US Army Corps of Engineers®

PDC TR-05-02
July 2005

Protective Design Center Technical Report

Component Explosive Damage Assessment Workbook *(CEDAW)*

WBE Project No. 02-0752-001

Contract No. DACA 45-01-D-0007

Prepared for

USACE Protective Design Center

Omaha District

https://pdc.usace.army.mil/software/cedaw

Notice

Baker Engineering and Risk Consultants, Inc. (BakerRisk) made every reasonable effort to perform the work contained herein in a manner consistent with high professional standards.

The work was conducted on the basis of information made available to BakerRisk. Neither BakerRisk nor any person acting on its behalf makes any warranty or representation, expressed or implied, with respect to the accuracy, completeness, or usefulness of this information. All observations, conclusions and recommendations contained herein are relevant only to the project, and should not be applied to any other facility or operation.

Any third party use of this Report or any information or conclusions contained therein shall be at the user's sole risk. Such use shall constitute an agreement by the user to release, defend and indemnify BakerRisk from and against any and all liability in connection therewith (including any liability for special, indirect, incidental or consequential damages), regardless of how such liability may arise.

BakerRisk regards the work that it has done as being advisory in nature. The responsibility for use and implementation of the conclusions and recommendations contained herein rests entirely with the client.

EXECUTIVE SUMMARY

This report summarizes the methods used by Baker Engineering and Risk Consultants, Inc. (BakerRisk) to develop the Component Explosive Damage Assessment Workbook (CEDAW) for the U.S. Army Corps of Engineers Protective Design Center (PDC). The workbook generates pressure-impulse (P-i) diagrams and charge weight-standoff (CW-S) graphs that are used to determine the Level of Protection (LOP) provided by an input structural component loaded by blast from an input equivalent TNT charge weight and standoff. The CEDAW workbook "unscales" scaled P-i curves applicable for the input component type and plots the unscaled curves on the P-i diagram and CW-S graphs. These curves create regions of constant LOP on the graphs that allow the user to visually determine the LOP for their input blast load scenario. CEDAW has scaled P-i curves for each LOP for fourteen different common structural component types.

The scaled P-i curves for each structural component type and LOP were determined primarily from available test data and single-degree-of-freedom (SDOF) analyses. The blast loads from both the tested components and SDOF analyses of representative components of each component type were scaled using Pbar and Ibar terms, which account for differences in component strength, stiffness, and mass, so that the blast loads and response of different components can be considered together in scaled terms. SDOF analyses were used to define the peak pressures and positive phase impulses of blast loads with a full range of durations that all caused a given non-dimensional response level in a representative component. These peak pressures and positive phase impulses were scaled into Pbar and Ibar terms, which defined scaled blast load points on a scaled P-i diagram that were curve-fit to define potential scaled P-i curves. The final scaled P-i curves were determined from SDOF analyses with response levels that caused the curves to create regions on the scaled P-i diagram that were consistent with scaled data points, where each region primarily contained data points that all had the same observed LOP response levels. The response levels for the final scaled P-i curves, which were determined in a trial and error method, represent the upper and lower response limits of each LOP for the given component type. The resistance-deflection relationships used in the SDOF analyses were consistent with applicable response modes for each component type, including flexural, tension membrane, concrete shear, and masonry arching from axial load. The blast loads in the SDOF analyses were determined from a full range of charge weight-standoff combinations, starting with a short standoff distance and progressing to very large distances, that produced the given response levels considering both positive and negative phase loads.

The most important steps in the development of the scaled P-i curves were the selection of the response limits corresponding to the upper and lower ranges of each LOP for each component type and the development of the Pbar and Ibar terms that scale the results from different components with the same component type and response mode into comparable terms. The response limits were determined using scaled data and SDOF analyses, as stated previously, except for component types and LOP response levels where insufficient data was available. In these cases, the response limits were determined using available information in the literature and comparisons to any similar component types with data.

The equations for the Pbar and Ibar terms were developed using a conservation of energy approach, where the strain energy from the dynamic response of a generic component was set equal to the work energy from a long duration blast load, which only involves the peak pressure of the blast load, and the kinetic energy of a short duration blast load, which only involves the impulse of the blast load. Each of these energy equivalency equations was solved for a non-dimensional load parameter (i.e. Pbar and Ibar) in terms of a non-dimensional response parameter (i.e. the ductility ratio of support rotation). These Pbar and Ibar terms, or equations, were used to generate the scaled P-i curves and to scale the relevant test data. The Pbar and Ibar terms were developed with different response parameters and response mode terms (i.e. for response in flexure, tension membrane, etc.) in the strain energy in the energy balance equations, depending on the component type. Some mathematical approximations were used to simplify the Pbar and Ibar equations that did not seem to significantly affect the accuracy of the scaling based on numerous SDOF analyses with a range of different component properties. Comparisons of scaled P-i curves calculated from SDOF analyses for different components with the same response mode and non-dimensional response parameter values, which ideally are identical, were typically within 10% for a flexural response mode and within 25% for the more complex response modes in the blast load range of interest for typical building blast assessments.

The Pbar and Ibar points on the scaled P-i curves for each LOP of the component type matching the input component are “unscaled” in the CEDAW workbook using the input component properties in the applicable Pbar and Ibar terms to solve for the peak pressure and impulse corresponding to each point. The workbook plots these peak pressure and positive phase impulse points to create unscaled P-i curves that are applicable only for the input component. The workbook also plots points defined by the charge weight and standoff causing each peak pressure and impulse point for free-field and fully reflected conditions to create CW-S curves.

CEDAW is not intended for use on single reinforced concrete components with high reinforcing ratios or heavy steel girders because the response limits used to develop the scaled P-i curves may be unconservative for these cases. Also, the CEDAW methodology is approximate because of simplifying assumptions and approximations incorporated into the derivations, data analysis, and calculation procedures used to develop the methodology, as discussed within the report. This is considered acceptable given that CEDAW is intended for generalized first-cut type damage assessments and it predicts response in terms of relatively general, qualitative LOP levels. The approximate approach in CEDAW allows it to calculate very rapid results, which is necessary for many first-cut type damage assessments that must assess a large number of buildings in a short time.

Table of Contents

EXECUTIVE SUMMARY ..... **I**

1.0 INTRODUCTION **1**

1.1 Scaled Pressure-Impulse (P-i) Diagrams 1

1.2 The FACEDAP Damage Assessment Method 2

2.0 METHODOLOGY FOR THE CEDAW WORKBOOK **4**

3.0 CURVE-FITTING EQUATIONS FOR SCALED P-I CURVES **9**

4.0 DERIVATION OF PBAR AND IBAR TERMS **12**

4.1 Pbar and Ibar Term Equations for Elastic, Perfectly Plastic Flexural Response 12

4.2 Pbar and Ibar Term Equations That Include Tension Membrane Response 14

4.3 Pbar and Ibar Term Equations for Brittle Flexural Response and Arching from Axial Force of Unreinforced Masonry Walls 16

4.4 Modifications to Pbar and Ibar Terms to Scale Negative Phase Load Effects 19

5.0 COMPONENT LEVELS OF PROTECTION (LOP) **25**

6.0 SCALED P-I CURVES FOR EACH COMPONENT TYPE **27**

6.1 P-i Curves for Corrugated Steel Panels 31

6.2 P-i Curves for Cold-Formed Girts and Purlins With Significant Tension Membrane 33

6.3 P-i Curves for Steel Beams and Cold-Formed Girts and Purlins Without Significant Tension Membrane 35

6.4 P-i Curves for Metal Stud Walls 37

6.5 P-i Curves for Reinforced Concrete Slabs and Beams 39

6.6 P-i Curves for One-Way Reinforced Masonry Slabs 40

6.7 P-i Curves for Open Web Steel Joists 42

6.8 P-i Curves for One-Way and Two-Way Unreinforced Masonry Walls 44

6.9 P-i Curves for Wood Stud Walls 47

6.10 P-i Curves for Reinforced Concrete Columns 48

6.11 P-i Curves for Steel Columns Limited by Connection Shear Capacity 53

6.12 P-i Curves for Steel Columns Not Limited by Connection Shear Capacity 56

7.0 ACCURACY OF CEDAW P-I CURVES 57

7.1 Comparisons of Unscaled P-i Diagrams from CEDAW and Directly from SDOF Calculations 57

7.2 Comparisons of Scaled P-i Curves for Similar Component Response 60

8.0 SUMMARY, CONCLUSIONS, AND RECOMMENDED FUTURE WORK.....65

8.1 Recommended Future Work.....67

9.0 REFERENCES 68

List of Appendices

Appendix A. Data from Shock Loading Tests on One-Way Spanning Unreinforced Masonry Walls 71

Appendix B. Data from Shock Loading Tests on Two-Way Spanning Unreinforced Masonry Walls 76

Appendix C. Data from Shock Loading Tests on One-Way Spanning reinforced Masonry Walls 80

Appendix D. Data from Shock Loading Tests on One-Way Spanning reinforced Concrete Walls 86

Appendix E. Data from Shock Loading Tests on Cold-Formed Girts with Tension Membrane 89

Appendix F. Data from Shock Loading Tests on Open Web Steel Joists 94

Appendix G. Data from Shock Loading Tests on Corrugated Steel Panels 97

Appendix H. Data from Shock Loading Tests on Wood Stud Walls 103

Appendix I. Data from Shock Loading Tests on Reinforced Concrete Columns Responding in Shear 106

Appendix J. Data from Shock Loading Tests on Steel Columns Limited by Connection Capacity 109

Appendix K. Comparison of P-i Diagrams Calculated with CEDAW and SDOF Analyses 111

Appendix L. Comparison of Scaled P-i Diagrams..... 117

Appendix M. Curve-Fitting Parameters for CEDAW P-i Curves for Each Component Type. 126

List of Tables

Table 1. DoD Level of Protection (LOP) Descriptions 26

Table 2. Response Modes, Response Parameter Types, and Pbar and Ibar Terms for Each Component Type in CEDAW 28

Table 3. Response Parameter Criteria for Upper Bound P-i Curves for Each LOP and CEDAW Component Type 30

Table 4. ASCE Response Criteria for Upper Bounds of Each Response Level in Steel Beams 37

Table 5. ASCE Blast Resistant Design Response Level Descriptions 37

Table 6. Assumed Concrete Shear DIF Values in CEDAW 52

Table 7. Statistical Summary of Comparison of P-i Diagrams Calculated with CEDAW and SDOF Analyses 60

Table 8. Trends From Comparisons of Scaled P-i Curves 64

List of Figures

Figure 1. General Scaled P-i Diagram for a Given Component Type Showing Levels of Protection (LOP) 2

Figure 2. Scaled P-i Curves-fits vs. Scaled SDOF Points in Terms of Support Rotation for Flexural Response of Reinforced Concrete Slabs 5

Figure 3. Scaled P-i Curves in Terms of Support Rotation vs. Scaled Data for Reinforced Concrete Slabs 6

Figure 4. Unscaled P-i Diagram for Specific Input Reinforced Concrete Slab 7

Figure 5. Charge Weight- Standoff Diagram for Reflected Blast Loads on Specific Input Reinforced Concrete Slab 8

Figure 6. Scaled P-i Diagram with Curve-Fits to Scaled Points from SDOF Analyses with Negative Phase Loads 9

Figure 7. Use of Equation 3 to Curve-Fit Scaled Points from SDOF Analyses Without Negative Phase Loads 11

Figure 8. Support Rotation Angle 13

Figure 9. Typical Resistance-Deflection Curve for Component Response with Flexure and Tension Membrane Showing Strain Energy 15

Figure 10. Response of Brittle Unreinforced Masonry Wall Under Combined Lateral and Axial Load 17

Figure 11. Resistance-Deflection Curves for Unreinforced Masonry with Brittle Flexural Response and Axial Load 18

Figure 12. Effect of Ultimate Resistance on Scaled P-i Diagram with Ductility Level of 4 21

Figure 13. Effect of Stiffness on Scaled P-i Diagram with Ductility Level of 4 22

Figure 14. Effect of Mass on Scaled P-i Diagram with Ductility Level of 4 22

Figure 15. Scaled P-i Diagram with Modified Ibar Term for Multiple Resistances with Ductility of 4 24

Figure 16. Typical SDOF Analysis Blast Load 29

Figure 17. Scaled P-i Curves-fits vs. Scaled SDOF Points in Terms of Ductility Ratio for Flexural Response of Corrugated Steel Panels without Significant Tension Membrane 31

Figure 18. Scaled P-i Curves-fits vs. Scaled SDOF Points in Terms of Support Rotation for Flexural Response of Corrugated Steel Panels without Significant Tension Membrane 31

Figure 19. Scaled P-i Curves in Terms of Ductility Ratio vs. Scaled Data for Flexural Response of Corrugated Steel Panels without Significant Tension Membrane 32

Figure 20. Scaled P-i Curves in Terms of Support Rotation vs. Scaled Data for Flexural Response of Corrugated Steel Panels without Significant Tension Membrane 32

Figure 21. Scaled P-i Curves in Terms of Support Rotation vs. Scaled Data for Flexural Response of Corrugated Steel Panels with Significant Tension Membrane..... 33

Figure 22. Scaled P-i Curves-fits vs. Scaled SDOF Points in Terms of Support Rotation for Flexural Response of Cold-Formed Girts with Significant Tension Membrane 34

Figure 23. Scaled P-i Curves in Terms of Support Rotation vs. Scaled Data for Flexural Response of Cold-Formed Girts with Significant Tension Membrane 35

Figure 24. Scaled P-i Curves-fits vs. Scaled SDOF Points in Terms of Ductility Ratio for Flexural Response of Steel Beams..... 36

Figure 25. Scaled P-i Curves-fits vs. Scaled SDOF Points in Terms of Support Rotation for Flexural Response of Steel Beams..... 36

Figure 26. Scaled P-i Curves-fits vs. Scaled SDOF Points in Terms of Ductility Ratio for Flexural Response of Metal Studs Not Connected to Top and Bottom Supports..... 38

Figure 27. Scaled P-i Curves-fits vs. Scaled SDOF Points in Terms of Ductility Ratio for Flexural Response of Metal Studs Connected to Top and Bottom Supports..... 38

Figure 28. Scaled P-i Curves-fits vs. Scaled SDOF Points in Terms of Support Rotation for Flexural Response of Reinforced Concrete Slabs..... 40

Figure 29. Scaled P-i Curves in Terms of Support Rotation vs. Scaled Data for Reinforced Concrete Slabs 40

Figure 30. Scaled P-i Curves-fits vs. Scaled SDOF Points in Terms of Support Rotation for Flexural Response of Reinforced Masonry Slabs..... 41

Figure 31. Scaled P-i Curves in Terms of Support Rotation vs. Scaled Data for Reinforced Masonry Slabs..... 42

Figure 32. Scaled P-i Curves-fits vs. Scaled SDOF Points in Terms of Support Rotation for Flexural Response of Open Web Steel Joists without Significant Tension Membrane 43

Figure 33. Scaled P-i Curves-fits vs. Scaled SDOF Points in Terms of Support Rotation for Flexural Response of Open Web Steel Joists with Significant Tension Membrane..... 43

Figure 34. Scaled P-i Curves in Terms of Support Rotation vs. Scaled Data for Open Web Steel Joists..... 44

Figure 35. Scaled P-i Curves-fits vs. Scaled SDOF Points in Terms of Support Rotation for Brittle Flexural and Arching Response of Unreinforced Masonry Walls with Low Ra/Ru. 45

Figure 36. Scaled P-i Curves-fits vs. Scaled SDOF Points in Terms of Support Rotation for Brittle Flexural and Arching Response of Unreinforced Masonry Walls with High Ra/Ru 46

Figure 37. Scaled P-i Curves in Terms of Support Rotation vs. Scaled Data for One-Way Unreinforced Masonry Walls..... 46

Figure 38. Scaled P-i Curves in Terms of Support Rotation vs. Scaled Data for Two-Way Unreinforced Masonry Walls..... 47

Figure 39. Scaled P-i Curves-fits vs. Scaled SDOF Points in Terms of Ductility Ratio for

Flexural Response of Wood Stud Walls 48

Figure 40. Scaled P-i Curves in Terms of Ductility Ratio vs. Scaled Data for Wood Stud Walls 48

Figure 41. Portion of Reinforced Concrete Frame Building Near Oklahoma City Bombing with Cladding Failure..... 49

Figure 42. Shear Damage to Reinforced Concrete Columns from DB6 Test..... 50

Figure 43. Damage to Concrete Column at 5 m from South Quay IRA Bombing in London 51

Figure 44. Scaled P-i Curves-fits vs. Scaled SDOF Points in Terms of Ductility Ratio for Flexural Response of Columns Up to Ultimate Shear Capacity..... 51

Figure 45. Scaled P-i Curves in Terms of Ductility Ratio vs. Scaled Data for Reinforced Concrete Columns Failing in Shear 53

Figure 46. Typical Pre-Engineered Steel Building and Multi-Story Steel Frame Building (in Background) with Cladding Failure Caused by Blast Loads..... 54

Figure 47. Failed Steel Column Connections in DB Tests 54

Figure 48. Scaled P-i Curves in Terms of Ductility Ratio vs. Scaled Data for Steel Columns Subject to Connection Failure..... 55

Figure 49. W14x38 Column After Blast Test 56

Figure 50. P-i Diagram Calculated Using SDOF Analyses for Corrugated Steel Panel 58

Figure 51. P-i Diagram Calculated with CEDAW for Corrugated Steel Panel 59

Figure 52. Comparison of Scaled P-i Curves Based on Ductility Ratio for Steel Beams with LOP Response 61

Figure 53. Comparison of Scaled P-i Curves Based on Support Rotation for Reinforced Concrete Slabs for MLOP Response (Uniform Load and Simple Supports) 62

Figure 54. Comparison of Scaled P-i Curves For Cold-formed Beams with Significant Tension Membrane for LLOP Response 62

Figure 55. Comparison of Scaled P-i Curves Controlled for Unreinforced Masonry Wall with Constant Ultimate Resistance and Variable Axial Load for LLOP Response..... 63

Figure 56. Comparison of Scaled P-i Curves Controlled for Unreinforced Masonry Wall with Variable Ultimate Resistance and Axial Load for LLOP Response..... 63

1.0 INTRODUCTION

Assessment of damage to military and civilian facilities from a terrorist or accidental explosion typically requires blast damage assessments for a large number of individual structural components. Overall building damage and potential injuries to building occupants can be determined based on the damage of individual components and consideration of any additional damage due to interdependence between components, such as progressive collapse. Component blast damage assessment can be performed with approaches ranging from simple charts based on the explosive charge weight and standoff distance to the component to dynamic finite element analyses, where the dynamic response of the component is modeled with a large number of degrees of freedom. A commonly used approach that is intermediate between these two extremes is the use of equivalent single-degree-of-freedom (SDOF) systems to represent the dynamic response of blast-loaded structural components.

1.1 Scaled Pressure-Impulse (P-i) Diagrams

SDOF analyses can be performed much more quickly than other approaches involving more degree of freedoms, but they can still be somewhat time consuming since a time-stepping solution method is generally required where the equation of motion is solved incrementally at each time-step using the response at the previous time step. A computationally efficient method to assess blast-loaded components using SDOF analyses is to develop scaled pressure-impulse (P-i) diagrams based on SDOF analyses that can be used in a look-up manner to determine component damage levels. In this approach, blast load parameters are scaled or divided by relevant dynamic response parameters of the blast-loaded component, so that the scaled blast load is a ratio of the applied blast load divided by key response parameters such as the mass and maximum dynamic load capacity of the blast-loaded component.

Figure 1 shows a scaled P-i diagram for a given component construction type (i.e. unreinforced masonry wall). The scaled blast load, in terms of the scaled peak blast pressure (Pbar) and scaled positive phase blast impulse (Ibar), define a point on the P-i diagram that lies in a region between bounding curves (P-i curves). Each region is associated with given component damage levels or levels of protection (LOP) to the building occupants and assets. The LOP, which range in Figure 1 from MLOP (i.e. Medium LOP) to VLLOP (Very Low LOP) and Blowout of the component, can be predicted based on the Pbar and Ibar terms calculated from the blast load applied to a component and the component properties. In order for a scaled P-i diagram to be valid for all components of a given component type, a wide range of blast loads causing the same blast damage or LOP in a wide range of structural components of the given component type should all have scaled Pbar and Ibar terms that define points in the same damage or LOP region of the diagram. Any significant response modes of the structural components or blast load effects not considered in the development of the equations for the Pbar and Ibar terms and scaled P-i diagram will tend to cause a discrepancy between the actual damage of given components and the damage or response level predicted with the P-i diagram. Simplifications and approximations are sometimes necessary in the consideration of more complex component response modes, but the corresponding discrepancies can often fit within the relatively broad definitions of damage levels or LOP predicted by the P-i diagram.

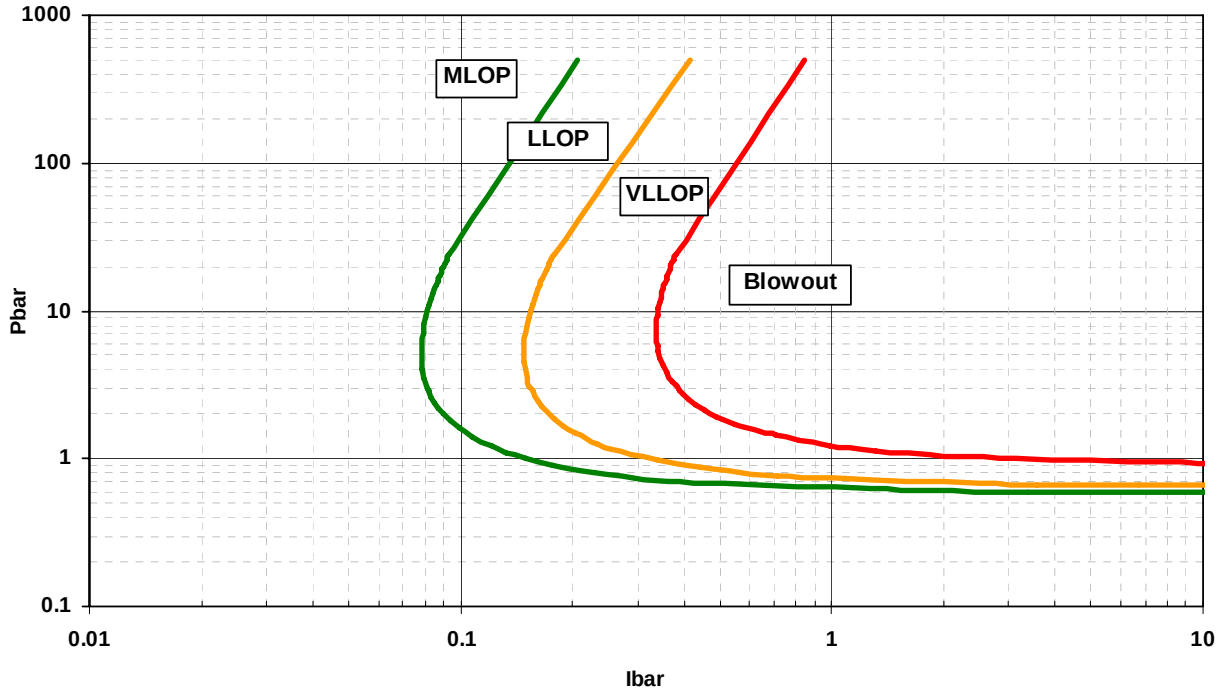

Figure 1. General Scaled P-i Diagram for a Given Component Type Showing Levels of Protection (LOP)

Scaled P-i diagrams can be created by analyzing equivalent single-degree-of-freedom (SDOF) systems of representative components for given component types (i.e., steel beams or reinforced concrete beams) to determine the full range of blast loads causing given component response levels that are assumed to correspond to the upper and lower bounds of each LOP, scaling these blast loads by the component dynamic response properties, plotting the scaled blast loads in terms Pbar and Ibar for each response level on a P-i diagram, and curve-fitting through the points. Other analytical methods that are more sophisticated than SDOF can be used in this same manner, but this is usually considered inefficient since the P-i diagrams generally divide component response only into relatively broadly defined damage or LOP levels. Empirical P-i diagrams can also be developed where Pbar and Ibar terms are calculated from explosive tests on components of the same component type using the known blast load and component properties from each test, and then each test is plotted on a P-i diagram in terms of the Pbar and Ibar representing each test and labeled with the known damage level or LOP. P-i curves can then be drawn separating the P-i diagram into regions where all the test data points have constant damage or LOP. A hybrid of these two approaches can also be used that depends on both SDOF analyses and explosive test data.

1.2 The FACEDAP Damage Assessment Method

The Facility and Component Explosive Damage Assessment Program (FACEDAP) was developed in the early 1980's to quickly assess blast damage to common building structural components using scaled pressure-impulse (P-i) diagrams (Oswald, 1993). It was the first comprehensive blast damage assessment method for conventional structural components to be

based on scaled P-i diagrams. The FACEDAP P-i diagrams or derivatives of these P-i diagrams have been used to assess blast damage to many facilities and have been incorporated into many newer, more user-friendly blast assessment computer tools that have been developed by the U.S. government to assess terrorist threats. The FACEDAP program has separate scaled P-i diagrams for fifteen structural component types that were derived using a hybrid of theory and empiricism and define component damage in terms of 0%, 30%, 60%, or 100% damage. The curves were initially developed theoretically using Pbar and Ibar terms from analyses of equivalent SDOF systems that caused given levels of response that were assumed to represent the upper bound of each damage level in representative components of each component type. Then, these curves were shifted on the P-i diagrams to better match points on the diagrams defined by empirical points with Pbar and Ibar terms calculated from applicable explosive test data.

Although the shapes of the theoretically derived P-i curves were preserved in the shifting process, it limits the generality of the FACEDAP scaled P-i diagrams so that the diagrams are most applicable only to components with similar properties as the test components used as the basis for the curve shifts. This limitation was considered as an acceptable tradeoff since the shifted curves empirically account for more complex response modes affecting the data that could not easily be accounted for in the theoretical SDOF analyses. Also, FACEDAP defines component damage only in terms of broadly defined damage levels and it is a quick assessment tool rather than a more exact blast design tool.

2.0 METHODOLOGY FOR THE CEDAW WORKBOOK

Since the development of FACEDAP, more refined SDOF techniques have become available that consider more complex response modes, including tension membrane and arching, and considerably more data from structural component response to blast loads has been generated. The SDOF Blast Effects Design Spreadsheets (SBEDS), which is distributed by the PDC, is an example of the currently available software that perform SDOF analyses considering more complex response modes (Nebuda and Oswald, 2004). Also, the importance of the negative phase of the blast load, which limits peak component response when the peak response occurs after the end of the positive phase of the blast load, is now understood better than during the development of FACEDAP. Therefore, the PDC contracted Baker Engineering and Risk Consultants, Inc. (BakerRisk) to develop updated scaled P-i diagrams for component damage, in terms of the Levels of Protection (LOP) currently used by the U.S. Department of Defense to classify blast damage, in an EXCEL® workbook named Component Explosive Damage Assessment Workbook (CEDAW).

There are two basic goals of the CEDAW workbook: 1) to very quickly generate "unscaled" P-i diagrams showing blast loads causing each LOP to a given input component based on unscaling component type-specific scaled P-i diagrams, and 2) to develop scaled P-i diagrams showing scaled blast loads causing each LOP for each component type that are as consistent as possible with both available test data and SDOF-based dynamic analyses. These goals involve a number of tasks that are discussed in detail in this report including: 1) develop scaling approaches for the blast loads that consider all relevant response modes and are as rational and practical as possible, 2) develop curve-fit equations for scaled P-i curves that match results from SDOF-based dynamic analyses and can be used to quickly "unscale" the curves to show the unscaled blast loads causing each LOP to a given component, 3) obtain as much relevant component blast test data as possible with sufficient detailed information, 4) define descriptions for each component LOP as shown in Section 5.0 and determine the LOP for the available data points based on these descriptions and available post-test photographs and damage descriptions, and 5) use both available test data information and SDOF-based analyses results to generate scaled P-i diagrams that are as consistent as possible with both approaches.

A short overview of the steps involved in developing the CEDAW methodology is presented in this section, followed by more detailed discussion in the following sections. In the first step of the development process, equations that transform the peak pressure and positive phase impulse from the blast load into the scaled blast load terms Pbar and Ibar, respectively, were developed. This development of these equations, which is discussed in Section 4.0, is based on conservation of energy and consideration of the response modes that affect given component types, including flexure, tension membrane, and arching from axial load. Essentially, the scaling process must normalize a given blast load on a given component by properties of the component so that two different components with different blast loads, but the same normalized or scaled blast load, will have the same response in terms of a non-dimensional response parameter such as ductility ratio or support rotation.

Scaled P-i curves for each LOP and component type were generated by using the Pbar and Ibar equations to scale the blast loads with a wide range of blast load durations that all cause a given non-dimensional response parameter in SDOF analyses. This is illustrated in Figure 2. Each point in the figure represents a scaled blast load casing the given support rotation (θ) and the curve-fits through the points represent scaled P-i curves. The overall figure is a scaled P-i diagram that shows curves of constant response in terms of the scaled peak blast pressure (Pbar) and scaled positive blast impulse (Ibar).

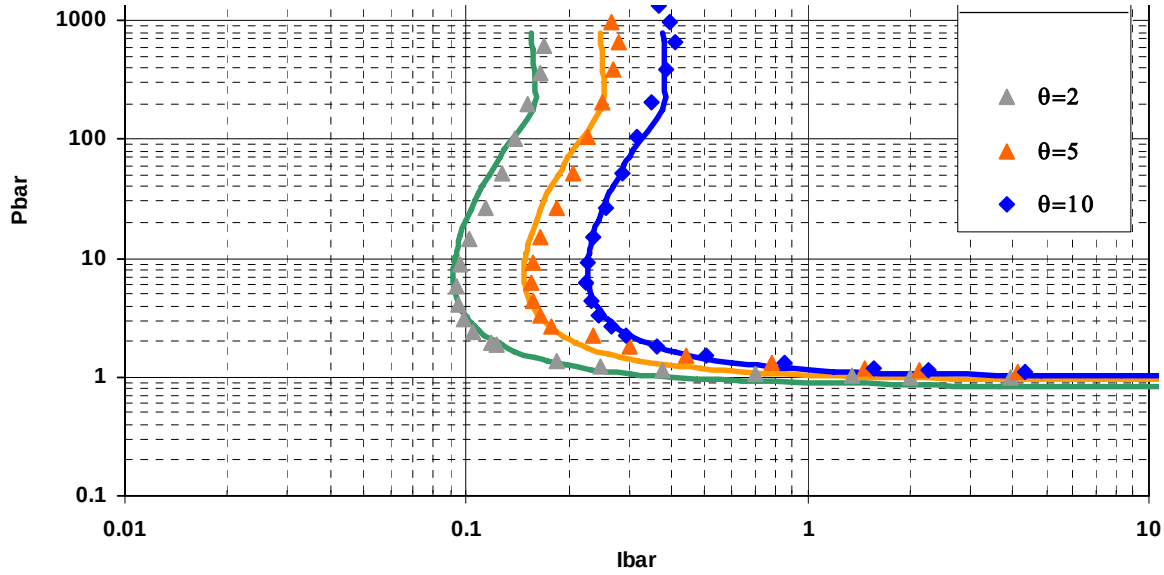

Figure 2. Scaled P-i Curves-fits vs. Scaled SDOF Points in Terms of Support Rotation for Flexural Response of Reinforced Concrete Slabs

The available test data for each component type were characterized in terms of the observed LOP response level using descriptions for each LOP in Section 5.0, the blast loads from the tests were scaled into Pbar and Ibar values using the appropriate scaling equations, and the test data were plotted as points on scaled P-i diagrams for each component type. Scaled P-i curves, such as those in Figure 2, were developed for each component type using a trial and error approach with different response levels (i.e., different θ values in the case of Figure 2) so that to the maximum extent possible, the scaled test points in the regions between adjacent scaled P-i curves all had the same observed LOP. The regions on the scaled P-i diagram between adjacent curves are therefore regions of constant LOP response based on available test data and response levels used in the SDOF analyses to define the bounding curves are response limits, or response criteria for the LOP.

Scaled P-i curves that created regions of constant LOP response in the available test data are illustrated in Figure 3. The curves were generated as described for Figure 2. The data points in Figure 3 were generated by scaling the blast loads from available tests on reinforced concrete slabs that caused the slabs to have LOP as shown in the figure with the same scaling equations used for the SDOF analysis blast loads. SDOF analyses with different support rotations were performed using a trial and error approach to determine the scaled P-i curves that caused the most consistency between the LOP regions on the scaled P-i diagram and the scaled data points.

This procedure was used to create scaled P-i diagrams for each of the fourteen component types in CEDAW. The SDOF analyses and scaling relationships considered applicable response modes for different component types including flexure, shear, tension membrane, and arching from axial load.

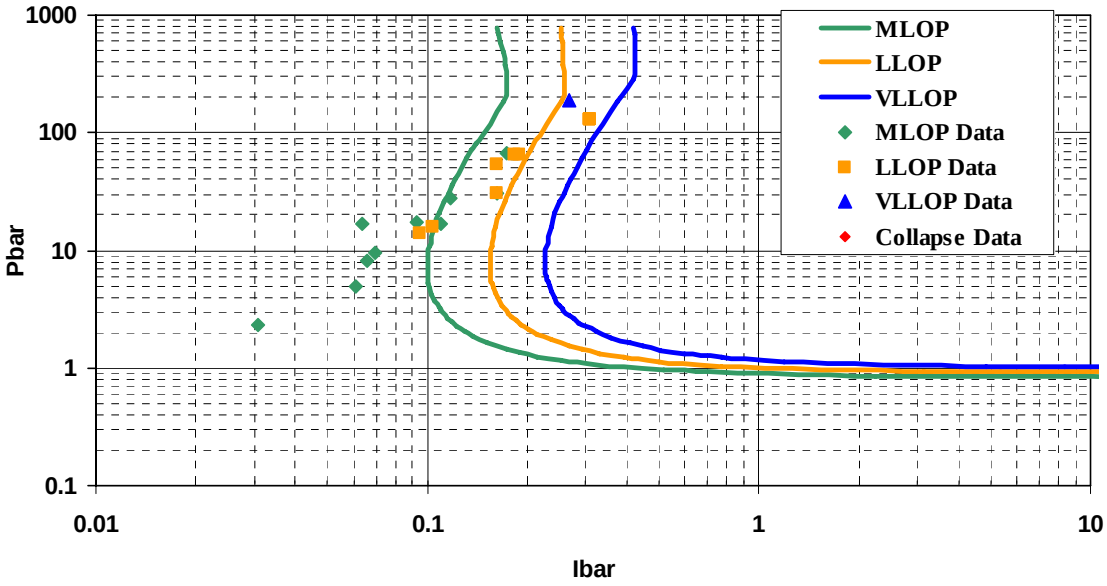

Figure 3. Scaled P-i Curves in Terms of Support Rotation vs. Scaled Data for Reinforced Concrete Slabs

In the final step of the CEDAW methodology, the CEDAW workbook "unscales" the scaled P-i curves of the component type matching an input component for each LOP by using the same Pbar and Ibar scaling equations used to create the scaled P-i curves in reverse. This transforms the scaled curves for the given component type, such as those in Figure 3, which are hard-coded into the CEDAW workbook, into similar curves on an unscaled P-i diagram, such as the P-i diagram in Figure 4, that are only applicable for the given input component. The unscaled P-i diagram is in terms of peak pressure and positive phase impulse, instead of Pbar and Ibar, and the peak pressure and impulse from a given explosive threat can be used directly in an unscaled P-i diagram to determine the LOP of the input component response. The CEDAW workbook makes this comparison for the reflected and side-on blast loads from an input explosive threat, as shown in Figure 4 for the input charge weight and standoff to the component. Since the scaled P-i curves are unscaled using specific properties of the input component, the unscaled P-i diagrams are only applicable for the input component

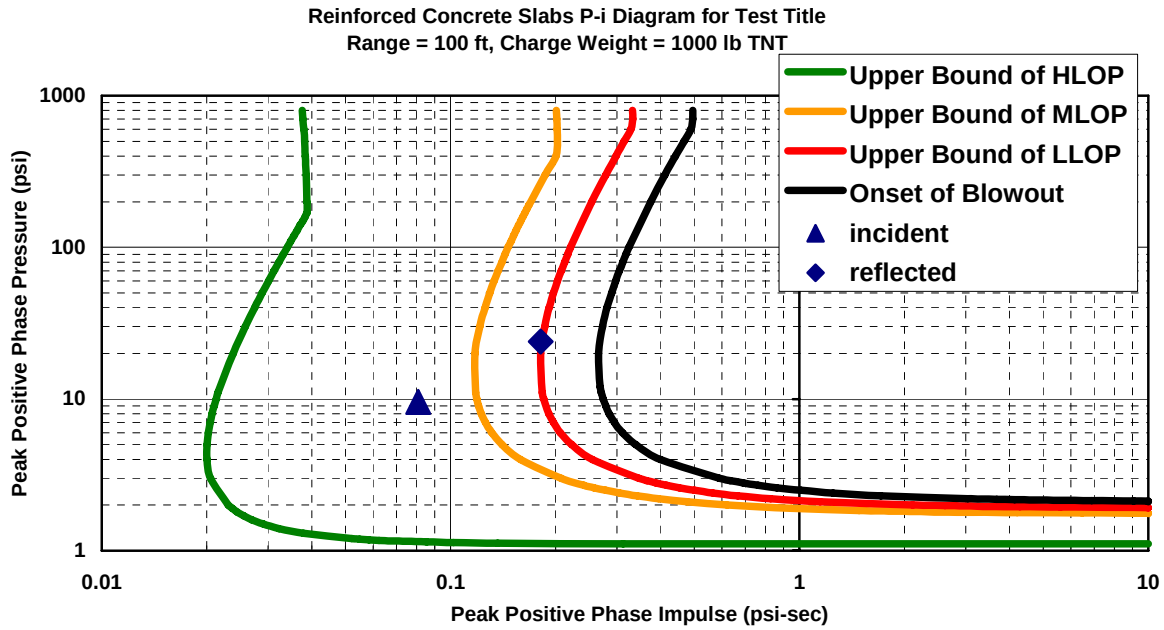

Figure 4. Unscaled P-i Diagram for Specific Input Reinforced Concrete Slab

For a number of component types, there are two sets of scaled P-i curves where one set of curves is for component LOP response defined in terms of ductility ratio and the other set of curves is for component LOP response defined in terms of support rotations. For other component types, such as reinforced concrete slabs, engineering judgment was used to determine that only one set of scaled P-i curves for component response at given LOP levels was necessary, and therefore LOP response was defined in terms of either ductility ratio or support rotations for these cases. This is discussed more in Section 6.0.

When there are two sets of scaled P-i curves for the component type matching the input component, the CEDAW workbook determines the lower unscaled P-i curve independently for each LOP and plots these unscaled curves on the output unscaled P-i diagram. Therefore, the P-i curve defining the upper bound of HLOP might be based on the upper bound scaled P-i curve for HLOP response defined in terms of ductility ratio while the P-i curve for the upper bound of MLOP might be based on the scaled P-i curve that is defined in terms of support rotation. The CEDAW program determines the lower unscaled curve by unscaling a point on the scaled P-i curves for ductility ratio and support rotation response that has a Pbar value 5 times greater than the Pbar asymptote and selecting the P-i curve with the lower impulse value at this point.

The points on the unscaled P-i diagrams are also converted into charge weight-standoff (CW-S) points causing the same peak pressure and positive phase impulse for the free-field and fully reflected conditions. These CW-S points create curves that define the upper and lower boundaries of each LOP for the input component. Figure 5 shows a CW-S diagram for the same component shown in Figure 4. The CEDAW workbook also generates a diagram similar to Figure 5 for side-on blast loading.

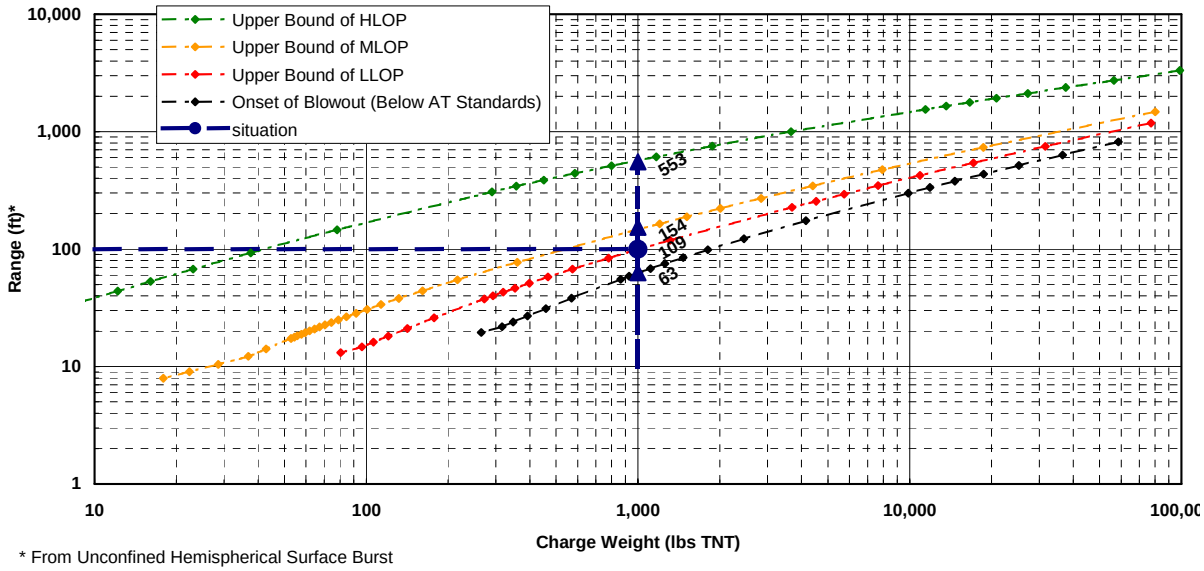

Figure 5. Charge Weight- Standoff Diagram for Reflected Blast Loads on Specific Input Reinforced Concrete Slab

The CEDAW methodology is approximate because of simplifications in the assumptions, derivations, and calculation procedures used to develop the methodology. This includes the use of some simplifying assumptions in the derivation of the blast load scaling equations that keep the scaling process from becoming too complex, the use of SDOF analyses that make the basic simplifying assumption that only one response mode dominates the component response, and the use of approximate curve-fit equations to develop scaled P-i curves from scaled blast loads generated with SDOF analyses. Also, engineering judgment was used to determine the LOP response of the tested components based on available photos and damage descriptions and all desired information was not available for all test data. In a relatively few cases, some tested component properties were assumed equal to typically used properties in construction where this was necessary and it was considered a reasonable approach. Test data is shown in detail in the appendices to the report. These simplifications and assumptions must be considered against the fact that CEDAW is intended primarily for generalized, first-cut type damage assessments and it only predicts response in terms of relatively general, qualitative LOP levels. Also, CEDAW provides very rapid results, which is necessary for damage assessments that must consider a large number of buildings in a short time.

The accuracy of the CEDAW P-i diagrams is discussed in Section 7.0. Comparisons in this section show that the approximate P-i diagrams generated by CEDAW generally match P-i diagrams generated with more a more exact, and more time-consuming iterative SDOF-based analyses within 5% to 15%. Also, many comparisons of scaled P-i curves developed for different components with the same response mode and response levels showed that these curves, which ideally lie on top of each other, were within 30% as a worse case. These comparisons indicate that the assumptions and approximations involved in scaling and unscaling the blast loads, and the curve-fitting of the scaled blast loads, that are used to create the scaled P-i curves do not typically have a very significant effect on the final unscaled P-i diagrams generated by CEDAW.

3.0 CURVE-FITTING EQUATIONS FOR SCALED P-I CURVES

As mentioned in Section 2.0, the peak pressure and positive phase impulse of blast loads causing given levels of component response in SDOF analyses are scaled into Pbar and Ibar values, respectively, that are plotted as (Ibar, Pbar) points on scaled P-i diagrams to define scaled P-i curves. Figure 6 shows a scaled P-i diagram with four sets of color coded points for Pbar and Ibar combinations representing blast loads causing four different levels of non-dimensional component response (i.e., ductility ratios or support rotations) calculated with SDOF analyses. In the case of Figure 6, all the square purple points are scaled blast loads from SDOF analyses caused a ductility ratio of 1.0. The other series of points were calculated from SDOF analyses causing higher ductility ratios. Each scaled blast load on the P-i diagram can be referred to as a "scaled SDOF point" or a "scaled point from SDOF analyses".

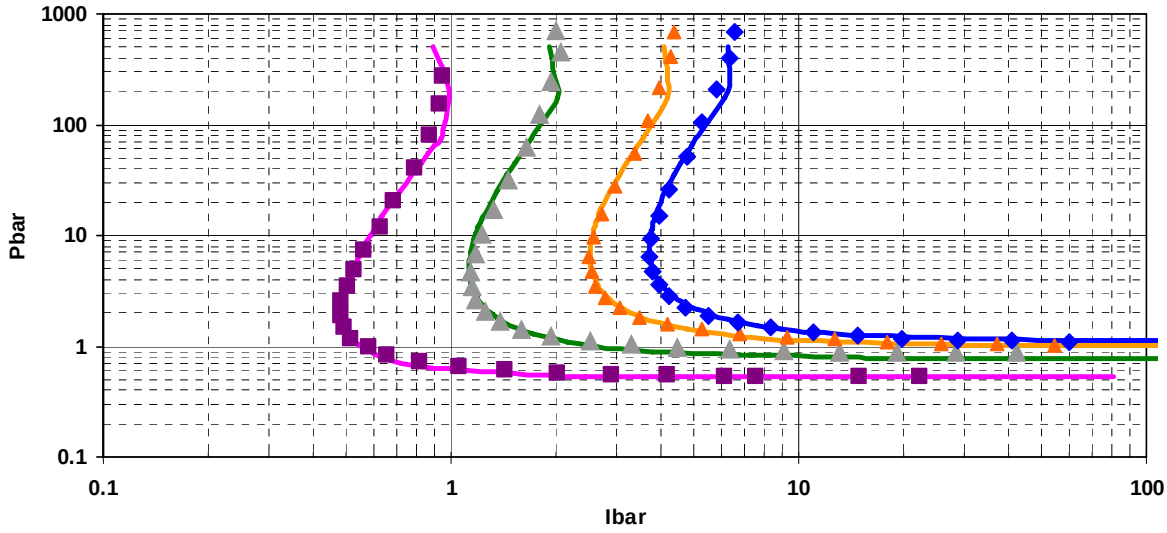

Figure 6. Scaled P-i Diagram with Curve-Fits to Scaled Points from SDOF Analyses with Negative Phase Loads

These points in Figure 6 can be curve-fit to form four scaled P-i curves, where each curve represents all the different scaled blast loads causing each level of response. The scaled P-i curves representing the upper bounds of each LOP for each component type represent the basis of the CEDAW methodology. Equation 1 is used in CEDAW as the curve-fit equation for these scaled P-i curves for all cases where the scaled P-i points were developed from SDOF analyses that include the effects of negative phase loading. Negative phase loading only affects component response when Pbar is high relative to Ibar, which corresponds to cases where the positive phase blast load durations are relatively short compared to component response time, and causes the curves of scaled (Ibar, Pbar) points to bend first to the right, and then to the left at higher Pbar values. The effects of negative phase loads are included for all component types except columns in shear response or subject to connection failure.

The parameters A through G in Equation 1 are curving fitting parameters that can be varied to typically cause a curved line that closely fits the scaled SDOF blast loads for given component levels of response representing upper bounds of each LOP, as shown in Figure 6. Equation 2

shows a special case for the unreinforced masonry wall component type where A and D in Equation 1 are functions of wall properties, including the applied axial load. The equations in Equation 2 were determined by trial and error to cause the curve-fits to match different sets of scaled SDOF points from SDOF analyses where walls had the same response in terms of support rotation but a range of different levels of axial load. These wall property dependent terms for A and D are necessary because of approximations in the derivations of the equations for Pbar and Ibar for unreinforced masonry walls, as discussed in Section 4.3. Typically, the effects of component properties are accounted for within the Pbar and Ibar scaling terms so that the scaled P-i curves are independent of the component properties used in the SDOF analyses that generate the scaled P-i points. Thus, all the curve-fit equation parameters in Equation 1 are only functions of the LOP and component type except as noted in Equation 2. Appendix M contains the curve-fit equation parameters causing Equation 1 (and Equation 2 where applicable) to fit scaled blast loads from SDOF analyses representing the upper bound of each LOP for each component type and applicable non-dimensional response parameter as discussed in Section 6.0.

$$Ibar = \frac{A(Pbar)^C}{(\ln[(B)(Pbar)])^D} \qquad for \quad Pbar \le E$$

$$Ibar = (Pbar - E)G + F \qquad for \quad Pbar > E \qquad where \quad F = \frac{A(E)^C}{(\ln[(B)(E)])^D}$$

Equation 1

where: A, B, C, D, E, F, G = curve fitting parameters, see Appendix M
Pbar = scaled pressure term applied to component on y-axis of scaled P-i diagram
Ibar = scaled impulse term applied to component on x-axis of scaled P-i diagram

$$A(MLOP) = -0.0096R'^2 + 0.039R' + 0.047$$
$$A(LLOP) = 1.6 \times A(MLOP)$$
$$A(VLLOP) = 3 \times A(MLOP)$$
$$D(MLOP) = -0.47R'^2 + 0.89R' + 0.236$$
$$D(LLOP) = D(MLOP) = D(VLLOP)$$

Note: Only applicable for unreinforced masonry walls (see paragraph above)

Equation 2

where: $R' = R_A/R_u$ for unreinforced masonry walls (see Section 4.3 and Equation 8)

Equation 3 was used as the curve-fit equation for the scaled P-i curves developed from SDOF analyses that did not include the effects of negative phase loading, which includes the curves for columns in shear response or subject to connection failure. It is the curve-fit equation for scaled P-i curves from FACEDAP. The parameters A through C are curving fitting parameters in

Equation 3 that can be varied to typically cause a curved line that closely fits the scaled SDOF blast loads for a given level of response component, as shown in Figure 7. In Figure 7, scaled SDOF blast loads are shown from three sets of SDOF analyses causing a column component to have responses equal to ductility ratios (μ) of 1, 2, and 6. Since there is no negative phase load in the SDOF analyses, the curves of scaled (Ibar, Pbar) points have asymptotic values along both the Pbar and Ibar axes. Negative phase blast loads were not considered in the SDOF analyses of column components because these components are typically stiff and strong enough so that their peak response occurs before the end of the positive phase blast load for charge weight-standoff combinations of practical interest. The scaled P-i curves for columns are discussed more in Section 6.10 and 6.11.

$$Ibar = \frac{0.4\left(\frac{A}{2}+\frac{B}{2}\right)^{C}}{Pbar - A} + B$$

Equation 3

where: A, B, C = curve fitting parameters, see Appendix M

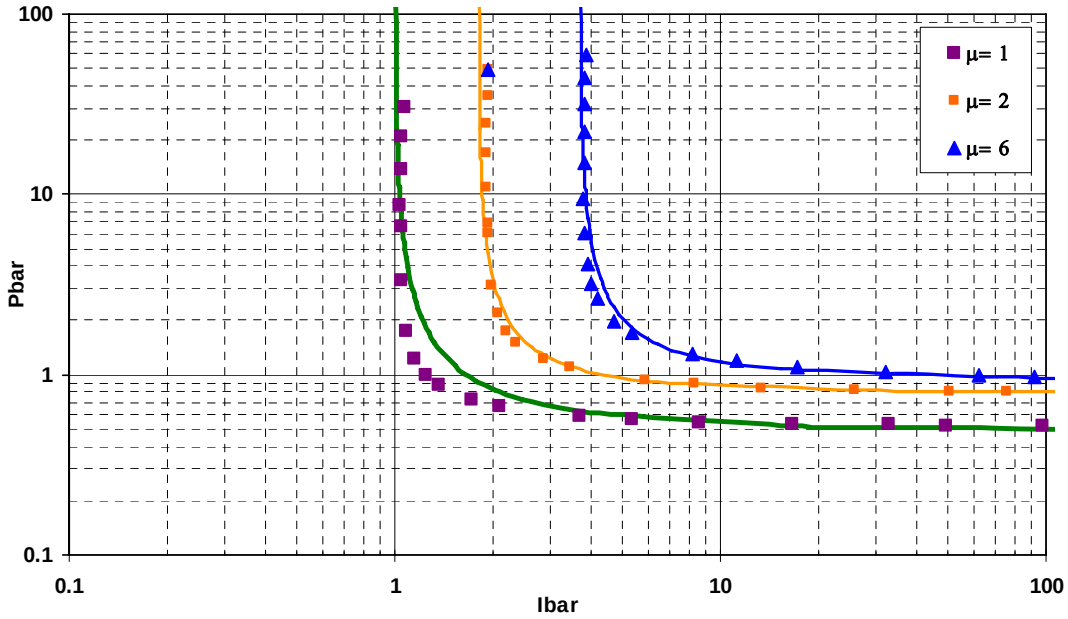

Figure 7. Use of Equation 3 to Curve-Fit Scaled Points from SDOF Analyses Without Negative Phase Loads

4.0 DERIVATION OF PBAR AND IBAR TERMS

The equations for the Pbar and Ibar terms in CEDAW vary depending on the assumed response modes for the component and the response criteria type (i.e., ductility ratio or support rotation) used to characterize component response. Elastic, perfectly plastic flexural response is assumed to predominate for all component types in CEDAW except for lightweight steel beams, open web steel joists, columns, and unreinforced masonry walls. Lightweight steel beams and open web steel joists in typical construction can also respond with significant tension membrane response at larger deflections, depending on support conditions. Unreinforced masonry components are assumed to respond in brittle flexural response followed by arching action from axial loads, including self-weight. Column components are assumed to have elastic flexural response until the to the component resistance equals the shear capacity through the cross section (for reinforced concrete columns) or through the connections (steel columns), if the connections control the ultimate component capacity. Limited ductile yielding is then assumed to occur with a resistance equal to the ultimate dynamic shear capacity. In all these cases, the different component types can have LOP that are associated with component response in terms of ductility ratio, support rotation, or both. Therefore, a suite of equations are needed for different Pbar and Ibar terms that are consistent with all the applicable combinations of response mode and response criteria type for the CEDAW component types. Response modes other than those discussed here are possible for all component types in CEDAW. However, the use of these assumed response modes dramatically simplified the blast assessment procedure and these response modes are considered as predominate for the component types based on blast test data and engineering judgment.

4.1 Pbar and Ibar Term Equations for Elastic, Perfectly Plastic Flexural Response

Equation 4 and Equation 5 show development of Pbar and Ibar terms for ductile flexural component response. The applied energy from the blast load is entirely described in terms of work energy for the Pbar equation and kinetic energy for the Ibar equation (Baker et al, 1983). In both cases, the energy from the blast load is set equal to the component strain energy for elastic, perfectly plastic flexural response. The equations are rearranged so that the blast load terms and the maximum structural response term are on opposite sides of the equations in non-dimensional terms and the non-dimensional response term is the ductility ratio or support rotation, which can both be correlated to component blast damage. The non-dimensional blast load terms with the peak blast pressure and impulse are called Pbar and Ibar, respectively. In general, component response to blast load is dependent on both the peak pressure and impulse, and therefore to both Pbar and Ibar.

$$Px_m = \frac{{x_m}^2 K}{2} \qquad let\mu = \frac{Kx_m}{R_u} \qquad Pbar1 = \frac{P}{R_u} = \frac{\mu}{2} \quad (ductility\_based\_elastic)$$

$$Px_m = R_u\left(x_m - \frac{x_e}{2}\right) \qquad x_e = \frac{R_u}{K} \qquad let\mu = \frac{x_m}{x_e} \qquad Pbar1 = \frac{P}{R_u} = 1 - \frac{1}{2\mu} \quad (ductility\_based\_yielding)$$

Equation 4

$$\frac{i^2}{2K_{LM}m}=\frac{x_m{}^2K}{2}\qquad \frac{i^2K}{K_{LM}mR_u{}^2}=\frac{\mu^2}{2}\qquad Ibar1=\frac{i}{R_u}\sqrt{\frac{K}{K_{LM}m}}=\frac{\mu}{2}(ductility\_based\_elastic)$$

$$\frac{i^2}{2K_{LM}m}=R_u\left(x_m-\frac{x_e}{2}\right)\qquad \frac{i^2}{K_{LM}mR_ux_e}=2\sqrt{\mu-0.5}\qquad Ibar1=\frac{i}{R_u}\sqrt{\frac{K}{K_{LM}m}}=\sqrt{2\mu-1}(ductility\_based\_yielding)$$

$$\frac{i^2}{2K_{LM}m}=R_u\left(x_m-\frac{x_e}{2}\right)\quad Let\left(x_m-\frac{x_e}{2}\right)\approx x_m=\theta\frac{L}{2}\quad Ibar2=i\sqrt{\frac{1}{K_{LM}mR_uL}}=\sqrt{\theta}(SupportRotation\_based)$$

Equation 5

where:
- P = peak pressure
- i = applied positive phase impulse
- m = mass of equivalent SDOF system for component
- K_{LM} = load-mass factor of equivalent SDOF system for component
- R_u = ultimate flexural resistance of equivalent SDOF system for component at yield (ultimate resistance based on shear capacity for reinforced concrete columns and connection shear capacity for steel columns, See Sections 6.10, 6.11)
- K = flexural stiffness of equivalent SDOF system for component
- x_m= maximum response of equivalent SDOF system for component
- θ = support rotation (radians) – see Figure 6 below
- L = component span length (twice minimum distance from support to yield line for two-way components)
- x_e = maximum deflection of component at ultimate flexural resistance
- μ = ductility ratio, equal to the ratio of maximum deflection divided by the deflection causing yield at all maximum moment locations

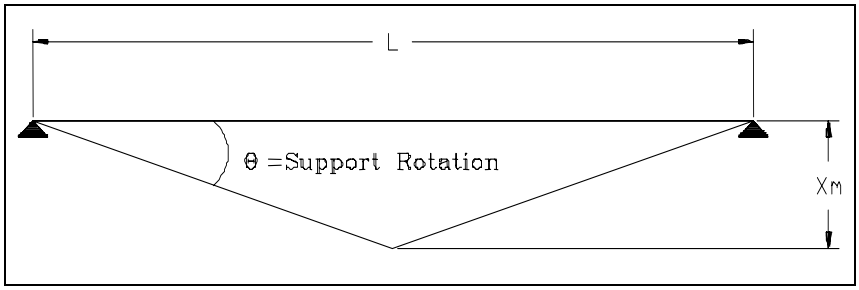

$$\theta=\tan^{-1}\left[\frac{2x_m}{L}\right]$$

Figure 8. Support Rotation Angle

The Ibar1 or Ibar2 terms in Equation 4 and Equation 5 are used to scale the blast loads from SDOF analyses or from data for a given component type in terms of ductility or support rotation, respectively. The response term built into the Ibar scaling equation varies since component damage can be correlated better to one term or the other, depending on the component type, or it is correlated to both terms in some cases. For the general case where the LOP for a given component type is correlated to both terms, two scaled P-i curves are needed based on the two different Ibar terms, they are both applied to the component of interest, and the unscaled P-i curves causing the lower predicted pressure and impulse values is used to construct the final unscaled P-i curve for the given LOP. Unscaling of scaled P-i curves is discussed in Section 2.0.
A Pbar term could not be derived for non-dimensional response in terms of support rotation with

the same approximation used for Ibar2 in Equation 5. However, Pbar is not very sensitive to the response term in general, whether it is based on either term, at ductility ratios greater than 3.0. For example, there is very little change in Pbar1 when ductility ratios of 3 and 10 are substituted into in Equation 4. SDOF analyses using very long duration blast loads, where the maximum response is only dependent on the peak pressure, could be used to show the same trend for responses with maximum support rotations past yield. Ductility ratios in the range of 3 or higher are typical for all LOP more severe than HLOP. Therefore, a Pbar term based on ductility level (i.e., Pbar1 in Equation 4) can be used to scale the peak pressure of blast loads causing LOP more severe than HLOP for component types where damage correlates better to support rotation and Ibar2 in Equation 5 is used to scale the impulse.

4.2 Pbar and Ibar Term Equations That Include Tension Membrane Response

Figure 9 shows a simplified resistance-deflection relationship for a component in combined ductile flexure response and tension membrane response, which is assumed in CEDAW to represent the response of light steel components with significant in-plane restraint at the supports. The available support restraint is typically not sufficient to develop tension membrane that is significantly more than the flexural resistance of heavy steel components such as most hot-rolled beams, which is greater than the flexural resistance of light steel components. After yielding from in-plane forces occurs in the cross section or in the connection, tension membrane resistance increases linearly with deflection at the slope K_{TM} in Figure 9. Elastic tension membrane occurring prior to this yielding tends to offset response mechanisms in light steel components that cause a loss in post-yield flexural capacity, such as local compression buckling in the maximum moment region, twisting of the cross section, or overall buckling of the compression flange, so that the combined resistance from elastic tension membrane and flexural response is assumed approximately equal to the flexural resistance assuming no post-yield reduction. Also, tension membrane forces tend to develop somewhat slowly with component deflection in many cases due to component slippage in the connections and support member flexibility and therefore do not contribute significantly to the overall component resistance at deflections less than the flexural yield deflection.

For the simplified case of combined ductile flexural response and tension membrane response in Figure 9, an extra term is added to the strain energy in the conservation of energy equations from Equation 4 and Equation 5, as shown in Equation 6 and Equation 7, and approximate Pbar and Ibar terms are derived as shown. The C term in Equation 6 and Equation 7 is a function of the component response and is therefore placed on the response parameter side of Equation 6 and Equation 7, so that it is not included in the Pbar and Ibar equations. Scaling with the $Pbar_{TM}$ equation breaks down if (P/R_u-1) becomes too close to zero. Based on trial and error iterations, $Pbar_{TM}$ should not be used when the maximum resistance including tension membrane, equal to r_m in Figure 9, is less than $1.27r_u$, as indicated in Equation 6. This implies that tension membrane resistance should be ignored and only flexural response considered for these cases where tension membrane causes less than a 27% increase in resistance above the flexural resistance at the maximum deflection corresponding to the given LOP. The exponent A in $Ibar_{TM}$ in Equation 7 was determined by trial and error iterations to best cause cases where various blast loads that all caused the same given support rotations to a wide range of components in SDOF analyses had the same $Ibar_{TM}$ terms.

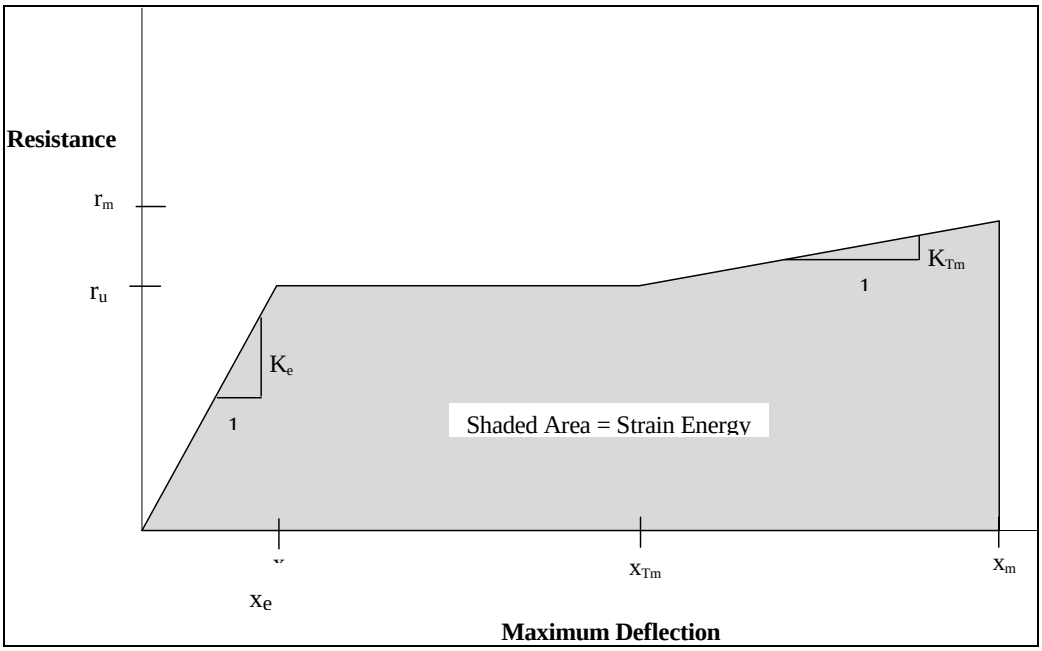

Figure 9. Typical Resistance-Deflection Curve for Component Response with Flexure and Tension Membrane Showing Strain Energy

$$Px_m = R_u\left(x_m - \frac{x_e}{2}\right) + x_{TM}{}^2\frac{K_{TM}}{2} \qquad Letx_{TM} = Cx_m \quad and \quad \frac{1}{L}\left(x_m - \frac{x_e}{2}\right) \approx \frac{x_m}{L}$$

$$\frac{P}{LR_u} = \frac{1}{L} + C^2\frac{x_m}{L}\frac{K_{TM}}{2R_u}$$

$$Pbar_{TM} = \left(\frac{P}{R_u} - 1\right)\frac{R_u}{K_{TM}L} = C^2\frac{x_m}{2L} \qquad for \quad \frac{R_u + K_{TM}\left(x_m - x_{TM}\right)}{R_u} > 1.27 \qquad otherwise\_only \quad flexural\_response$$

Equation 6

$$\frac{i^2}{2K_{LM}m} = R_u\left(x_m - \frac{x_e}{2}\right) + x_{TM}{}^2\frac{K_{TM}}{2} \qquad Let x_{TM} = Cx_m \quad and \quad \frac{1}{L}\left(x_m - \frac{x_e}{2}\right) \approx \frac{x_m}{L}$$

$$\frac{i^2}{2K_{LM}mLR_u} = \frac{x_m}{L} + \left(\frac{x_m}{L}\right)^2 C^2\frac{LK_{TM}}{2R_u}$$

This results in a compliated quadratic exp*ression for* $\frac{x_m}{L}$ *not appropriate for Ibar Therefore pattern* $Ibar_{TM}$ *after* $Pbar_{TM}$

$$Ibar_{TM} = \frac{i}{\sqrt{K_{LM}mLR_u}}\left(\frac{R_u}{LK_{TM}}\right)^A$$

Equation 7

where:

x_{TM} = deflection at beginning of tension membrane response (See Figure 9)
C = ratio of deflection at beginning of tension membrane to maximum deflection (C<=1)
K_{TM} = slope of plastic region of tension membrane response (See Figure 9)
A = factor determined by trial and error to cause nearly identical scaled tension membrane response in impulsive realm for different components
A=0.1 for components with R_u>0.6 psi, otherwise A=0.125

See Equation 4 and Equation 5 for definitions of other parameters

4.3 Pbar and Ibar Term Equations for Brittle Flexural Response and Arching from Axial Force of Unreinforced Masonry Walls

Unreinforced masonry components are assumed to respond in flexure up to the ultimate flexural capacity and then respond in a brittle mode where the only post-yield resistance is provided by the resisting moment from arching caused by axial load, including the wall self-weight above mid-span. The assumed response is summarized in Figure 10. Figure 11 shows the assumed resistance-deflection curve, where r_1 and r_2 are the initial yield and ultimate resistances in flexural response, respectively, and r_3 or R_A is the peak resistance from axial load arching calculated based on axial load and self-weight as shown in Equation 8. The resisting moment from the axial load has a moment arm equal to the wall thickness minus the wall deflection, as shown in Figure 10. Based on the very small yield deflections of typical unreinforced masonry walls, the moment arm for R_A, can be assumed equal to the wall thickness. The resistance is assumed to transition from flexural response to arching response with a negative stiffness equal to the flexural stiffness, as shown in Figure 11, because some finite stiffness value is needed for dynamic response calculation purposes. The elastic and elastic-plastic stiffnesses are typically much larger than the stiffnesses implied in Figure 11. The arching resistance from axial load decays to zero when the wall deflection equals the wall thickness. This assumed resistance-deflection relationship is largely based on the WAC computer program (Jones, 1989).

The strain energy is the area under the resistance-deflection curve in Figure 11. Typically the resistance from axial load arching (r_3, also referred to as R_A) is significantly less than that from flexure (r_2, also referred to as R_u), unless the axial load is in the range of at least 150 lb/in to 200 lb/in. Pbar and Ibar terms were derived for unreinforced masonry response as shown in Equation 9 using some simplifications to keep the terms from becoming too complex. The $Pbar_{URM}$ term is based primarily on the peak resistance from either axial load arching or flexure since response to long duration load is primarily dependent on the peak overall resistance. As the minimum resistance term approaches the value of the larger resistance term, $Pbar_{URM}$ is decreased by a numerically determined factor with a minimum value of 0.6 (i.e., C_p in Equation 9). C_p was determined numerically to cause equal $Pbar_{URM}$ values for blast loads calculated from SDOF analyses for masonry walls with the same support rotation, but different ratios of R_A/R_u. Note from the equation for C_p in Equation 9 that as R_A and R_u become more equal maximizing the relative amounts of strain energy from both response modes, a lower $Pbar_{URM}$ is calculated for a given peak pressure and maximum overall resistance implying lower predicted damage.

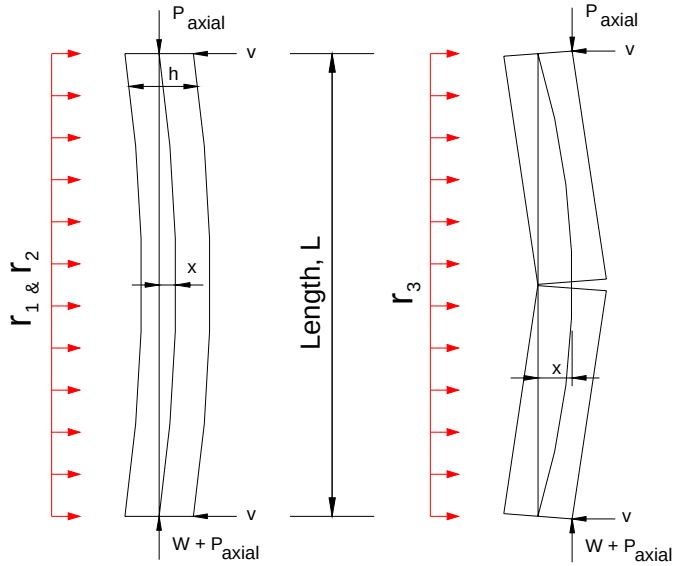

Response prior to ultimate flexural resistance, r_2 Response after r_2 where x= arching moment arm

Figure 10. Response of Brittle Unreinforced Masonry Wall Under Combined Lateral and Axial Load

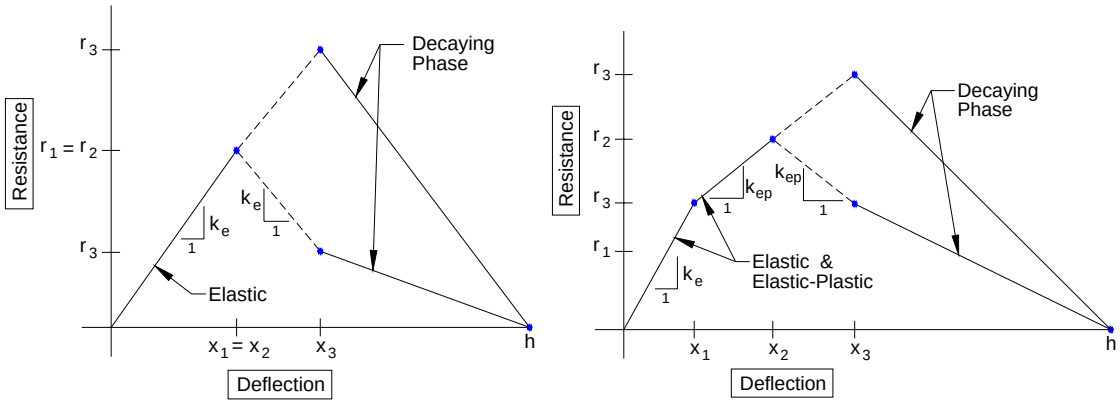

Determinate Component (Note $r_2=R_u$) Indeterminate Component

Figure 11. Resistance-Deflection Curves for Unreinforced Masonry with Brittle Flexural Response and Axial Load

$$r_3 = R_A = \frac{8}{L^2}(h - x_2)\left(P + \frac{WL}{2}\right)$$

Equation 8

where: r_3 = maximum resistance from axial load effects (also designated as R_A)
r_2 = ultimate flexural resistance (also designated as R_u)
x_3 = flexural deflection at $r_2 + (r_3 - r_2)/K_{ep}$
K_{ep} = elastic-plastic stiffness for indeterminate components, otherwise equal to elastic stiffness
x_2 = flexural yield deflection
h = overall wall thickness
P = input axial load per unit width along wall, P_{axial}
W = area self-weight of wall
L = wall height (assumed equal to minimum span of two-way components)

$$Px_m = R_u \frac{x_e}{2} + R_A x_m C_A \quad where \quad C_A \approx 0.5\left(\frac{h}{x_m} - 1 + \frac{x_m}{h}\right) for\_x_m >> x_e \quad where \quad \frac{x_m}{h} \le 1 and \quad C_A \le 0.5$$

$$P = R_u \frac{x_e}{2x_m} + R_A C_A \qquad \frac{P - R_A C_A}{R_u} = \frac{1}{2\mu}$$

$$Let \quad Pbar_{URM} = \frac{P}{R_{MAX}} C_P \quad where \quad R_{MAX} = Max(R_u, R_A) \quad C_P = -0.38R_F^{\,2} - 0.038R_F + 1 \quad R_F = \frac{Min(R_u, R_A)}{R_{MAX}}$$

$$\frac{i^2}{2K_{LM} m} = R_u\left(x_m - \frac{x_e}{2}\right) + R_A x_m C_A \qquad Let \quad \frac{1}{L}\left(x_m - \frac{x_e}{2}\right) \approx \frac{x_m}{L}$$

$$\frac{i^2}{K_{LM} mLR_u} = \frac{2x_m}{L}\left(1 - \frac{R_A C_A}{R_u}\right)$$

$$Ibar_{URM} = \frac{i}{\sqrt{K_{LM} mLR_u}}\left(\frac{R_u}{R_A}\right)^B \approx \sqrt{\frac{2x_m}{L}} \qquad where \quad B = -0.1$$

Equation 9

where: R_A= arching resistance from axial load acting through a moment arm based on the wall thickness minus the wall deflection at maximum flexural yielding (see Equation 8)
See Equation 4 and Equation 5 for definitions of other parameters

The exponent B in $Ibar_{URM}$ in Equation 9 was determined numerically in a similar manner as C_P, where a B value equal to -0.1 caused scaled P-i curves determined from SDOF analyses of walls with the same support rotation, but different ratios of R_A/R_u, to have nearly identical scaled blast loads in the impulse sensitive regions of the curves. Finally, it should be noted that the $Pbar_{URM}$ and $Ibar_{URM}$ terms in Equation 9 are based on maximum support rotation. Response controlled by maximum thickness to span ratio could also be assumed as the non-dimensional response term that correlates best to component damage, but the use of support rotation is considered acceptable and is more consistent with the non-dimensional response terms used for other component types.

4.4 Modifications to Pbar and Ibar Terms to Scale Negative Phase Load Effects

The Pbar and Ibar terms are used to "scale" a full range of blast loads on a full range of components that all cause a given non-dimensional response parameter (i.e., ductility ratio or support rotation) in SDOF analyses into a single scaled P-i curve of (Ibar, Pbar) points. The basic requirement for meaningful Pbar and Ibar terms, therefore, is that any two different components, subject to the restrictions below, will have nearly identical scaled P-i curves. Once such a scaled P-i curve has been constructed, it can be unscaled for any given component by dividing each Pbar points by Pbar/P and each Ibar point by Ibar/i by to determine an unscaled P-i curve for that component subject to the restrictions below.

1. The resistance-deflection curves for the two components have the same basic type of response that was assumed in the development the Pbar and Ibar terms (i.e., flexural response).

2. The two components have equal response in terms of the same non-dimensional response term used to develop the Pbar and Ibar terms (i.e., the same support rotation or ductility ratio).

3. The two components are subject to blast loads with identical shapes, including both positive and negative phase loading.

It has been shown that scaled P-i curves can be constructed for the basic case of response to a triangular shaped blast load with only positive phase load for response criteria expressed in terms of a ductility ratio (Baker et al, 1983). The Pbar and Ibar term derivations in Equation 4 and Equation 5 are therefore considered exact for this case. Also, the approximations involved in deriving Pbar and Ibar for the slightly more complicated case of positive phase loading with the non-dimensional response term equal to support rotation are minor as long as the support rotations correlate to ductility ratios greater than 3, as discussed previously. This ductility ratio requirement is not usually a problem for response levels more severe than HLOP. The Pbar and Ibar terms for cases involving strain energy from tension membrane and axial load arching response involve more significant approximations and assumptions, but they were derived to with numerically determined constants that are intended to minimize the effects of these approximations and assumptions. The error introduced into the scaling by these simplifications and assumptions in the Pbar and Ibar derivations is addressed in Section 7.0.

A major parameter not addressed to this point is the effect of the negative phase blast load. The derivation of all Pbar and Ibar terms has been only in terms of the positive phase peak pressure and impulse but these terms are intended for predicting component response to the entire blast load including the negative phase blast load. Including the negative phase blast load in SDOF analyses of component response causes the scaled P-i curve in the impulsive region, which corresponds to very short duration blast loads, to be a function of the scaled peak pressure rather than becoming asymptotic (i.e. independent of peak pressure) as it does for the case where only positive phase loading is considered. Test data indicates that this is a realistic behavior, as shown in Section 6.8 and Section 6.6. However, inclusion of negative phase blast load also violates requirement No. 3 above to some extent because the varying charge weight-standoff combinations needed to cause the same response level in components of varying resistance, mass, and stiffness generally cause blast loads that have somewhat different shapes from each other. Based on comparisons from SDOF analyses where charge weight-standoff combinations with short blast load durations were used to cause the same non-dimensional response term in different components, the blast wave shapes have differing ratios of the following parameters: positive phase to negative phase durations, the positive phase to negative phase impulses, and positive phase to negative phase peak pressures. The last parameter ratio is of least importance since the negative phase primarily affects component response only for cases where the blast load duration is so short that response is primarily a function of the blast load impulse.

A study of SDOF analyses that included negative phase loading was conducted to determine the effect of component resistance, stiffness, and mass on the resulting scaled P-i curves for ductile flexural response of a component with a ductility ratio of 4. The results are shown in Figure 12

through Figure 14, where the points are blast loads from the SDOF analyses scaled in terms of Pbar and Ibar from Equation 4 and Equation 5 and the curves are fit through the points using Equation 1.

The parameters A through G that cause Equation 1 to fit the scaled blast load points for each of the four analyzed cases in each figure are shown in the figures. The SDOF analyses considered a wide range of component resistance, stiffness, and mass, where each of these three parameters was changed independently of the others, as shown in Figure 12 through Figure 14. Ideally, a single scaled P-i curve would be calculated for all cases in Figure 12 through Figure 14 because the same non-dimensional response criteria equal to a ductility ratio of 4 was calculated for all scaled points of all cases. This is true (within some acceptable scatter) only for all the stiffness and mass combinations in Figure 13 and Figure 14. The differences in component resistance caused the curve-fits of the scaled blast loads from the SDOF analyses to change enough to so that they did not lie on top of each other, as shown in Figure 12. Therefore, this study indicates that blast loads causing a given constant response level in components with significantly different resistances can have different blast load shapes when the negative phase load is included, so that the simple Pbar and Ibar scaling terms that only include the positive phase peak pressure and impulse do not scale the blast loads into a single scaled P-i curve. However, similar differences in mass and stiffness do not cause as much of a change in the shapes of the blast loads causing a constant level of component response and there is relatively little scatter in scaled P-i curves that are based on scaling that only considers the positive phase peak pressure and impulse.

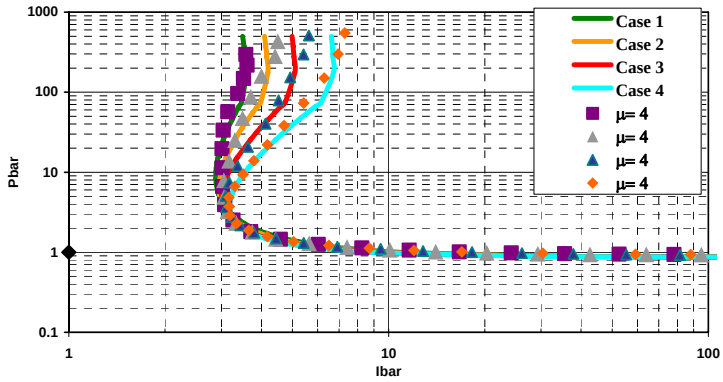

Case	mu	Ru (psi)	K (psi/in)	Mass (psi-ms^2/in)
1	4	20	5	1500
2	4	6	5	1500
3	4	2	5	1500
4	4	0.75	5	1500

Case	1	2	3	4
A	2.70	2.50	2.30	2.20
B	1.15	1.15	1.15	1.15
C	0.3	0.35	0.41	0.48
D	0.7	0.7	0.7	0.7
E	100	100	100	100
F	3.61	4.21	5.11	6.75
G	-0.3	-0.3	-0.3	-0.3

Figure 12. Effect of Ultimate Resistance on Scaled P-i Diagram with Ductility Level of 4

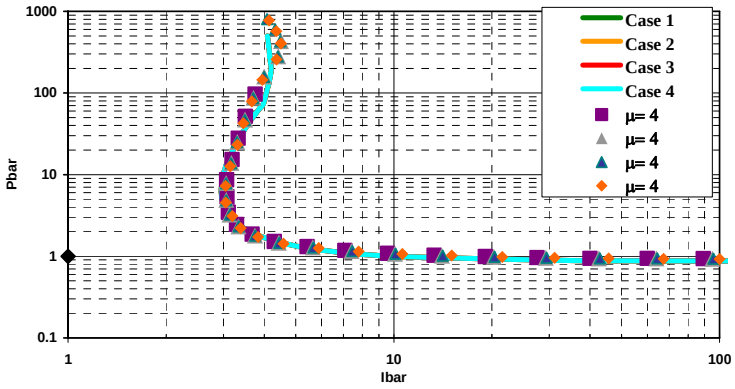

Case	mu	Ru (psi)	K (psi/in)	Mass (psi-ms^2/in)
1	4	6	50	1500
2	4	6	5	1500
3	4	6	1	1500
4	4	6	0.5	1500

Case	1	2	3	4
A	2.50	2.50	2.50	2.50
B	1.15	1.15	1.15	1.15
C	0.35	0.35	0.35	0.35
D	0.7	0.7	0.7	0.7
E	100	100	100	100
F	4.21	4.21	4.21	4.21
G	-0.3	-0.3	-0.3	-0.3

Figure 13. Effect of Stiffness on Scaled P-i Diagram with Ductility Level of 4

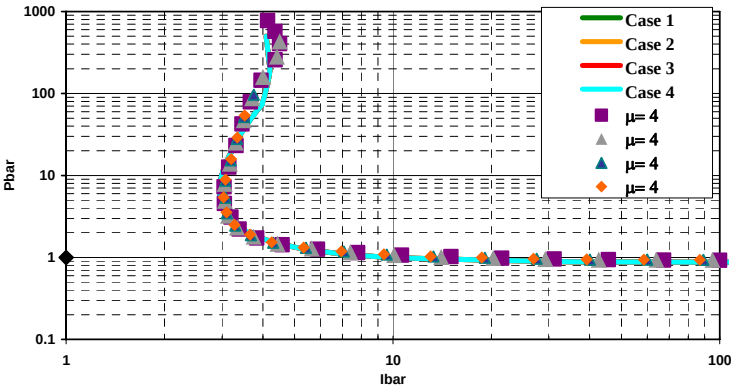

Case	mu	Ru (psi)	K (psi/in)	Mass (psi-ms^2/in)
1	4	6	5	15000
2	4	6	5	1500
3	4	6	5	150
4	4	6	5	70

Case	1	2	3	4
A	2.50	2.50	2.50	2.50
B	1.15	1.15	1.15	1.15
C	0.35	0.35	0.35	0.35
D	0.7	0.7	0.7	0.7
E	100	100	100	100
F	4.21	4.21	4.21	4.21
G	-0.3	-0.3	-0.3	-0.3

Figure 14. Effect of Mass on Scaled P-i Diagram with Ductility Level of 4

As shown in Figure 12, the scaled P-i curves vary in the impulsive realm, where the Pbar term is high relative to the Ibar term. This implies very short duration blast loads, which occur at smaller standoffs, are causing the response in this part of the P-i curve. At a given small standoff, a smaller charge weight is needed to cause a given ductility ratio in a low resistance component than in a high resistance component. The difference in load shape is that the smaller close-in charge tends to have a higher ratio of negative to positive phase impulse and a lower ratio of negative to positive phase load duration. The time to peak response does not seem to be very dependent on resistance. The end result is that the low resistance component gets a higher ratio of effective negative phase load compared to positive phase load within its response time to maximum deflection in the impulsive loading realm. The effect of the difference in resistance of a high and low resistance component is accounted for in the Pbar and Ibar scaling terms, but not the effect of a higher ratio of negative phase to positive phase impulse. Therefore, there is a larger "layover" effect in the impulse asymptote of the scaled P-i curve for low resistance components, as seen in Figure 12.

A "first principles" type approach was tried initially to correct this problem, where a net impulse up to the time of maximum response was used in the Ibar term rather than only the positive phase impulse. The net impulse included both positive phase impulse and the portion of the

negative phase impulse occurring prior to the time of peak response. This would presumably account for different ratios of negative to positive phase blast load impulse for high and low resistance components and therefore "scale" this effect. This did not work well, however, probably because the effect of applied impulse on response prior to the time of peak response is not a simple linear relationship. The times at which differing proportional amounts of impulse are applied during component response up to the time of peak response is as important as the overall net impulse that is applied.

Rather than trying to go further with first principles approaches that could possibly get quite complex, a numerical approach was developed. The effect of resistance on the curve-fitting parameters for Equation 1, as shown in Figure 12, was determined mathematically and this effect was built into the Ibar term so that the effect of resistance on the scaled P-i curves could be accounted for, or scaled, within the Ibar term. The resulting Ibar terms are shown in Equation 10 where Rbar is the ratio of the component resistance to the atmospheric pressure at standard sea-level atmospheric conditions. Therefore, Rbar is the component resistance in dimensionless units of atmospheres. The Pbar term is unchanged. Note that Pbar is used within the Ibar calculation since the effect of resistance on the shapes of the P-i curves in Figure 12 increases with Pbar. Figure 15 shows the same scaled P-i curves from Figure 12 plotted in terms of Ibar1 in Equation 10 with the correction factor Y. Similar results were achieved for components with different resistances at different ductility ratios and for cases where the Pbar and Ibar terms were derived based on maximum response in terms of support rotation. As shown in Figure 15, the correction factor does a good job except at very high Pbar values. These very high Pbar values typically correspond to very close-in scaled standoffs where other response modes, such as spalling and localized shear behavior can predominate, and the blast loading over the full component area is very non-uniform.

A similar approach was used to derive a different Y value to account for the effect of component resistance on the shape of the scaled P-i curves for components with tension membrane, where the $Ibar_{TM}$ term in Equation 7 is multiplied by the Y_{TM} term for tension membrane in Equation 10. Pbar is equal to $Pbar_{TM}$ from Equation 7 for this case. See Equation 10 for final Pbar and Ibar scaling equations for different response modes and non-dimensional response parameters considered in CEDAW. The Pbar and Ibar equations in Equation 10 are used in the CEDAW spreadsheet and were used to determine all the scaled P-i curves shown in Section 6.0, Section 7.0, and the appendices of this report.

See Equation 4 through Equation 9 for definition of terms and information on derivation of equations

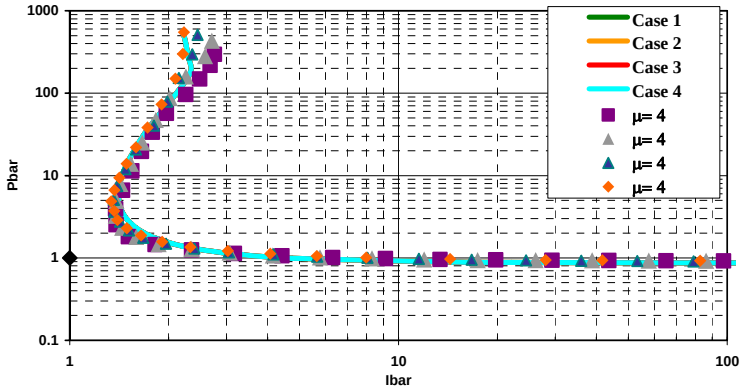

Case	mu	Ru (psi)	K (psi/in)	Mass (psi-ms^2/in)
1	4	20	5	1500
2	4	6	5	1500
3	4	2	5	1500
4	4	0.75	5	1500

Case	1	2	3	4
A	1.15	1.15	1.15	1.15
B	1.15	1.15	1.15	1.15
C	0.37	0.37	0.37	0.37
D	0.7	0.7	0.7	0.7
E	150	150	150	150
F	2.33	2.33	2.33	2.33
G	-0.3	-0.3	-0.3	-0.3

Figure 15. Scaled P-i Diagram with Modified Ibar Term for Multiple Resistances with Ductility of 4

$$Pbar1 = \frac{P}{R_u} \quad for \quad ductlity \quad and \quad \sup port \quad rotation \quad criteria$$

$$Pbar_{URM} = \frac{P}{R_{MAX}} C_p \quad for \quad unre\inf .masonry \quad with \quad \sup port \quad rotation$$

$$Pbar_{TM} = \left(\frac{P}{R_u} - 1\right)\frac{R_u}{K_{TM} L} \quad for \quad tension \quad membrane \quad with \quad \sup port \quad rotation$$

$$Ibar_{COL} = \frac{i}{R_u}\sqrt{\frac{K}{K_{LM} m}} \quad for \quad column \quad shear\_and \quad connection \quad response$$

$$Ibar1 = \frac{i}{R_u}\sqrt{\frac{K}{K_{LM} m}} Y \quad for \quad ductility \quad criteria$$

$$Ibar2 = i\sqrt{\frac{1}{K_{LM} m R_u L}} Y \quad for \quad \sup port\_rotation \quad criteria$$

$$Ibar_{TM} = \frac{i}{\sqrt{K_{LM} m L R_u}}\left(\frac{R_u}{L K_{TM}}\right)^A Y_{TM} \quad for \quad tension \quad membrane \quad with \quad \sup port \quad rotation$$

$$Ibar_{URM} = \frac{i}{\sqrt{K_{LM} m L R_u}}\left(\frac{R_u}{R_A}\right)^B Y \quad for \quad unre\inf . \quad masonry \quad with \quad \sup port \quad rotation$$

$$Y = \frac{Pbar^{\left(0.5-0.39 Rbar^{-0.127}\right)}}{2.59 Rbar^{0.067}} \quad for \quad no \quad tension\_membrane\_cases \quad except \quad columns \quad in \quad shear$$

$$Y_{TM} = \frac{Pbar_{TM}^{\left(0.5-0.19 Rbar^{-0.28}\right)}}{1.32 Rbar^{0.058}} \quad for \quad tension\_membrane$$

$$Rbar = \frac{R_u}{P_a} \quad where \quad P_a = s\tan dard \quad atmospheric \quad pressure$$

$$Y = 1 \quad for \quad columns\_responding\_in\_shear \quad including \quad connection\_failure$$

Equation 10

5.0 COMPONENT LEVELS OF PROTECTION (LOP)

The Pbar and Ibar equations described in the previous section can be used to create scaled P-i curves representing maximum response in terms of any given value of ductility ratio or support rotation for a component with a given assumed response mode. From a practical viewpoint, it is beneficial to the PDC to have specific scaled P-i curves defined for each component type that correspond to the ductility ratio or support rotation that cause the upper and lower bounds of each level of protection (LOP) to building occupants and assets contained in the building because these P-i curves can be used to determine the LOP for a given blast load and component. This can be achieved to a large extent using blast test data that has known applied blast loads, component properties, and response in terms of LOP, as discussed in Section 6.0. However, the test data is typically expressed in terms of maximum deflection, observed damage, and/or photographs. It is not typically directly described by the test researchers in terms of LOP. The observed response of test data must be translated into a LOP based on descriptions of the component response corresponding to each LOP.

The DoD has defined LOP in terms of overall building structural damage, as shown in Table 1 (UFC, 2003). However, there are no DoD LOP definitions specific to given component types. This is problematic since the CEDAW workbooks are intended to determine the LOP for input components. Therefore, component LOP definitions were developed as shown in Table 1 so that available blast test data could be categorized into LOP levels based on the observed response and used in Section 6.0 to help determine the ductility ratio or support rotation that cause the upper and lower bounds of each level of protection (LOP). Table 1 shows the level "Below AT Standards" that is not a DoD LOP. This response level represents "blowout" type structural failure, where the component is overwhelmed by the blast so that its debris is thrown with enough velocity to travel across the width of a typical room (i.e. approximately 15 ft). This structural response realm, which is more severe of the lowest LOP, can be useful when predicting the extent of severe injuries to room occupants. The building LOP information is shown in Table 1 for reference purposes only. Components at each LOP do not necessarily cause the overall building to have the same LOP. A separate correlation between component LOP and building LOP based in part on component type (i.e., is the component a cladding component or a primary framing component) is necessary, but this correlation is outside the scope of this report.

The CEDAW workbook can be used to determine the LOP provided for a given input component and charge weight-standoff combination. The acceptable LOP for the component must be determined separately by the CEDAW user based on the amount of protection the component needs to provide to building occupants and assets and a consideration of how the component response affects the response of any attached components. Typically, first floor bearing wall components with a very low LOP will have enough damage to cause collapse of the roof or floors above and therefore affect the LOP of building occupants and assets over a much larger area of the building than a similar non-load bearing wall.

This logic is also generally true, although to a lesser extent, for any failed roof framing components, such as roof girders, that can cause failure of attached secondary components, such as purlins or cladding. However, from a practical perspective, cladding components and even

secondary framing components typically fail at blast loads much less than those needed to fail primary framing components. The lower strength and failure of these components often limits the blast load actually transferred into primary framing components, which is not accounted for in CEDAW. Therefore, the response of cladding components generally controls the LOP provided to building occupants and assets except in the case where a very low LOP occurs for a load-bearing wall or column causing significant progressive collapse. Columns are analyzed in CEDAW only to determine whether they have a LOP less than VLLOP. This is equivalent to determining whether the column fails or not. Column response is only of practical importance for the case of column failure and associated progressive collapse, since lesser column damage may only potentially affect the very small percentage of building occupants and assets in the floor space directly behind the column. The analysis of column response is discussed in more detail in Section 6.10 through Section 6.12.

Table 1. DoD Level of Protection (LOP) Descriptions

Level of Protection	Potential Overall Structural Damage [1]	Component Damage[2]
Below AT standards [3] (Blowout)	Severely damaged. Frame collapse/massive destruction. Little left standing.	The component is overwhelmed by the blast load causing failure and debris with significant velocities
Very Low (VLLOP)	Heavily damaged - onset of structural collapse: Major deformation of primary and secondary structural members, but progressive collapse is unlikely. Collapse of non-structural elements.	A portion of the component has failed, but there are no significant debris velocities.
Low (LLOP)	Building is damaged beyond repair. Major deformation of non-structural elements and secondary structural members and minor deformation of primary structural members, but progressive collapse is unlikely.	The component has not failed, but it has significant permanent deflections causing it to be unrepairable. The component is not expected to withstand the same blast load again without failing.
Medium (MLOP)	Building is damaged, but repairable. Minor deformations of non-structural elements and secondary structural members and no permanent deformation in primary structural members.	The component has some permanent deflection. It is generally repairable, if necessary, although replacement may be more economical and aesthetic. The component is expected to withstand the same blast load again without failing.
High (HLOP)	Superficially damaged. No permanent deformation of primary and secondary structural members or non-structural elements.	No visible permanent damage

Note 1: Department of Defense definition in terms of overall building damage. Shown only for reference.
Note 2: Definitions developed for CEDAW components. Components at each LOP do not necessarily cause the overall building to have the same LOP. A separate correlation between component LOP and building LOP based in part on component type is necessary, but is outside scope of this report.
Note 3: This is not an official level of protection. It only defines a realm of more severe structural response that can provide additional useful information in some cases.

6.0 SCALED P-I CURVES FOR EACH COMPONENT TYPE

Scaled P-i curves were developed for each component type listed in Table 2, as described in this section, based on available test data and results from SDOF analyses that were scaled with Pbar and Ibar terms that were based on the applicable non-dimensional response parameter(s) and response mode for the component type. The applicable non-dimensional response parameter(s) (i.e. support rotation or ductility ratio) and response mode (i.e. flexure, flexure and tension membrane, arching) for each component type were assumed as shown in Table 2 based on the applicable response modes and response criteria parameters in established guidelines such as TM 5-1300, ASCE, and response limits criteria from the PDC, as well as a review of the available test data. In all cases except for column components, for HLOP response level was assumed to occur in flexural response at a ductility level of 1.0, as required by the PDC based on their definition of the HLOP response level. For column components, only the boundary between LLOP and VLLOP is defined in CEDAW, corresponding to column failure. When more than one type of response parameter is applicable for a given LOP, the CEDAW workbook plots the P-i curve that causes the LOP to occur at the lowest blast loads. Table 2 also shows the Pbar and Ibar terms from Equation 10 that were used to scale the test data and SDOF analyses results for each component type. In all cases, Pbar1 and Ibar1 from Equation 10 were used to create the scaled P-i curves for HLOP response, since this response level is always assumed to occur at a ductility level of 1.0.

SDOF calculations were performed for each component type to determine the blast loads from charge weight and standoff combinations with varying load durations that caused given response levels, in terms of the applicable non-dimensional response term, to representative components responding in the applicable response mode. The positive phase impulse, peak pressure, and component dynamic response properties from these analyses were used to calculate Pbar and Ibar terms for each given response criteria level, using the applicable Pbar and Ibar equations, and the (Ibar, Pbar) combinations for each blast load were plotted to form scaled P-i curves.

The resistance-deflection relationships in the SDOF analyses were consistent with the response modes in Table 2, along with 2% of critical damping. The representative components had typical properties for each component type, but the exact values of the component properties was not considered critical because the Pbar and Ibar scaling terms generalized the results of the SDOF analyses to be independent of the component properties and geometry. The blast loads in the SDOF analyses, which included both positive and negative phase loading, were generated by starting with a very small standoff, typically 5 ft, and then increasing the standoff at given intervals and determining the TNT charge weight at each standoff that caused the desired response with a goal-searching algorithm. These charge weight-standoff combinations caused blast loads with a full range of load durations that produced the given response criteria. Curve-fits from TM 5-1300 (1990) for fully reflected surface burst explosions were used to get positive and negative phase peak pressures and impulses and the positive blast load duration, which defined the beginning of the negative phase load, for each charge weight-standoff combination. The blast load shapes were idealized as linear pressure histories that preserved the positive and negative phase impulse and the beginning time of the negative phase blast loading, as illustrated in Figure 16. The assumed blast load shape had a peak negative phase pressure at the quarter

point of the negative phase duration. Equation 1 or Equation 3 were used to curve-fit the Pbar and Ibar points calculated from the blast loads causing each response level and create the actual scaled P-i curves from the SDOF analyses.

Table 2. Response Modes, Response Parameter Types, and Pbar and Ibar Terms for Each Component Type in CEDAW

Component Type	Type of Response Parameter	Response Mode	Pbar and Ibar Terms from Equation 10
Reinforced masonry spanning 1-way [2]	Ductility ratio[1], support rotation	Elastic-perfectly plastic flexural response	Pbar1, Ibar1[1], Ibar2
Unreinforced masonry spanning 1-way and 2-way [2]		Brittle elastic response and arching based on axial self-weight	Pbar1[1], Ibar1[1], $Pbar_{URM}$,$Ibar_{URM}$
Reinfored concrete slab spanning 1-way or 2-way		Elastic-perfectly plastic flexural response	Pbar1, Ibar1[1], Ibar2
Reinfored concrete beam			
Reinfored concrete column	Ductility ratio	Shear response	Pbar1[3], $Ibar_{COL}$[3]
Hot rolled steel beam	Ductility ratio, support rotation	Elastic-perfectly plastic flexural response	Pbar1, Ibar1, Ibar2
Open web steel joist	Ductility ratio[1], support rotation	Elastic-perfectly plastic flexural response with or without tension membrane	Pbar1, Ibar1[1], Ibar2, Pbar $Pbar_{TM}$,$Ibar_{TM}$
Steel column	Ductility ratio	Connection shear response	Pbar1[4], Ibar[4]
	Ductility ratio, support rotation	Elastic-perfectly plastic flexural response	Pbar1, Ibar1, Ibar2
Cold-formed steel girts and purlins	Ductility ratio, support rotation	Elastic-perfectly plastic flexural response with or without tension membrane	Pbar1, Ibar1, Ibar2, $Pbar_{TM}$,$Ibar_{TM}$
Cold-formed metal stud wall	Ductility ratio	Elastic-perfectly plastic flexural response with and without top connection	Pbar1, Ibar1
Corrugated steel panels and Standing seam steel panels	Ductility ratio, support rotation	Elastic-perfectly plastic flexural response	Pbar1, Ibar1, Ibar2,
Wood beam	Ductility ratio	Elastic-perfectly plastic flexural response	Pbar1, Ibar1

Note 1: Used only for HLOP
Note 2: Masonry components include Brick, CMU, and European Clay Tile in single walls or cavity walls
Note 3: Ultimate resistance in Pbar and Ibar terms using ultimate shear resistance rather than flexural resistance, where the shear capacity includes the dynamic concrete shear strength and shear strength of any closely spaced steel ties. See Section 6.10 for CEDAW equation for ultimate resistance based on shear capacity.
Note 4: Ultimate resistance in Pbar and Ibar terms using ultimate connection shear resistance rather than flexural resistance, where the shear capacity is based on ultimate shear strength of bolted connections. See Section 6.11 for CEDAW equation for ultimate resistance based on connection capacity.

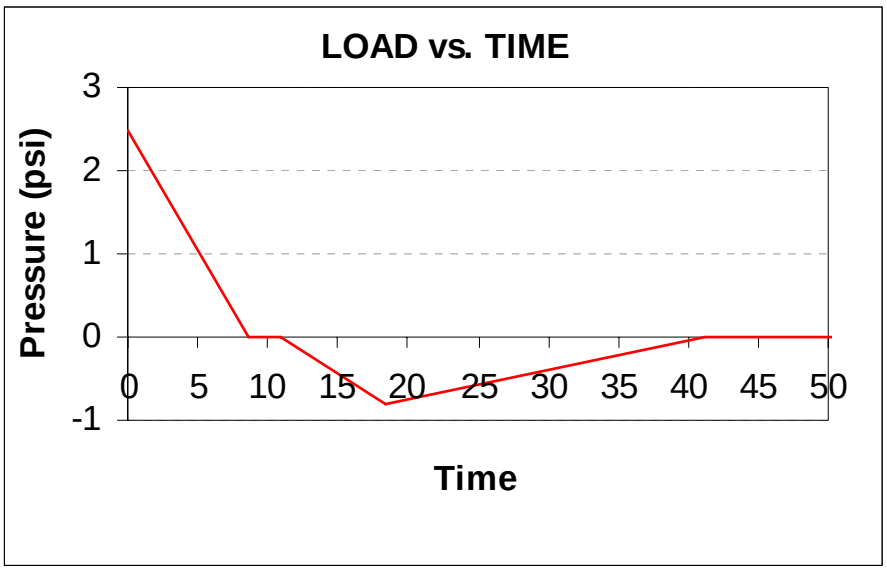

Figure 16. Typical SDOF Analysis Blast Load

Values of the applicable non-dimensional response parameters (i.e. ductility ratio and/or support rotation values) used in the SDOF analyses to create scaled P-i curves that bounded each LOP response level for each component type were determined separately for each LOP and component type using trial and error so that the scaled P-i curves were as consistent as possible with available component test data scaled with the applicable Pbar and Ibar terms (i.e., the same Pbar and Ibar terms used to scale the blast loads from the SDOF analyses). All test data was also assigned an LOP based on the component LOP definitions in Table 1. For some component types without much available data, the values of the applicable non-dimensional response parameters used in the SDOF analyses to create scaled P-i curves bounding each LOP response level were based on other published blast response, damage, and design criteria considering the LOP definitions in Table 1. The values of the non-dimensional response parameters that cause scaled P-i curves bounding each LOP response level for each component type are referred to as response criteria. The process of determining the response criteria for each component type and LOP is discussed in more detail throughout this section.

Table 3 summarizes the response criteria selected for each LOP and component type. Response criteria in the grey cells were assumed due to a lack of available test data. The response criteria for HLOP for all component types is assumed equal to a ductility ratio of 1.0, as required by the U.S. Army Corps of Engineers. In all other cases, response criteria are based on available data as described in Sections 6.1 through 6.12. Column components in Table 3 only have response criteria for the upper bound of LLOP as discussed in Section 6.10 and 6.11. Scaled P-i curves based on the response criteria in Table 3 for all LOP of the applicable component type are "unscaled" for an input component by the CEDAW workbook and displayed to allow the user to visually determine the component LOP for an input charge weight-standoff combination, as described in Section 2.0.

Table 3. Response Parameter Criteria for Upper Bound P-i Curves for Each LOP and CEDAW Component Type

Component	Ductility Ratio [3]				Support Rotation [3]			Support Rotation w/ Tension Membrane [1,3]		
	HLOP	MLOP	LLOP	VLLOP	MLOP	LLOP	VLLOP	MLOP	LLOP	VLLOP
One-Way Corrugated Metal Panel	**1**	3	6	12	3	6	10			
Hot Rolled Steel Beam	**1**	***3***	***12***	***25***	***3***	***10***	***20***			
Cold-Formed Girt and Purlins [2]	**1**				***3***	***10***	***20***	4	12	20
Metal Studs Connected Top and Bottom	***0.5***	***1***	***2***	***3***						
Metal Stud Wall Not Connected at Top	***0.5***	***0.8***	***0.9***	***1***						
Open-Web Steel Joist [2]	**1**				3	6	10	3	6	10
One-Way or Two-Way Reinforced Concrete Slab	**1**				2	5	10			
Reinforced Concrete Beam	**1**				2	5	10			
One-Way Reinforced Masonry	**1**				2	8	15			
One-Way or Two-Way Unreinforced Masonry	**1**				1.5	4	From data w/o SDOF			
Wood Stud Wall	**1**	2	3	4						
Reinforced Concrete Column (shear failure)			6							
Steel Column (connection failure)			1							
Steel Column (flexural failure)			***4***			***6***				

Note 1: Tension membrane only used in CEDAW when maximum resistance with tension membrane at given support rotation limits is more than 1.27 times ultimate flexural resistance.
Note 2: Support rotation values with tension membrane are used for cold-formed girts/ purlins and open web steel joists except when tension membrane resistance is too low according to Note 1. Even though CEDAW does not explicitly consider tension membrane in this case, limited tension membrane is assumed to allow relatively large support rotations shown in the table.
Note 3: Bold numbers indicate response criteria based on definition of HLOP with an upper bound ductility ratio of 1.0. Bold, shaded numbers indicate component types with a lack of blast data where CEDAW response criteria is based on other available response criteria that is interpreted and used based on LOP component definitions in Table 1. In all other cases, response criteria are based on data. See Sections 6.1 through 6.12 for discussion of response criteria for each component type.

6.1 P-i Curves for Corrugated Steel Panels

Figure 17 and Figure 18 show the scaled P-i curves in CEDAW for corrugated steel panels for all applicable response modes and response parameter types in Table 2. These figures show the scaled P-i curve-fits using Equation 1 to Pbar and Ibar points calculated with applicable Pbar and Ibar equations for each response mode and response parameter type, as indicated in Table 2, from SDOF analyses with response parameter values shown in the figures and in Table 3. The values for each of the curve-fitting parameters in Equation 1 for each curve are shown in Appendix M.

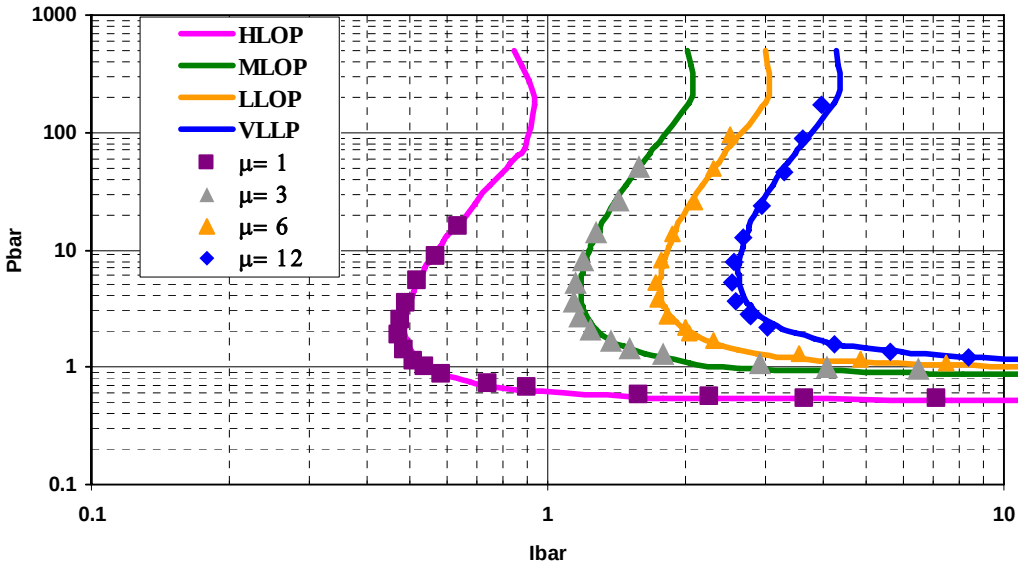

Figure 17. Scaled P-i Curves-fits vs. Scaled SDOF Points in Terms of Ductility Ratio for Flexural Response of Corrugated Steel Panels without Significant Tension Membrane

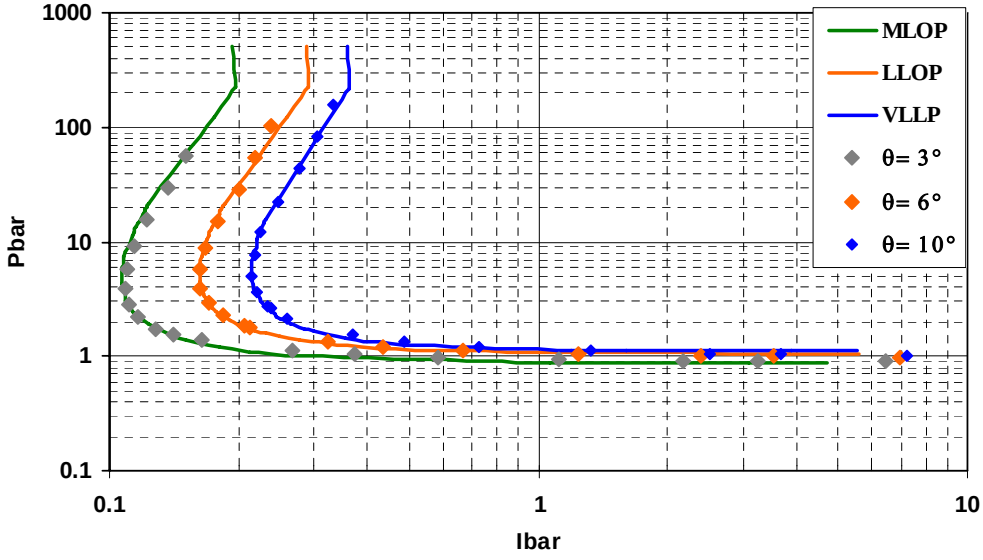

Figure 18. Scaled P-i Curves-fits vs. Scaled SDOF Points in Terms of Support Rotation for Flexural Response of Corrugated Steel Panels without Significant Tension Membrane

Figure 19 and Figure 20 show data scaled using the same Pbar and Ibar equations compared to the applicable scaled P-i curve-fits in CEDAW from Figure 17 and Figure 18. The scaled data for each LOP should ideally fall between the upper bound curve for the given LOP and the next curve below and to the left. The scaled data is conservative if it lies above or to the right of the upper bound curve for the given LOP. The data is primarily from testing on two-span continuous full-scale steel panels ranging from light 24 gauge panels to heavy 3-inch deep, 20 gauge panels with spans between 4 and 6 ft. Most of the tests were on corrugated steel panels attached to supporting members with self-tapping screws, but the data includes several standing seam panels and insulated steel panels. Most of the data is from a test series conducted for the U.S. Army by ARRADCOM in support of the development of TM 5-1300 for panels supported on rigid frames. The data also includes shock tube testing of panels supported by lightweight girts, and data from a DoD test series on a full-scale pre-engineered building. See Appendix G for detailed test data information and test data references.

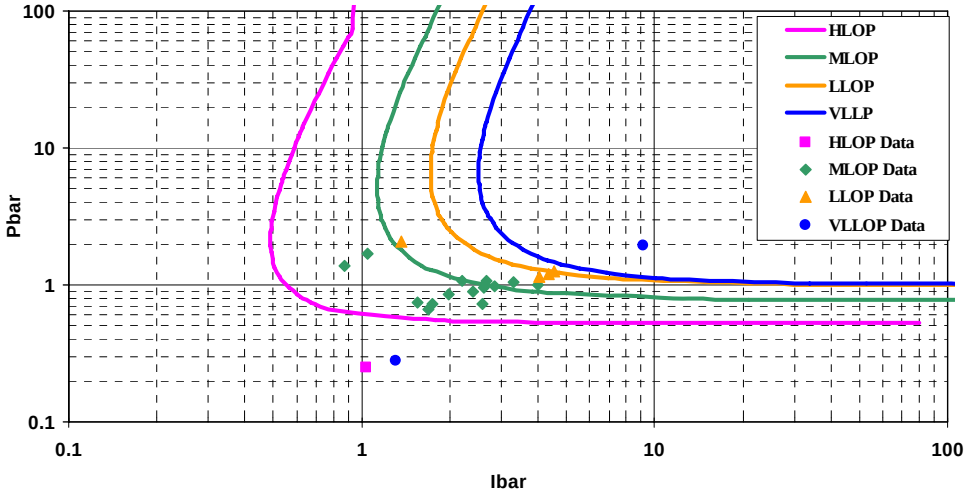

Figure 19. Scaled P-i Curves in Terms of Ductility Ratio vs. Scaled Data for Flexural Response of Corrugated Steel Panels without Significant Tension Membrane

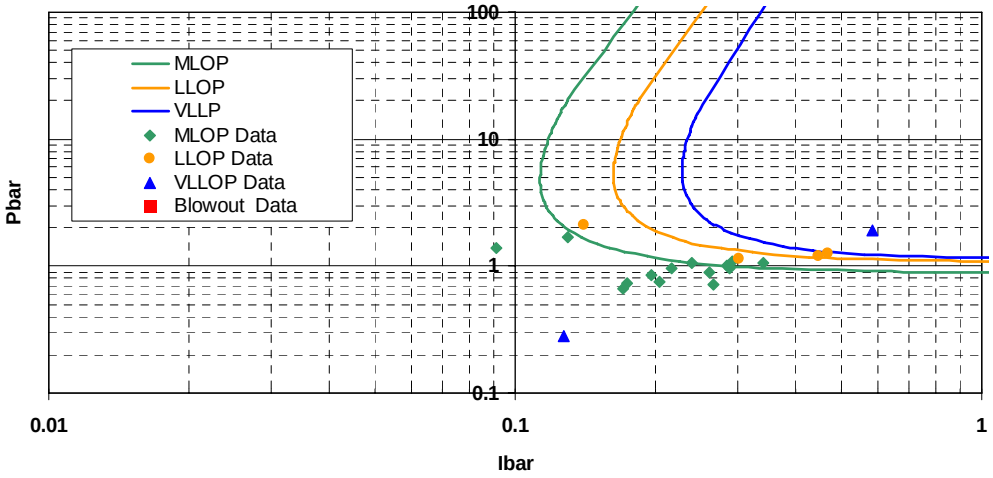

Figure 20. Scaled P-i Curves in Terms of Support Rotation vs. Scaled Data for Flexural Response of Corrugated Steel Panels without Significant Tension Membrane

Figure 21 shows a scaled P-i diagram using $Pbar_{TM}$ and $Ibar_{TM}$ from Equation 10. The scaled curves are from SDOF analyses with tension membrane and the support rotations shown in the figure. The resistance-deflection relationship was as shown in Figure 9 with x_{TM} at 2 degrees support rotation. The scaled data points using $Pbar_{TM}$ and $Ibar_{TM}$ are from test panels assumed to have significant tension membrane response based on a the screw spacing of 6 inches or less and girts with strengthened in-plane bending resistance. The maximum tension membrane force was assumed equal to the lesser of the ultimate shear capacity of the screws or the bearing capacity of the surrounding panel material. The data is from a test series conducted in the BakerRisk shock tube on panels supported by a strengthened top girt, or eave girt, and floor connection that supplied much more in-plane support to the panels than would be provided in a typical pre-engineered building.

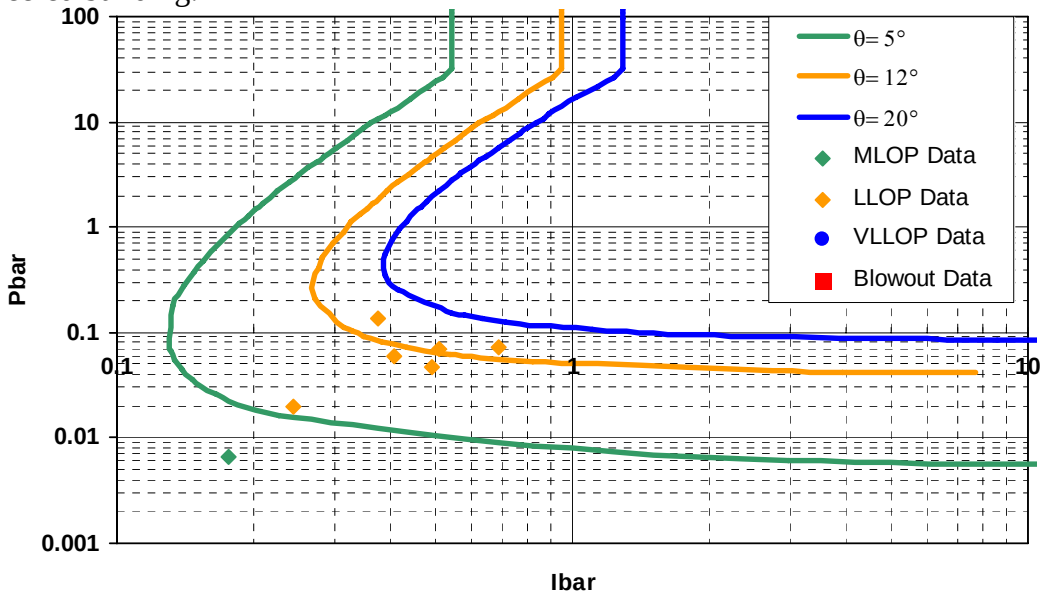

Figure 21. Scaled P-i Curves in Terms of Support Rotation vs. Scaled Data for Flexural Response of Corrugated Steel Panels with Significant Tension Membrane

Photographs of the tests in Figure 21 showed that panels without oversized washers failed by tearing away around the screws, indicating that the panels went into significant tension membrane response and the tension capacity was controlled by the connections. The data in Figure 21 was originally plotted on Figure 20, but it plotted in very low LOP regions relative to the observed LOP from the tests indicating significant tension membrane was present that was not accounted for in a scaled P-i diagram that only accounted for flexural response. The capacity to analyze corrugated metal panels with tension membrane is not included in CEDAW because eave struts with large in-plane flexural capacity compared to typical construction are necessary to develop significant tension membrane in the panels.

6.2 P-i Curves for Cold-Formed Girts and Purlins With Significant Tension Membrane

Figure 22 shows the scaled P-i curves in CEDAW for combined flexure and tensile membrane response of cold-formed girts and purlins in terms of support rotation for all LOP except HLOP, which is based on a ductility ratio of 1.0 in flexure. The scaled P-i curve for flexural response with a ductility of 1.0 is the same for all component types and is shown in Figure 17. Figure 22

shows the scaled P-i curve-fits using Equation 1 to Pbar and Ibar points calculated with applicable Pbar and Ibar equations shown in Table 2 from SDOF analyses for response parameter values shown in the figure and in Table 3 for MLOP through VLLOP response. These are the scaled P-i curves used for this component type and these LOP in CEDAW. The values for each of the curve-fitting parameters in Equation 1 for each curve in Figure 22 are shown in Appendix M. Figure 23 shows data scaled using the same Pbar and Ibar equations compared to the CEDAW scaled P-i curve-fits in Figure 22. The scaled data for each LOP should ideally fall between the upper bound curve for the given LOP and the next curve below and to the left. The scaled data is conservative if it lies above or to the right of the upper bound curve for the given LOP.

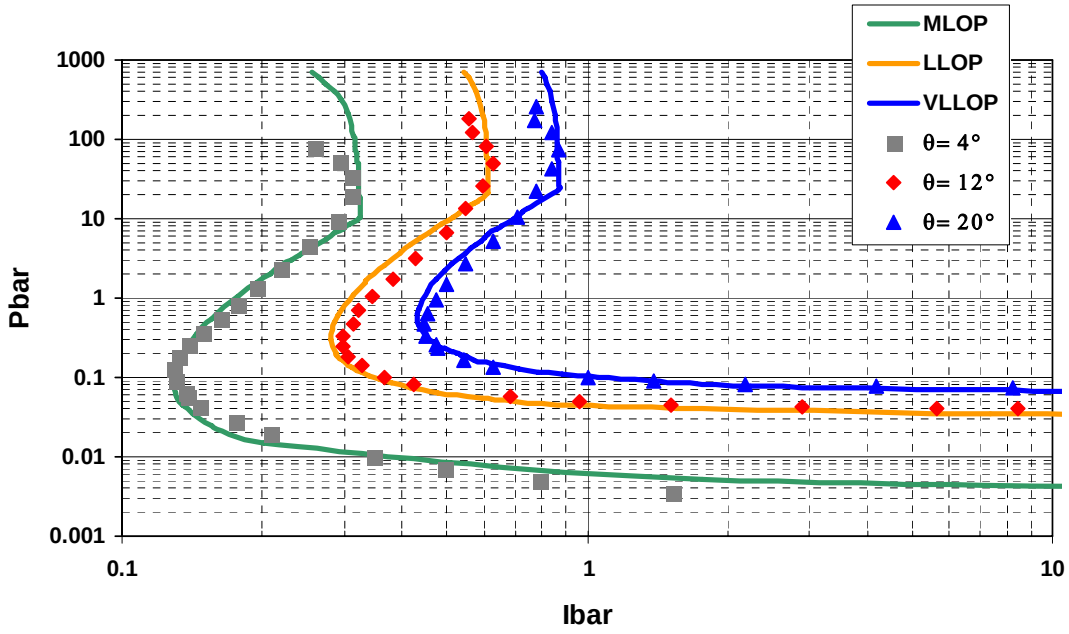

Figure 22. Scaled P-i Curves-fits vs. Scaled SDOF Points in Terms of Support Rotation for Flexural Response of Cold-Formed Girts with Significant Tension Membrane

The data in Figure 23 is from testing on full-scale, half-scale, and quarter-scale cold-formed steel girts, where full-scale represents approximately an 8-inch deep girt with a 3-inch flange width and a material thickness in the range of 0.06 to 0.105 inches (16 gauge to 12 gauge) with spans of 16 ft to 25 ft. Girts were assumed to have tension membrane equal to the lesser of the ultimate shear capacity of the bolts, the bearing capacity of the surrounding girt material, or the tensile capacity of the cross section. The data is from half-scale shock tube wall panel tests conducted by BakerRisk, quarter-scale tests conducted with high explosive on wall panels in the UK, several U.S. government test series on whole pre-engineered buildings, and two U.S. government test series where closely spaced, full-scale vertical steel girts were bolted to a supporting frame to develop the full tensile capacity of the cross section and subjected to high explosive loads. In all the tests except those with vertical girts, the girts supported typical corrugated steel panels. See Appendix E for detailed test data information and test data references.

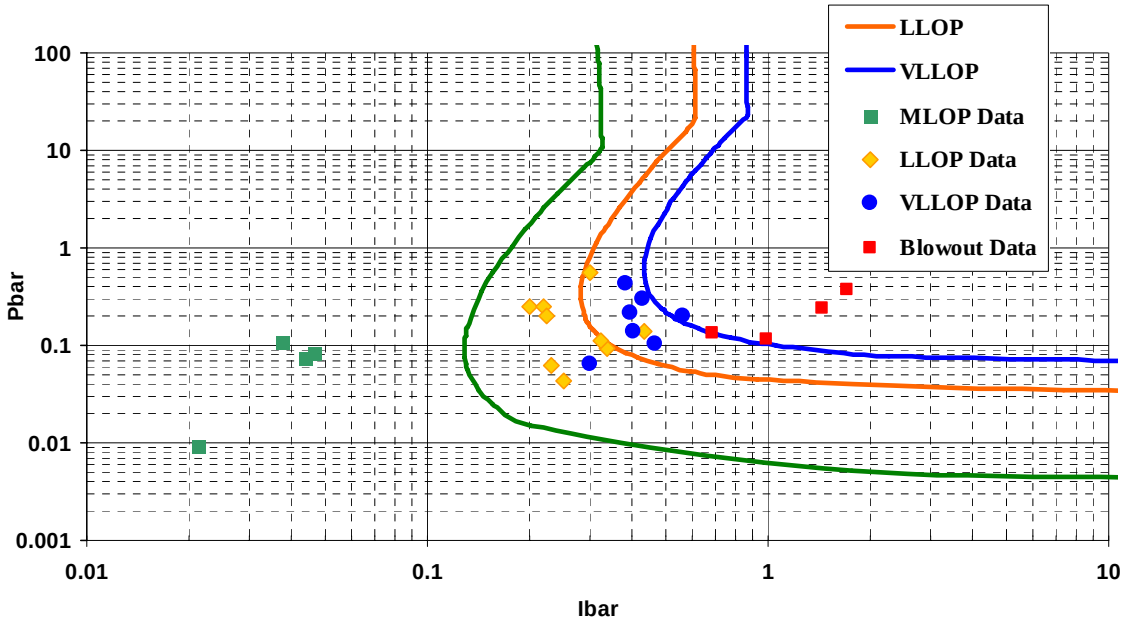

Figure 23. Scaled P-i Curves in Terms of Support Rotation vs. Scaled Data for Flexural Response of Cold-Formed Girts with Significant Tension Membrane

6.3 P-i Curves for Steel Beams and Cold-Formed Girts and Purlins Without Significant Tension Membrane

Figure 24 and Figure 25 show the scaled P-i curves in CEDAW for ductile flexural response of steel beams in terms of the response parameter types shown for this component in Table 2. These figures show the scaled P-i curve-fits using Equation 1 to Pbar and Ibar points calculated with applicable Pbar and Ibar equations, as indicated in Table 2, from SDOF analyses with the response parameter values shown in the figures and in Table 3. The values for each of the curve-fitting parameters in Equation 1 for each curve are shown in Appendix M.

There was no available data for ductile flexural response of steel beams without tension membrane. All the available steel beam data was for light, cold-formed beams that were attached to steel framing. Response criteria for steel beams without tension membrane are available in *Design of Blast Resistant Buildings in Petrochemical Facilities* (ASCE, 1997) and *Structural Design for Physical Security* (ASCE, 1999). The ASCE blast design criteria for Low, Medium, and High response levels and the ASCE physical security criteria for Light, Medium, and Severe damage are shown in Table 4. The definitions for blast design response levels are shown Table 5. There is no such available stated description of the physical security damage levels.

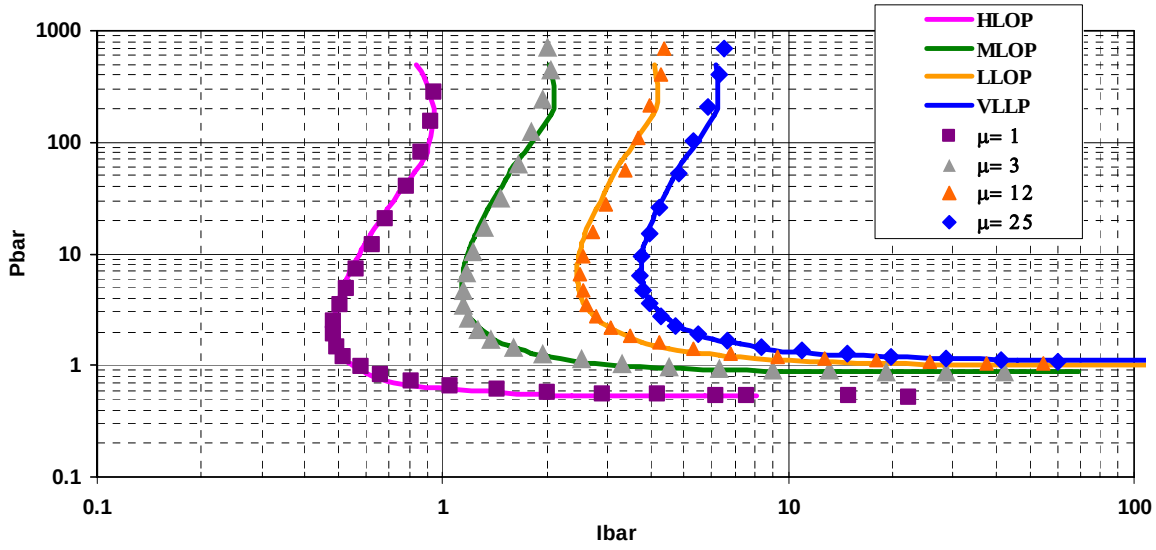

Figure 24. Scaled P-i Curves-fits vs. Scaled SDOF Points in Terms of Ductility Ratio for Flexural Response of Steel Beams

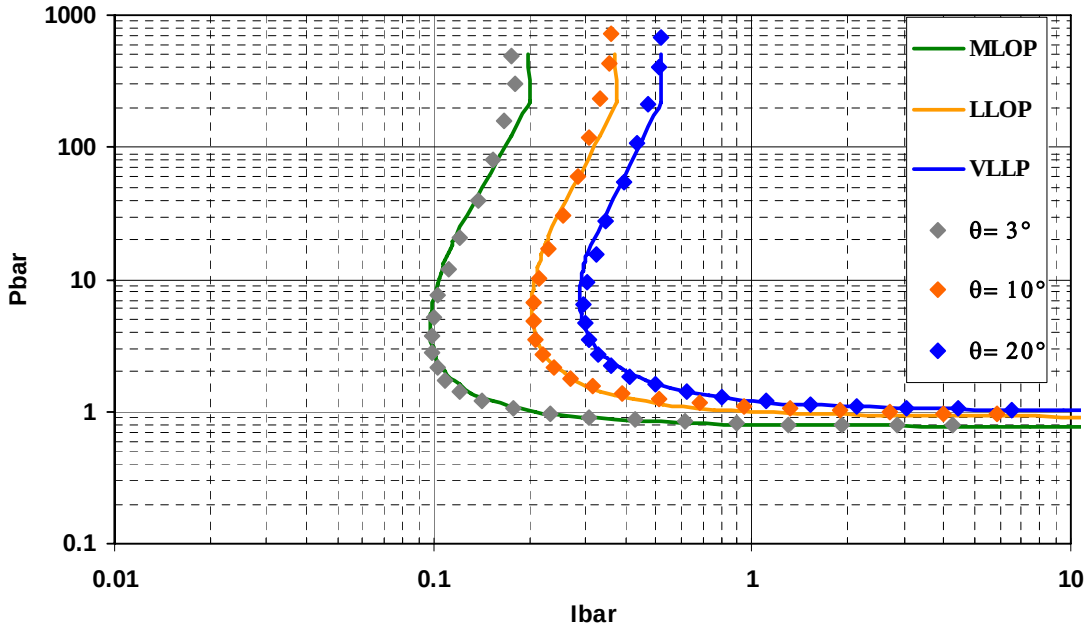

Figure 25. Scaled P-i Curves-fits vs. Scaled SDOF Points in Terms of Support Rotation for Flexural Response of Steel Beams

Table 4. ASCE Response Criteria for Upper Bounds of Each Response Level in Steel Beams

Source	Criteria for Each Response Level					
	Low Response, Light Damage, or MLOP		Medium Response or Damage, or LLOP		High Response or Severe Damage, or VLLOP	
	μ_a	θ_a	μ_a	θ_a	μ_a	θ_a
ASCE Blast Resistant Design Document	3	2	10	6	20	12
ASCE Physical Security Document		5.7		13.7		28.5
CEDAW for cold-formed girts w/ tension membrane (based on data)		4		12		20
Selected CEDAW criteria for steel beams	3	3	12	10	25	20

The blast design response criteria definitions for Low and High response approximately match the definitions for MLOP and LLOP, except the Low response definition may be a little more conservative than MLOP and the High response definition is a little less conservative than LLOP. The ASCE physical security criteria in Table 4 are much less conservative than the ASCE blast design criteria. The support rotation criteria from Table 3 for cold-formed girts with tension membrane, which are supported by available test data as discussed in Section 6.2, are also shown in Table 4. The last row in Table 4 shows the response criteria selected for CEDAW for steel beams without significant tension membrane response, such as hot-rolled steel beams, based primarily on the information in the first three rows.

Table 5. ASCE Blast Resistant Design Response Level Descriptions

Component Consequence	ASCE Response Level
Localized component damage, component can be repaired at moderate cost.	Low
Widespread component damage. Building cannot be used until component repaired. Total cost of repair may be significant.	Medium
Component has lost structural integrity and may collapse from environmental loads. Total repair cost is approaching replacement cost.	High

6.4 P-i Curves for Metal Stud Walls

Figure 26 and Figure 27 show the scaled P-i curves in CEDAW for flexural response of metal studs without and with connections to the top support, respectively, in terms of ductility ratio. These figures show the scaled P-i curve-fits using Equation 1 to Pbar and Ibar points calculated with applicable Pbar and Ibar equations, as indicated in Table 2, from SDOF analyses with the response parameter values shown in the figures and in Table 3. The values for each of the curve-fitting parameters in Equation 1 for each curve are shown in Appendix M.

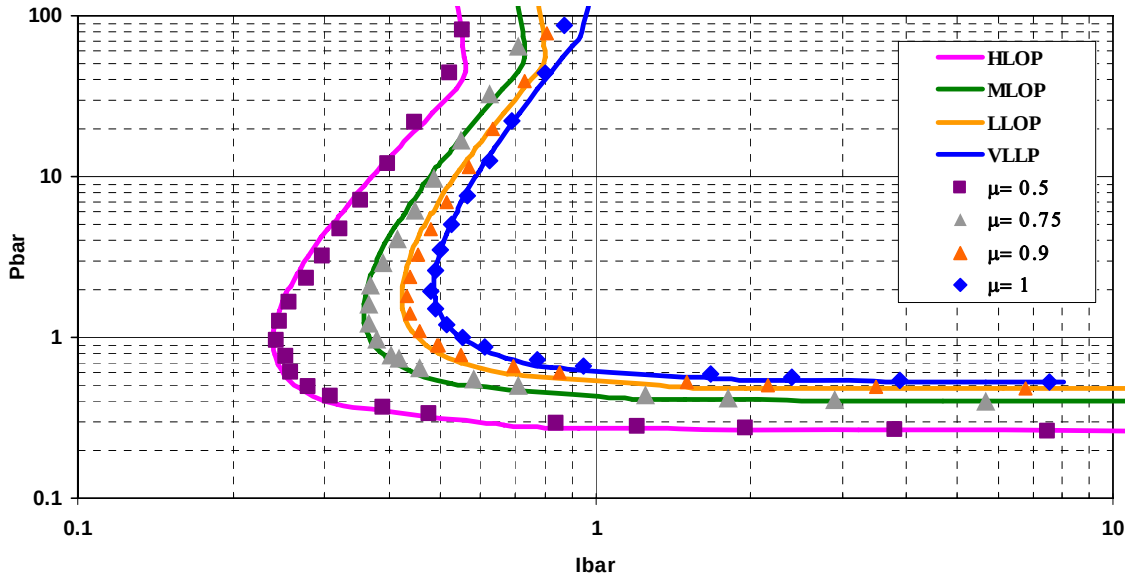

Figure 26. Scaled P-i Curves-fits vs. Scaled SDOF Points in Terms of Ductility Ratio for Flexural Response of Metal Studs Not Connected to Top and Bottom Supports

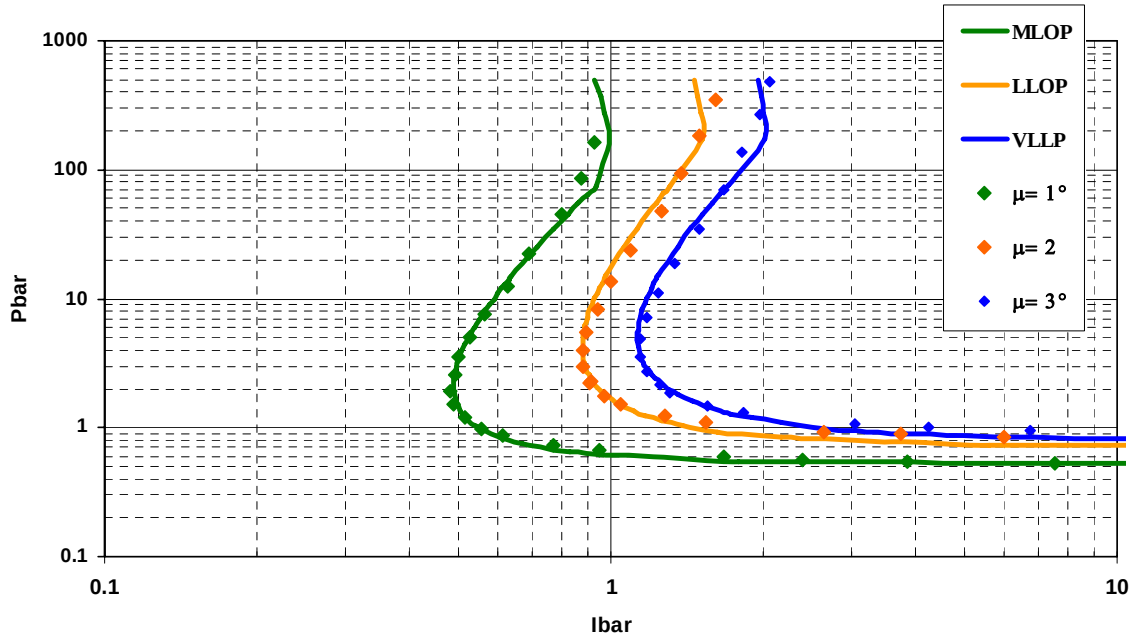

Figure 27. Scaled P-i Curves-fits vs. Scaled SDOF Points in Terms of Ductility Ratio for Flexural Response of Metal Studs Connected to Top and Bottom Supports

There is no available data for typical metal stud walls subject to blast loads. These are very light components that are typically considered to have a very low blast resistance, unless they are very well connected to their supports and can develop significant tension membrane capacity. If this is the case, the beam component type with tension membrane should be used in CEDAW. Metal studs are assumed to have light connections that cannot develop any significant tension membrane capacity.

A small static test series conducted by the University of Missouri showed that metal studs not screwed to the top track (i.e., with a slip track connection) did not develop their full moment flexural capacity before pushing through the vertical leg of the top track. In other tests where the top track legs were made much more rigid, so that the wall could not push through at the top, the metal studs developed their full flexural moment capacity and some limited ductile yielding. More ductile yielding was developed in subsequent tests where the stud was screwed onto the bottom support track with two screws instead of one screw. In all cases, the tested walls were non-load bearing walls.

The Protective Design Center at the U.S. Army Corps of Engineers, Omaha District has developed a set of response criteria for each LOP to metal stud walls with and without a positive connection of the stud to both supports. Since no blast test data was available, these response criteria were adopted for CEDAW, are shown in Table 3, and are used as the basis for Figure 26 and Figure 27. Limited blast test data is available for heavier metal studs that are bolted into concrete framing, but this data was used in Section 6.2 to develop the scaled P-i curves for steel girts with tension membrane since the metal studs in this case are acting much more similarly to steel girts well attached to heavy framing members than to typically constructed metal studs.

6.5 P-i Curves for Reinforced Concrete Slabs and Beams

Figure 28 shows the scaled P-i curves in CEDAW for ductile flexural response of reinforced concrete slabs and beams in terms of support rotation criteria for all LOP except HLOP, which is based on a ductility ratio of 1.0 in flexure and has a scaled P-i curve as shown in Figure 17. The scaled P-i curves were curve-fit with Equation 1 to Pbar and Ibar points calculated with applicable Pbar and Ibar equations, as indicated in Table 2, from SDOF analyses with the response parameter values shown in the figure and in Table 3. The values for each of the curve-fitting parameters in Equation 1 for each curve are shown in Appendix M. Figure 29 shows data scaled using the same Pbar and Ibar equations compared to the CEDAW scaled P-i curve-fits in Figure 28. The scaled data for each LOP should ideally fall between the upper bound curve for the given LOP and the next curve below and to the left. The scaled data is conservative if it lies above or to the right of the upper bound curve for the given LOP.

The data in Figure 29 is from blast testing of full-scale, half-scale, and quarter-scale one-way spanning reinforced concrete slabs. No data is available for reinforced concrete beams. The quarter-scale tests were performed in the UK on slabs with equivalent full-scale dimensions of a 20 ft span, 8-inch thickness, and reinforcing ratio of 0.7%. Full-scale tests from Sweden were performed on 8 ft spanning walls with 6-inch and 8-inch thicknesses and reinforcing ratios of 0.2% and 0.25%. Half-scale tests were also performed by the U.S. government on a box-type concrete structure with 24-inch, full-scale wall thickness and steel reinforcing ratios of 0.25% to 1.0% and shear reinforcement. See Appendix D for detailed test data information and test data references.

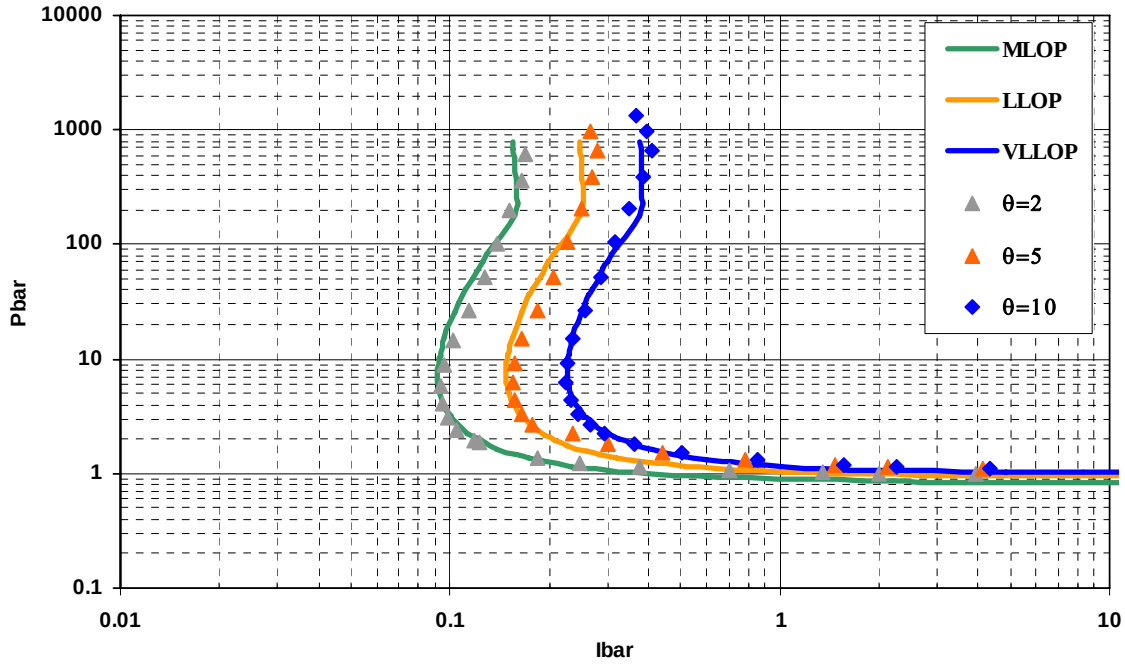

Figure 28. Scaled P-i Curves-fits vs. Scaled SDOF Points in Terms of Support Rotation for Flexural Response of Reinforced Concrete Slabs

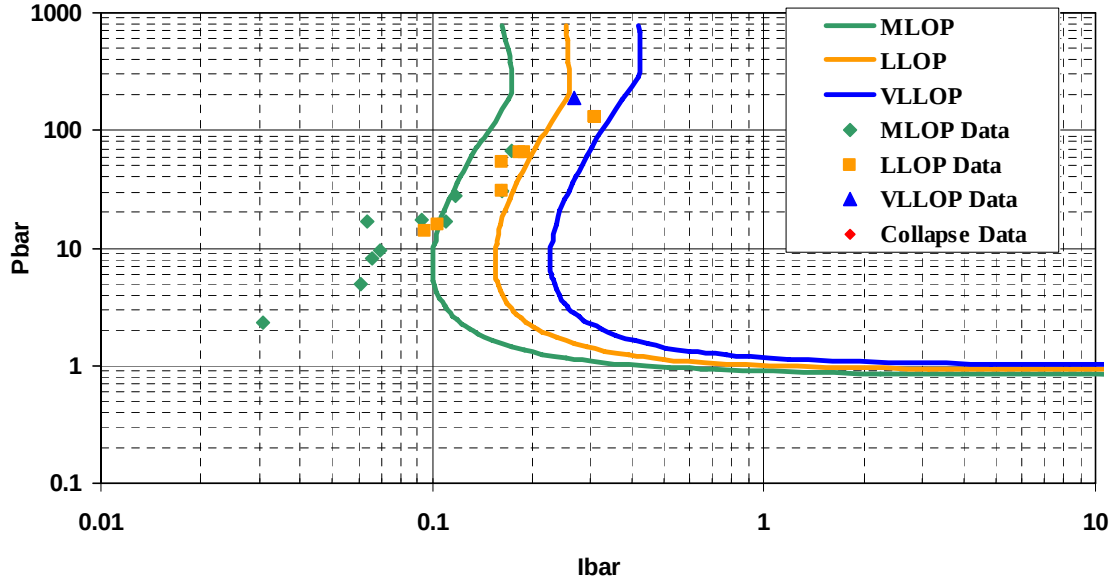

Figure 29. Scaled P-i Curves in Terms of Support Rotation vs. Scaled Data for Reinforced Concrete Slabs

6.6 P-i Curves for One-Way Reinforced Masonry Slabs

Figure 30 shows the scaled P-i curves in CEDAW for flexural response of one-way reinforced masonry walls in terms of support rotation criteria for all LOP except HLOP, which is based on the P-i curve for a ductility ratio of 1.0 in flexure as shown in Figure 17. The scaled P-i curves were curve-fit with Equation 1 to Pbar and Ibar points calculated with applicable Pbar and Ibar

equations, as indicated in Table 2, from SDOF analyses with the response parameter values shown in the figure and in Table 3. The values for each of the curve-fitting parameters in Equation 1 for each curve are shown in Appendix M.

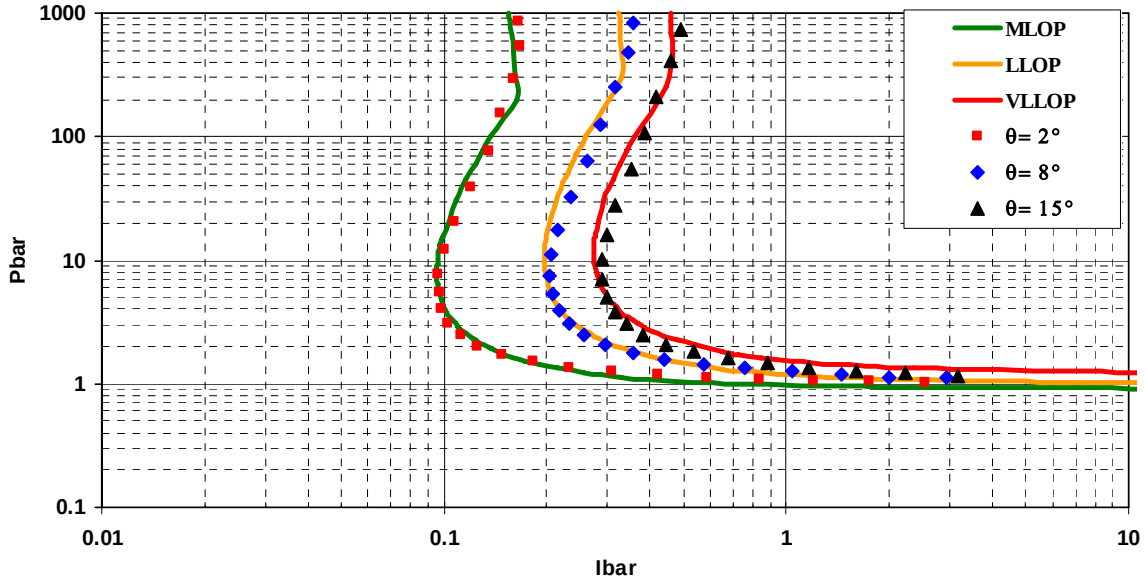

Figure 30. Scaled P-i Curves-fits vs. Scaled SDOF Points in Terms of Support Rotation for Flexural Response of Reinforced Masonry Slabs

Figure 31 shows blast test data scaled using the same Pbar and Ibar equations compared to scaled CEDAW P-i curve-fits in Figure 30. The scaled data for each LOP should ideally fall between the upper bound curve for the given LOP and the next curve below and to the left. The scaled data is conservative if it lies above or to the right of the upper bound curve for the given LOP. The data is from blast testing of full-scale and quarter-scale reinforced CMU walls. All of the data is from the CMUDS database and are explained in full in the CMUDS database report (Wesevich, et. al. 2002). The full-scale equivalent dimensions for the data have spans of 8 ft to 11 ft, thicknesses of 6 inches to 8 inches, and reinforcing ratios of 0.15% to 1%. Most of the data has reinforcing ratios from 0.15% to 0.3%. The data includes full-scale shock tube testing performed by BakerRisk and high explosives testing performed by the U.S. government at EMRTC and ERDC. See Appendix C for detailed test data information.

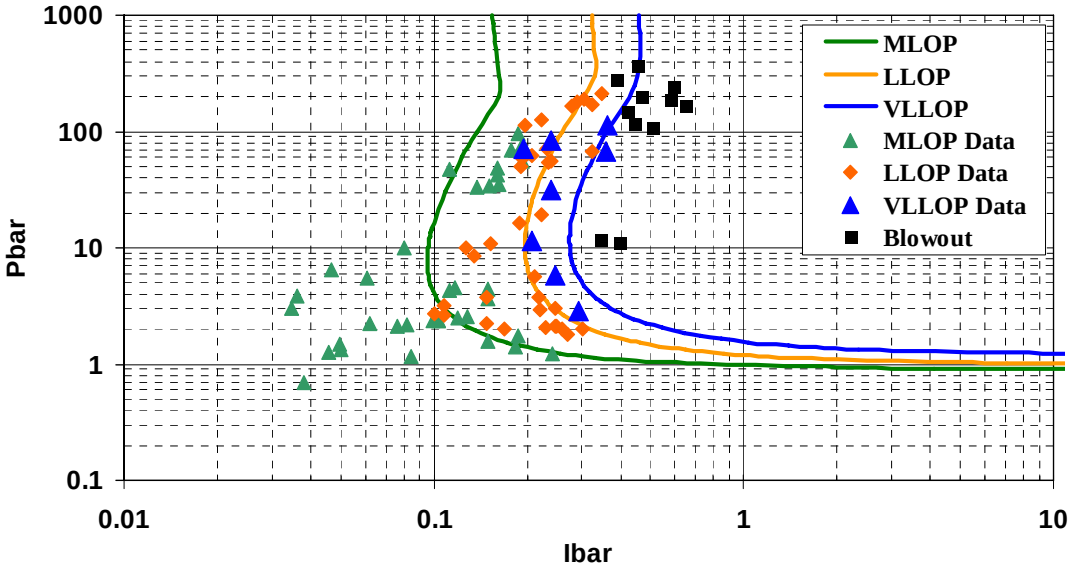

Figure 31. Scaled P-i Curves in Terms of Support Rotation vs. Scaled Data for Reinforced Masonry Slabs

6.7 P-i Curves for Open Web Steel Joists

Figure 32 and Figure 33 show the scaled P-i curves in CEDAW for flexural response of open web steel joists without and with tension membrane, respectively, in terms of support rotation criteria for all LOP except HLOP, which has a scaled P-i curve based on a ductility ratio of 1.0 in flexure as shown in Figure 17. The scaled P-i curves were curve-fit with Equation 1 to Pbar and Ibar points calculated with applicable Pbar and Ibar equations, as indicated in Table 2, from SDOF analyses with the response parameter values shown in the figure and in Table 3. The values for each of the curve-fitting parameters in Equation 1 for each curve are shown in Appendix M.

Figure 34 shows scaled data compared to the scaled CEDAW P-i curve-fits in Figure 33 for open web steel joists with significant tension membrane. The scaled data for each LOP should ideally fall between the upper bound curve for the given LOP and the next curve below and to the left. The scaled data is conservative if it lies above or to the right of the upper bound curve for the given LOP. The data is from one blast test series on full-scale joists that supported a light metal deck roof system sponsored by the U.S. government. The joists were 12K1 joists spanning 20 ft at 4 ft spacing. The joists were welded to steel plate embedded in the supporting reinforced concrete walls. See Appendix F for detailed test data and test data references.

The tension membrane force used to scale the data in Figure 34 was assumed equal to 9 kips for first three tests, where typical joist configurations were tested, based on the ultimate dynamic shear strength of the minimum specified weld of the joist top chord to the supports using a dynamic increase factor of 1.2. This is consistent with the method recommended in the CEDAW workbook for calculating the maximum tensile force for tension membrane response of joists. The minimum specified weld size for a 12K1 joist is 2 inches of 1/8-inch weld at each support. The actual weld length was somewhat larger in some of the tests. The welds did not fail in these

tests and finite element analyses of the tests showed that the welds had to develop the full tension membrane force associated with the joist deflection, which was up to 30 kips, in order for the calculated deflection to match the measured deflection (Bogozian and Dunn, 2000). If the data points were scaled using 30 kips of tension force, they would be somewhat more conservative compared to the scaled P-i curves than shown in Figure 34.

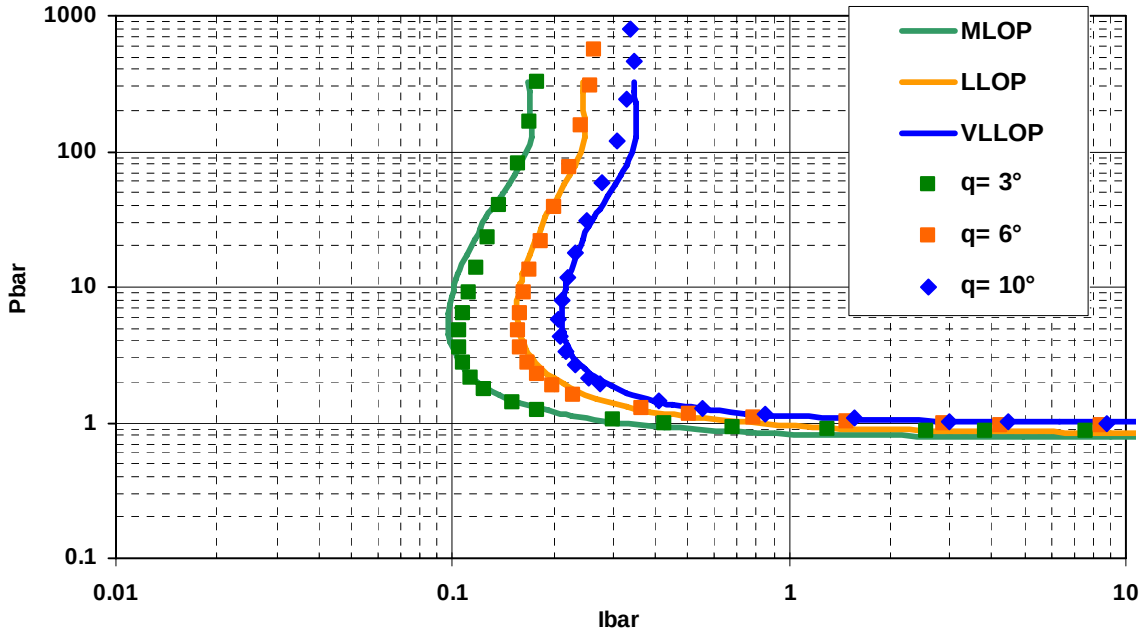

Figure 32. Scaled P-i Curves-fits vs. Scaled SDOF Points in Terms of Support Rotation for Flexural Response of Open Web Steel Joists without Significant Tension Membrane

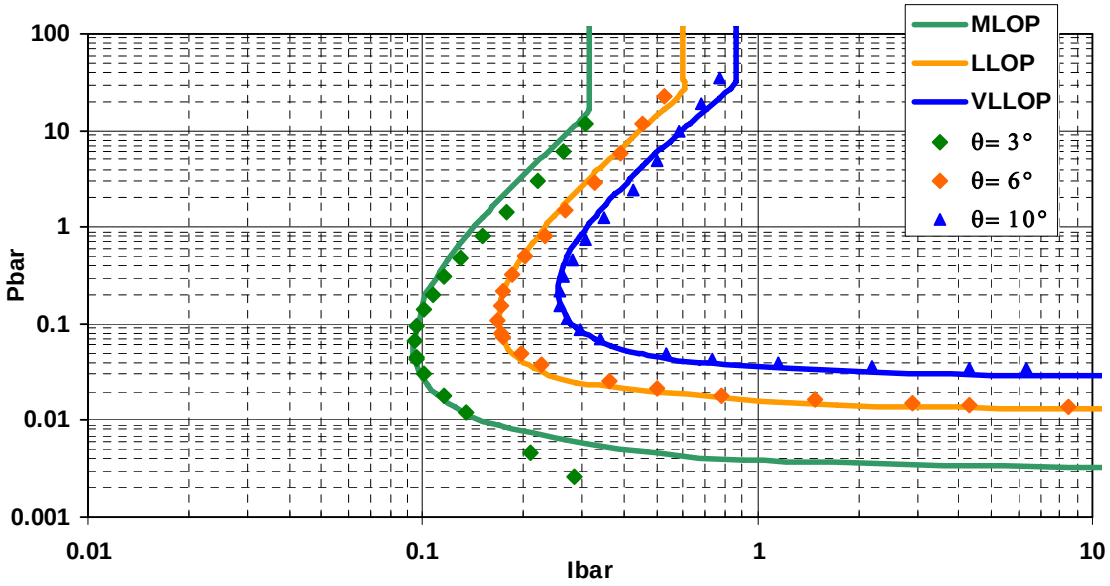

Figure 33. Scaled P-i Curves-fits vs. Scaled SDOF Points in Terms of Support Rotation for Flexural Response of Open Web Steel Joists with Significant Tension Membrane

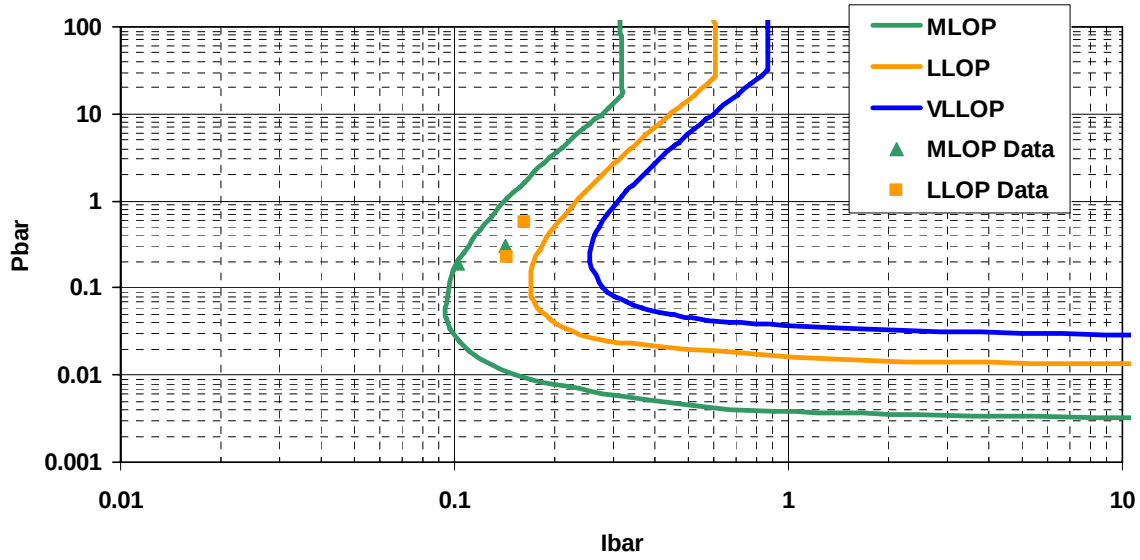

Figure 34. Scaled P-i Curves in Terms of Support Rotation vs. Scaled Data for Open Web Steel Joists

In the final test, where an upgraded joist was attached to the supports with 8 inches of weld, the tension membrane force used to scale the data in Figure 34 was taken as 31 kips based on the dynamic tensile capacity of the top chord of the joists. The chord had a minimum area of 0.5 in^2 and a minimum specified yield strength of 50 ksi. The upgraded joist had a weld failure during the response that did not cause the joist to fail into the building. It is not known why the welds on the non-upgraded joists did not fail, although the very significant observed rotation of the ends of the joists in these tests may indicate that the small welds were not confined or constrained and could therefore respond more ductilely than the longer welds on the upgraded joist.

6.8 P-i Curves for One-Way and Two-Way Unreinforced Masonry Walls

Figure 35 and Figure 36 show scaled P-i curves in CEDAW for unreinforced masonry walls with brittle flexural response and arching from axial load in terms of support rotation criteria for all LOP except HLOP, which has scaled P-i curve based on a ductility ratio of 1.0 in flexure as shown in Figure 17. The scaled P-i curves in Figure 35 and Figure 36 were curve-fit with Equation 1 and Equation 2 to Pbar and Ibar points calculated with applicable Pbar and Ibar equations, as indicated in Table 2, from SDOF analyses with ratios of R_a to R_U as explained below and the response parameter values shown in the figure and in Table 3. As explained in Section 4.3 and at the end of Section 3.0, the curve-fitting parameters A and D from Equation 1 for this component and response mode type are a function of the ratio of the peak resistance from axial load arching (R_a) to the ultimate flexural resistance (R_U) as shown in Equation 2. For illustrative purposes, scaled P-i curves are plotted in Figure 35 for a low ratio of the peak resistance from axial load arching (R_a) to the ultimate flexural resistance (R_U), equal to 0.05 to 0.1, which represents the case of a non-load bearing wall with only self weight axial loading. Also, scaled P-i curves are plotted in Figure 36 for a high ratio of R_a to R_U, equal to about 1.0, which represents the case for a ground floor wall of a typical three or four story load-bearing building with an axial load of around 200 lb/in.

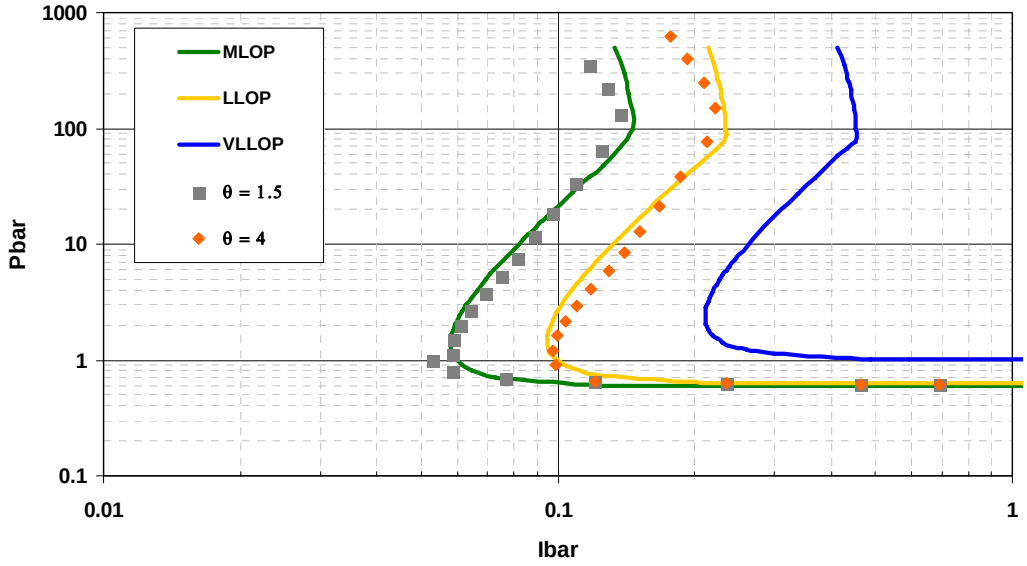

Figure 35. Scaled P-i Curves-fits vs. Scaled SDOF Points in Terms of Support Rotation for Brittle Flexural and Arching Response of Unreinforced Masonry Walls with Low Ra/Ru

The scaled P-i curve for VLLOP in Figure 35 is based on scaled data, as explained in the next paragraph. No such data exists for cases of high R_a to R_U ratio, but the scaled P-i curve for VLLOP response for this component and response mode for all higher R_a to R_U ratios is assumed to have the approximately the same relative position to the other two scaled curves, which can both be determined from SDOF analyses, as shown in Figure 35. It is not possible to calculate a response level much higher than 4 degrees with SDOF analyses because the strain energy in the resistance-deflection curve for unreinforced masonry goes to zero at response levels greater than the wall thickness, as shown in Figure 11, and therefore the blast loads do not increase for higher SDOF response levels. The values for the constant curve-fitting parameters in Equation 1 for each curve are shown in Appendix M. The equations for the curve-fitting parameters dependent on the ratio of R_a to R_U are shown in Equation 1.

Figure 37 and Figure 38 show data scaled with the same Pbar and Ibar equations compared to the scaled CEDAW P-i curve-fits in Figure 35 representing a low R_a to R_U ratio. In all cases the tests did not have any axial load except self-weight. The scaled data for each LOP should ideally fall between the upper bound curve for the given LOP and the next curve below and to the left. The scaled data is conservative if it lies above or to the right of the upper bound curve for the given LOP. The one-way spanning data in Figure 37 are from the CMUDS database, which includes full-scale shock tube testing performed by BakerRisk and high explosives testing performed by the U.S. government at EMRTC on full-scale walls and at ERDC on one-quarter scale walls. It also includes full-scale tests on brick walls with long duration blast loads conducted at the URS shock tunnel in the 1970s. The span lengths were 8 ft to 10 ft and the thicknesses ranged from 6 inches to 8 inches. Most of tests walls were constructed with unreinforced CMU blocks or bricks. See Appendix A for detailed test data information and test data references.

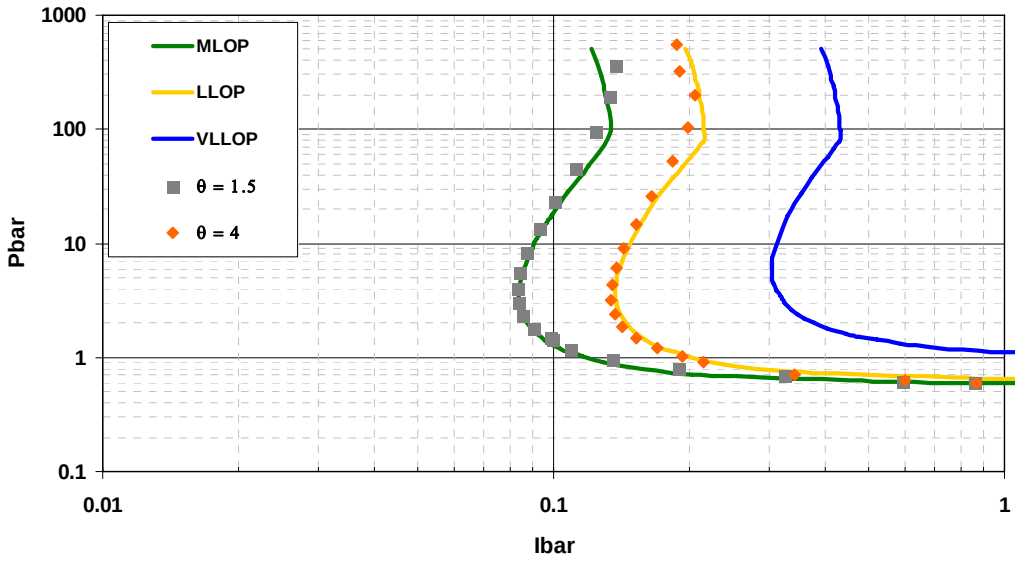

Figure 36. Scaled P-i Curves-fits vs. Scaled SDOF Points in Terms of Support Rotation for Brittle Flexural and Arching Response of Unreinforced Masonry Walls with High Ra/Ru

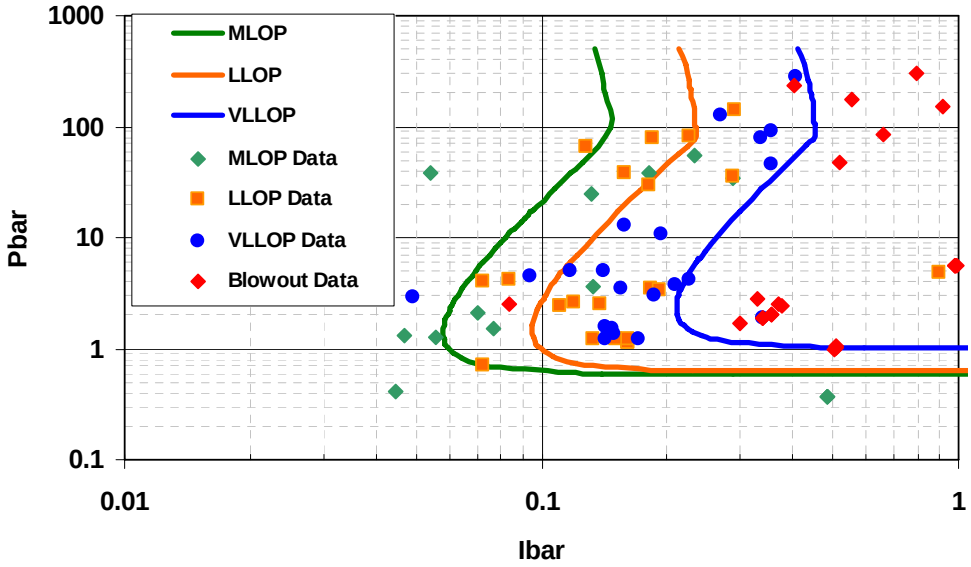

Figure 37. Scaled P-i Curves in Terms of Support Rotation vs. Scaled Data for One-Way Unreinforced Masonry Walls

The two-way spanning data in Figure 38 includes a few one-quarter scale tests performed by BakerRisk in a small shock tube and 34 full-scale tests conducted by the Indian Ministry of Defense with high explosive loading. The BakerRisk walls modeled unreinforced CMU walls with 8 ft spans and simple supports along all four edges. The Indian Ministry of Defense tests were conducted on square brick walls with thicknesses ranging from 9 inches to 18 inches, a span length of nearly 10 ft, and simple supports along all four sides. See Appendix B for detailed test data information and test data references.

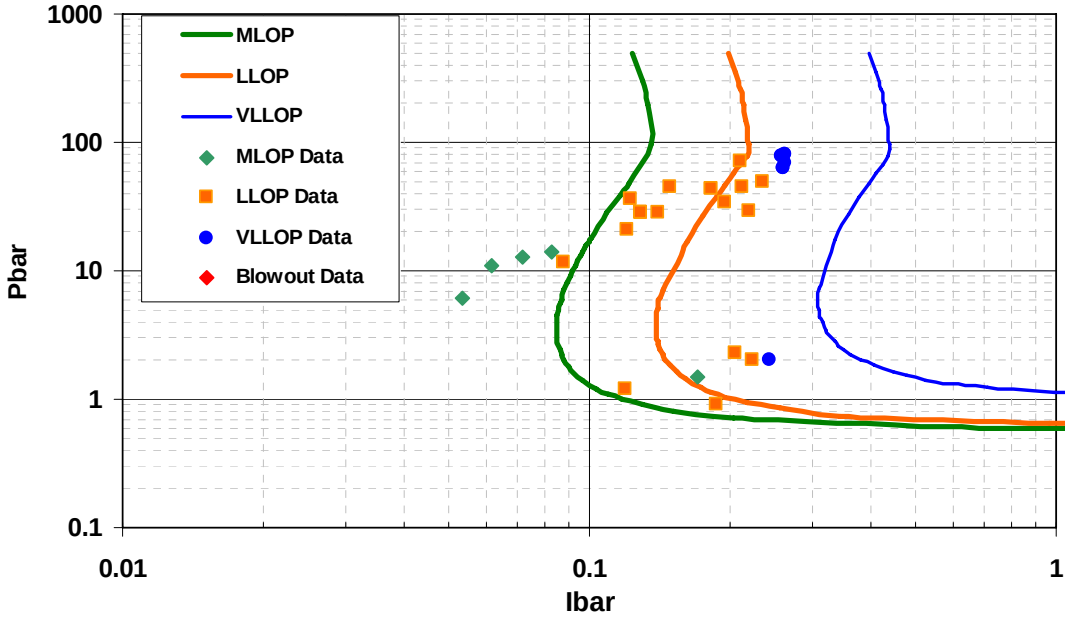

Figure 38. Scaled P-i Curves in Terms of Support Rotation vs. Scaled Data for Two-Way Unreinforced Masonry Walls

6.9 P-i Curves for Wood Stud Walls

Figure 39 shows the scaled P-i curves in CEDAW for ductile flexural response of wood stud walls in terms of ductility ratio criteria for all LOP. The scaled P-i curves in Figure 39 were curve-fit with Equation 1 to Pbar and Ibar points calculated with applicable Pbar and Ibar equations, as indicated in Table 2, from SDOF analyses with the response parameter values shown in the figure and in Table 3. The values for each of the curve-fitting parameters in Equation 1 for each curve are shown in Appendix M.

Figure 40 shows data scaled with the same Pbar and Ibar equations compared to the scaled CEDAW P-i curve-fits in Figure 39. The scaled data for each LOP should ideally fall between the upper bound curve for the given LOP and the next curve below and to the left. The scaled data is conservative if it lies above or to the right of the upper bound curve for the given LOP. Most of the data in Figure 40 is from the BAITS tests, where lightly constructed wood "SEA Huts" representing Air Force expeditionary wood stud structures were loaded with large high explosion charges at large standoffs. The walls of the SEA Huts had typical 2-inch x 4-inch wood studs at 16 inches on center supporting 5/8-inch thick plywood panels. The researchers reported the measured reflected blast loads and generally described damage to the huts. Data from the SEA Hut walls subject to side-on loads were not used if the roof failed or had severe damage since the roof helped support these walls. Figure 40 also includes some data from shock tube tests conducted by BakerRisk on heavy wood stud walls, where 2-inch x 6-inch and 8-inch studs were spaced at 6 inches supporting 5/8-inch plywood on one side or both sides of the wall. The studs spanned 8 ft. In some of these tests the plywood was nailed to the studs with nail spacing as close as 3 inches, but the peak measured dynamic reaction forces were consistent with

reactions based only on the maximum resistance of studs with no composite action from the plywood. See Appendix H for detailed test data information and test data references.

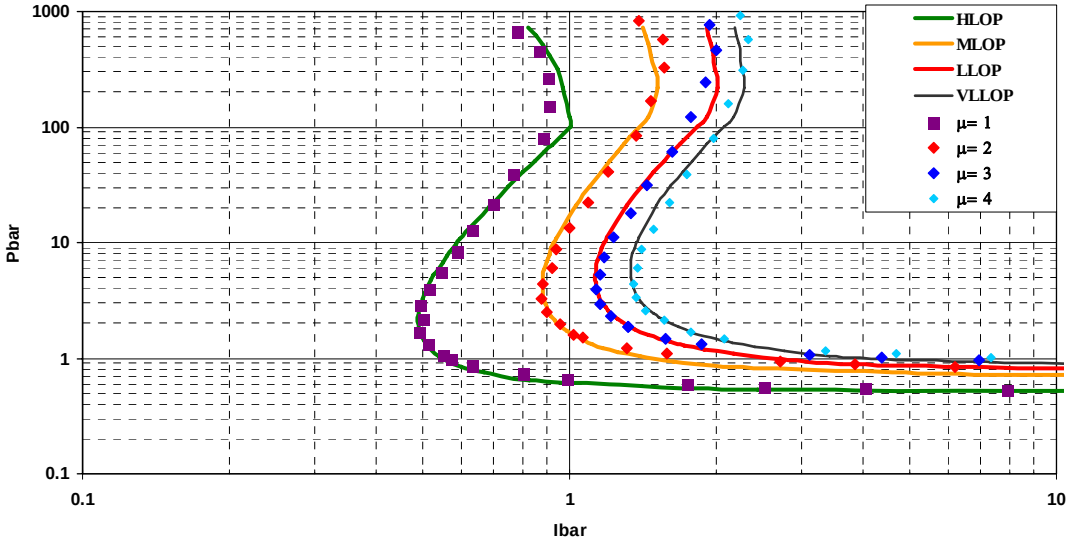

Figure 39. Scaled P-i Curves-fits vs. Scaled SDOF Points in Terms of Ductility Ratio for Flexural Response of Wood Stud Walls

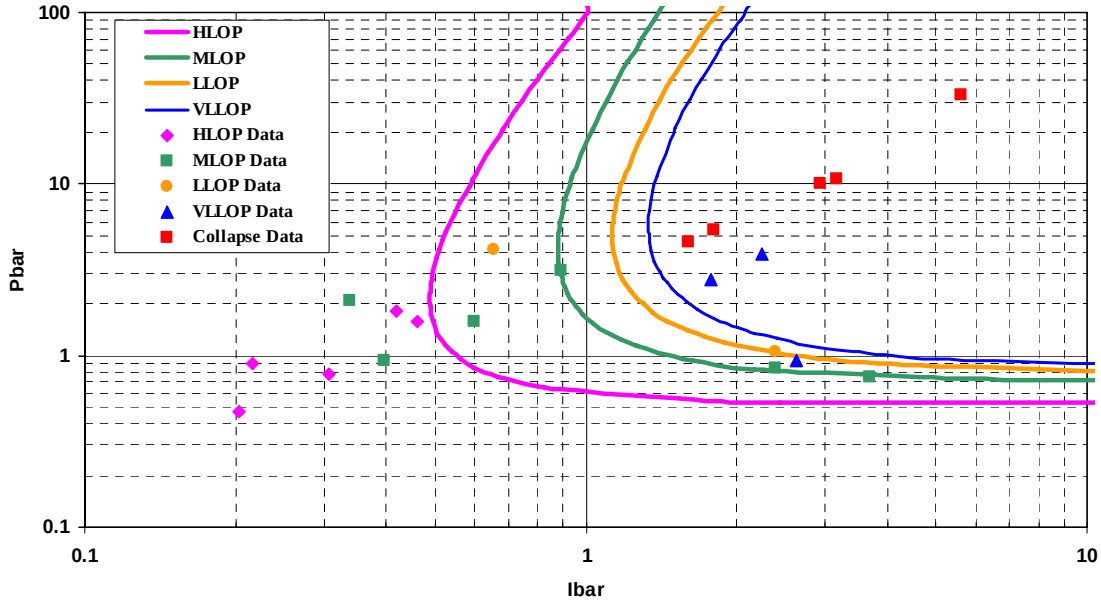

Figure 40. Scaled P-i Curves in Terms of Ductility Ratio vs. Scaled Data for Wood Stud Walls

6.10 P-i Curves for Reinforced Concrete Columns

Available data from typical reinforced concrete frame buildings, such as the blast damaged building shown in Figure 41, indicate that the columns are much more resistant to blast loads than the surrounding wall cladding components. Typically, the cladding in reinforced concrete frame buildings spans vertically between floors and does not transfer blast load into the columns,

so that the columns are only loaded over their self-width. Also, the columns are required to have a significant percentage of longitudinal steel to resist conservatively high, design-level, axial loads, and this steel acts as flexural steel under lateral blast loads to provide a very significant flexural moment resisting capacity. This is true even when considering P-delta effects from axial loads because the columns are also very stiff laterally and therefore tend to have small lateral deflections. Except in earthquake zones, the only lateral steel reinforcement in columns is typically column ties that are too widely spaced to provide shear strength (i.e., at a spacing greater than one-half the depth of the longitudinal steel from the opposite face of the column). Due to the large amount of column longitudinal reinforcement and the relatively low shear strength, even in columns with closely spaced stirrups, the lateral load capacity of conventional reinforced concrete columns is almost always controlled by the column shear strength instead of flexural strength. The Pbar and Ibar terms in CEDAW assume that the ultimate column capacity is always controlled by the column shear capacity.

Figure 41. Portion of Reinforced Concrete Frame Building Near Oklahoma City Bombing with Cladding Failure

The LOP provided to building occupants and assets is generally controlled by the cladding components, rather than column components, because the cladding components almost always fail before the columns due to have a much lower blast load capacity. However, column failure from severe, close-in blast loading can lead to progressive collapse of portions of all supported areas of a concrete frame building, including sections where severe damage to cladding is not caused by directly applied blast loads. This occurred in the Murrah Building adjacent to the 1995 Oklahoma City Bombing, where column failure at the first floor level caused progressive collapse of building components and occupant fatalities up to the ninth floor, where the directly applied blast loads were not particularly severe. Therefore, column failure is considered in the CEDAW workbook.

Failure of perimeter ground floor concrete columns is assumed in CEDAW to be controlled by diagonal tension type shear based on observed column damage in the Devine Buffalo (DB) test

series (Plamondon and Sheffield, 1999) and near the South Quay IRA bombing in London. It is worth noting that in both of these cases, surrounding cladding components were failed and thrown into the building with significant velocities by the blast loads, indicating that the cladding components cause the lower LOP due to direct component to blast load (i.e., excluding any progressive collapse effects). Figure 42 shows column damage from Test DB6, where the column failed primarily in shear response. Figure 42 also shows diagonal shear cracks near the top of the second floor column above, which did not fail. Figure 43 shows a column at about 5 m from the South Quay IRA bombing where severe shear damage occurred. The damage at midspan in these columns is not nearly as severe as damage in the high shear region at the supports. Calculations of typical concrete column response to close-in explosion loads using an SDOF-based approach (Morrill et al, 1999) also showed that shear typically controlled maximum column capacity.

Overall View of Failed Column Bottom of Failed Column Damaged Second Floor Column

Figure 42. Shear Damage to Reinforced Concrete Columns from DB6 Test

Figure 44 shows scaled P-i curves for a reinforced concrete column responding in flexure up to the ultimate shear resistance, followed by ductile yielding, in terms of ductility ratio criteria for three ductility ratios. The scaled P-i curves in Figure 44 were curve-fit using Equation 3 to Pbar and Ibar points calculated with applicable equations in Table 2 from SDOF analyses with the response levels shown in the figure. The resistance used in the Pbar and Ibar equations, which is based on the ultimate concrete shear strength including a dynamic increase factor (DIF), is shown in Equation 11. The DIF values used in CEDAW and for the scaled test data in Figure 45 are shown in Table 6. They are based on analyses of typical columns with the SPAN32 code v1.3 (2001), which calculates concrete tension DIF for use in shear strength calculations. Charge weights between 1000 lb and 3000 lb TNT were used against square columns with 12-inch to 24-inch dimensions and 1% to 2% steel ratios. Note that the highest ductility ratio in Figure 44, equal to 6.0, corresponds to the scaled P-i curve used to predict the upper bound of LLOP for

perimeter ground floor columns in CEDAW, as indicated in Table 3. The values for the curve-fitting parameters from Equation 3 fitting the scaled blast load points from SDOF analyses with a ductility ratio of 6.0 are shown in Appendix M.

Figure 43. Damage to Concrete Column at 5 m from South Quay IRA Bombing in London

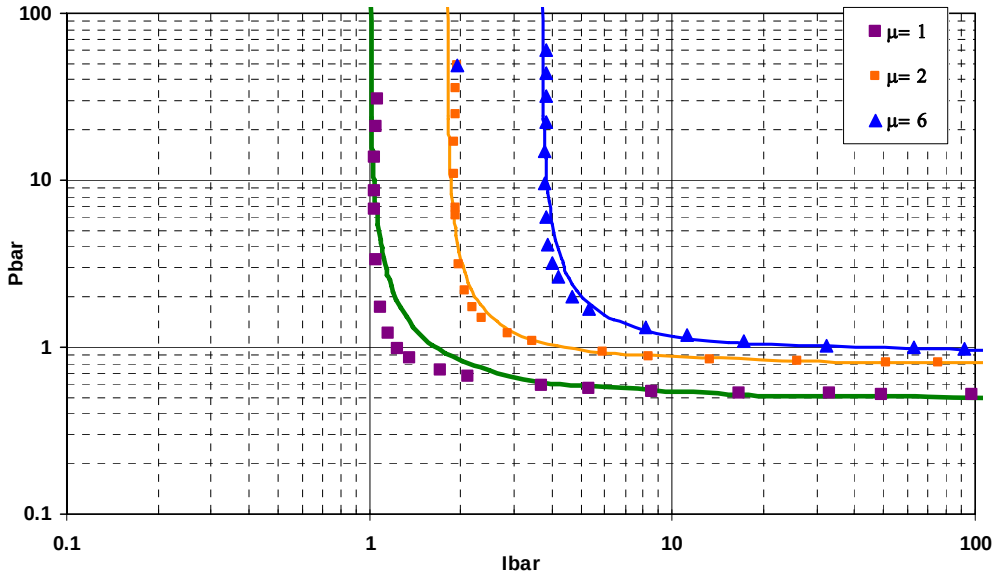

Figure 44. Scaled P-i Curves-fits vs. Scaled SDOF Points in Terms of Ductility Ratio for Flexural Response of Columns Up to Ultimate Shear Capacity

$$R_u = \frac{\left[2\sqrt{1.1f'c}bd\right]DIF + f_{dy}A_v\frac{d}{s}}{B(kL-d)}$$

Equation 11

where: R_u = ultimate resistance of column based on shear capacity (lb/in^2)
f'_c = concrete cylinder compression strength (lb/in^2), where 1.1 is an aging strength increase factor
b = column width (in)
d = column depth (in)
L = column span (in)
k = 0.675 for fixed simple support, otherwise k = 0.5
B = supported width (in)
f_{dy} = dynamic yield strength of shear reinforcing steel
A_v = area of shear reinforcing steel with spacing less than d/2 near supports (in^2)
s = spacing of shear reinforcing steel (in)
DIF = dynamic increase factor for concrete shear strength, see Table 6

Table 6. Assumed Concrete Shear DIF Values in CEDAW

Scaled Standoff Range (Z) (ft/lb$^{1/3}$)	Assumed Concrete Shear DIF
$Z \geq 1.0$	2.1
$1.0 < Z < 2.3$	1.7
$Z > 2.3$	1.35

Figure 45 shows scaled data of column response to close-in high explosive blast loads compared to scaled P-i curve-fits for response of reinforced concrete columns with ductility ratios ranging from 1 to 6. The same Pbar and Ibar equations used to scale the SDOF analyses, as shown in Table 2, were used to scale the data. The data in Figure 45 are from the previously mentioned Devine Buffalo series and from the closest buildings to the South Quay and Bishopgate IRA bombings in London. See Appendix I for detailed test data information and test data references.

Conservatively, three non-failing scaled data points lie inside of the scaled P-i curve (i.e., above or to the right) in Figure 45 for a ductility ratio of 6, which is used in CEDAW for the upper bound of LLOP response, and none of the failing data points lie outside this curve. Note that the P-i curves for column response in Figure 44 and Figure 45 conservatively do not have any "layover" in the impulse sensitive range. The columns are typically quite stiff and respond quickly to blast load so that peak column response occurs prior to the negative phase blast load except for very short duration loads, with very high pressures from charge weight and standoff combinations that are typically outside the range of interest. These cases would typically cause more of a breaching threat, which is not included in the CEDAW methodology, than flexural response that causes high shear stresses at the supports.

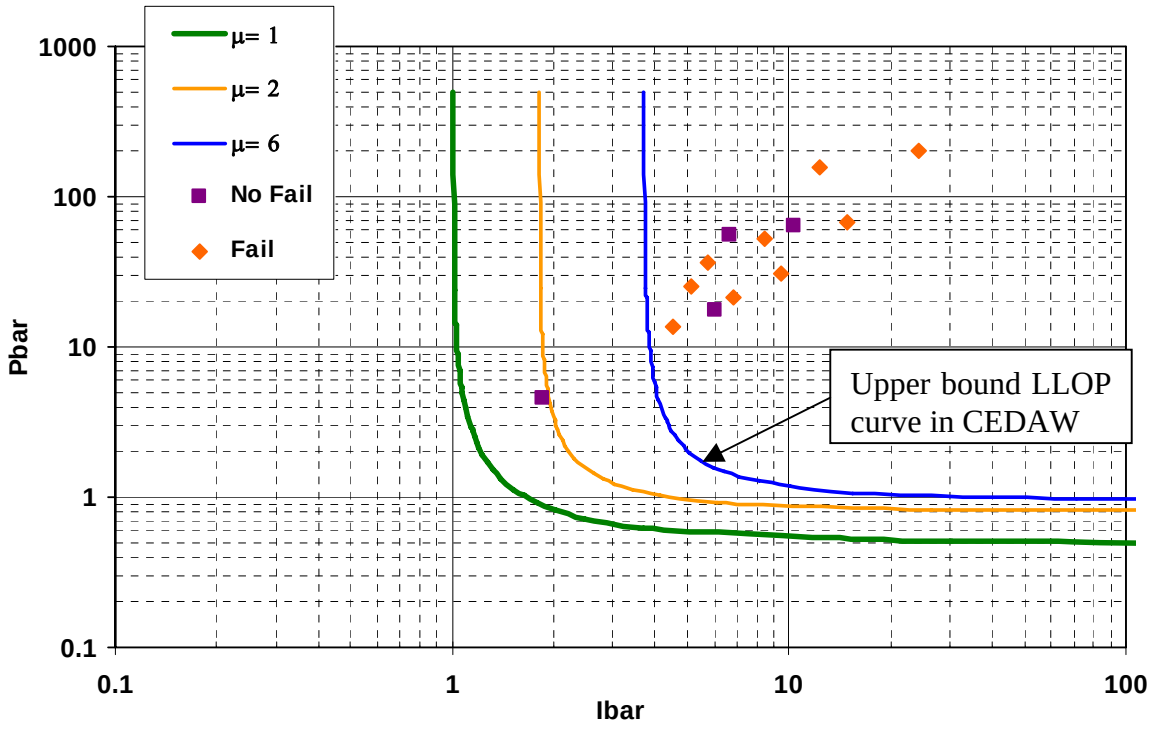

Figure 45. Scaled P-i Curves in Terms of Ductility Ratio vs. Scaled Data for Reinforced Concrete Columns Failing in Shear

6.11 P-i Curves for Steel Columns Limited by Connection Shear Capacity

This component type is intended for perimeter ground level steel columns where the connections are in shear. This typically occurs at the bottom connection of the column when there is a shear plane through the anchor bolts connecting the column bearing plate to the concrete slab. The same rationale described in Section 6.10 to limit consideration of reinforced concrete column damage to failure (i.e., a VLLOP) also generally applies to steel columns. The cladding does transfer blast loads into steel columns for some steel frame building types, such as pre-engineered buildings, but the cladding typically has a much lower blast capacity than the columns for these building types and fails before the frame members, as shown in Figure 46 for a lightly clad steel frame building in a petrochemical plant near a large accidental explosion. Steel column failure can lead to progressive collapse as described for reinforced concrete columns in Section 6.10. However, steel columns with relatively weak connections at the ground floor level, such as those in light metal buildings, can have significantly less blast capacity against close-in blast loading than reinforced concrete columns. Limited available blast test data for steel columns subject to severe blast loads (Stanley and Osowski, 2002) indicates that connection failure is the weakest response mode when conventional types of column baseplate connections are used (see Figure 47).

Figure 46. Typical Pre-Engineered Steel Building and Multi-Story Steel Frame Building (in Background) with Cladding Failure Caused by Blast Loads

Figure 47. Failed Steel Column Connections in DB Tests

Figure 48 shows scaled data from the tests where steel column failure was caused by failure of typical anchor bolt connections compared to scaled P-i curves for steel columns with ductility ratios ranging from 1 to 2. The scaled P-i curves are based on SDOF analyses where flexural response was assumed to occur up to an ultimate resistance based on the connection shear capacity followed by ductile yielding up to the ductility ratios shown in the figure. The blast loads from the SDOF analyses and test data were scaled with the Pbar and Ibar equations indicated in Table 2. The ultimate resistance of the column based on the connection shear capacity in the Pbar and Ibar equations is calculated in CEDAW as shown in Equation 12. This equation assumes equal distribution of shear force between the top and bottom columns supports. In some cases, depending on the relative amounts of rotational restraint provided by the anchor bolts at the bottom connection and the top connection of the column, this assumption can be conservative the 0.5 factor in the denominator of Equation 12 can be closer to 0.38. The curves

in Figure 48 fit through the Pbar and Ibar points calculated by scaling the blast loads from SDOF analyses with response levels equal to the two ductility ratios were generated with Equation 3. The curve-fitting parameters in Equation 3 for the scaled P-i curve in Figure 48 with a ductility ratio of 1.0, which is used to define the upper bound of LLOP response in CEDAW, are shown in Appendix M.

$$R_u = \frac{f_{dy} A_v N_b}{0.5BL}$$

Equation 12

where: R_u = ultimate resistance of column based on connection shear capacity
L = column span (in)
B = supported width (in)
f_{dy} = ultimate dynamic shear strength of bolts
A_v = nominal shear area of typical bolt
N_b = number of bolts
Note: input any combination of $f_{dy}A_vN_b$ = shear strength of welded connection for the unusual case where weld controls connection strength

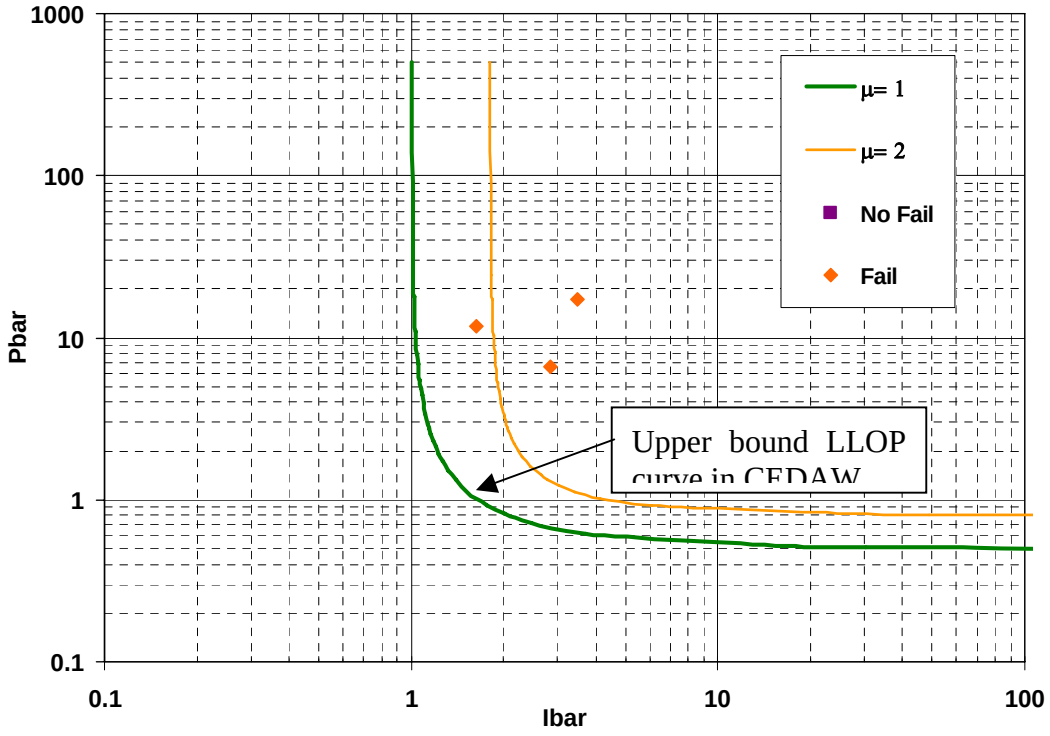

Figure 48. Scaled P-i Curves in Terms of Ductility Ratio vs. Scaled Data for Steel Columns Subject to Connection Failure

The very limited number of available scaled data points in Figure 48 fall outside the P-i curve for a ductility ratio of 1. The scaled data indicates that a ductility ratio of 2 may be a nonconservative criterion for this type of column failure and the lack of data also dictates use of a more conservative ductility ratio as a basis for the scaled P-i curve in the CEDAW workbook. Therefore, scaled P-i curve corresponding to a ductility ratio of 1 in Figure 48 is used in CEDAW as the upper bound for LLOP response of steel columns subject to connection failure. See Appendix J for detailed test data information and test data references. The P-i curves in Figure 48 do not layover in the impulsive region for the same reasons discussed for concrete columns in Section 6.10.

6.12 P-i Curves for Steel Columns Not Limited by Connection Shear Capacity

There are also cases in steel frame buildings where the perimeter column baseplates are buried in the concrete slab or the columns are continuous into a basement so that the column bears against the ground floor slab. If the column is also continuous over the second floor slab (or the 'first floor' slab, according to common European designation), so the ground floor column capacity is not controlled by connection capacity, flexure is expected to control column response to close-in blast loads. The columns can be considered vertical steel beams loaded over their flange widths, or width exposed to blast.

Column flexural failure criteria equal to a ductility ratio of 6 or a support rotation of 4 were assumed to define steel column flexural failure for CEDAW (i.e. upper bound of LLOP), which are twice the criteria recommended for "High" response in ASCE (1997) for beam-columns. Scaled P-i curves were curve-fit using Equation 1 to SDOF points from analyses causing these two response criteria that were scaled using Pbar1, Ibar1 and Ibar2 from Equation 10 for the applicable response parameter types. This approach is conservative compared to limited test data. W14x82 and W14x38 columns with an axial load of 133,000 lbs were loaded in the strong axis by 1200 lb ANFO at 15 ft (Stanley and Osowski, 2002). Neither column failed. The W14x38 column shown in Figure 49 had the larger deflections, equal to 3.5 inches in the strong direction corresponding to a rotation of about 2.5 degrees and a ductility ratio of 7.

Figure 49. W14x38 Column After Blast Test

7.0 ACCURACY OF CEDAW P-I CURVES

CEDAW is an approximate method where blast loads from test data and blast loads causing given response levels in SDOF systems representing common structural component types have been scaled into generalized non-dimensional Pbar and Ibar terms and used to develop scaled P-i curves that can be unscaled in an EXCEL® workbook to very quickly determine the LOP provided by a given structural component. CEDAW is approximate because of assumptions that fall into three main categories: 1) simplifying assumptions related to the theoretical development of the Pbar and Ibar scaling terms; 2) selection of the most appropriate response mode and non-dimensional parameter type (i.e., ductility ratio, support rotation, or both parameters) for each component type; and 3) assumptions related to the development of the response criteria in Table 3 associated with the upper bounds of each LOP for each component type. The effect of approximations related to the Pbar and Ibar scaling terms is investigated in this section. It is important to balance these inaccuracies against the fact that CEDAW only predicts component response in terms of LOP, which includes a relatively broad range of responses rather than a discrete value, such as the maximum deflection value, and the fact that CEDAW is intended primarily for initial blast assessments of structural components.

The assumptions involved in the development of the response criteria used to create the scaled P-i curves and in the selection of the most appropriate response mode and non-dimensional parameter type for each component type are not investigated in this section. All the available data was used as described in Section 6.0 to help develop the response limits in Table 3 and there are no independent data available to assess the accuracy of these limits. As assessment of the accuracy or reasonableness of these assumptions is best determined by an independent engineering review.

Simplifying assumptions related to the theoretical development of the Pbar and Ibar scaling terms are discussed in Section 4.0, which include some numerically determined, "back-calculated" adjustment factors. Error related to the Pbar and Ibar scaling terms will be assessed in this section by comparing scaled P-i curves developed for different components with the same component type, response mode, and response level, which should ideally be identical, and by unscaling the scaled P-i curves for given components and comparing them to unscaled P-i curves developed directly from SDOF calculations that do not involve the scaling and unscaling procedures in CEDAW. P-i curves developed directly from SDOF calculations are significantly more laborious and time consuming than unscaling the appropriate scaled P-i curves in CEDAW, but they can be calculated with automated processes such as that within the SBEDS workbook.

7.1 Comparisons of Unscaled P-i Diagrams from CEDAW and Directly from SDOF Calculations

The scaled P-i curves in the CEDAW methodology can be unscaled for a given structural component, as described in Section 2.0. Ideally, these unscaled curves would be identical to P-i curves generated for the same component and response criteria with iterative SDOF-based analyses. Figure 50 shows a P-i diagram generated for a typical corrugated steel panel with a 5 ft span and fixed-simple boundary conditions using the SBEDS workbook (Nebuda and Oswald, 2004). This spreadsheet performs iterative SDOF-based analyses to determine a full range of

blast loads, in terms of the positive phase peak pressure and impulse, which cause a constant input target component deflection. The effects of negative phase blast pressures from the charge weight-standoff combinations causing each blast load are included in the SDOF analyses. Target deflections were input into SBEDS to cause the non-dimensional response criteria in Table 3 for HLOP, MLOP, LLOP, and VLLOP response for the applicable component type.

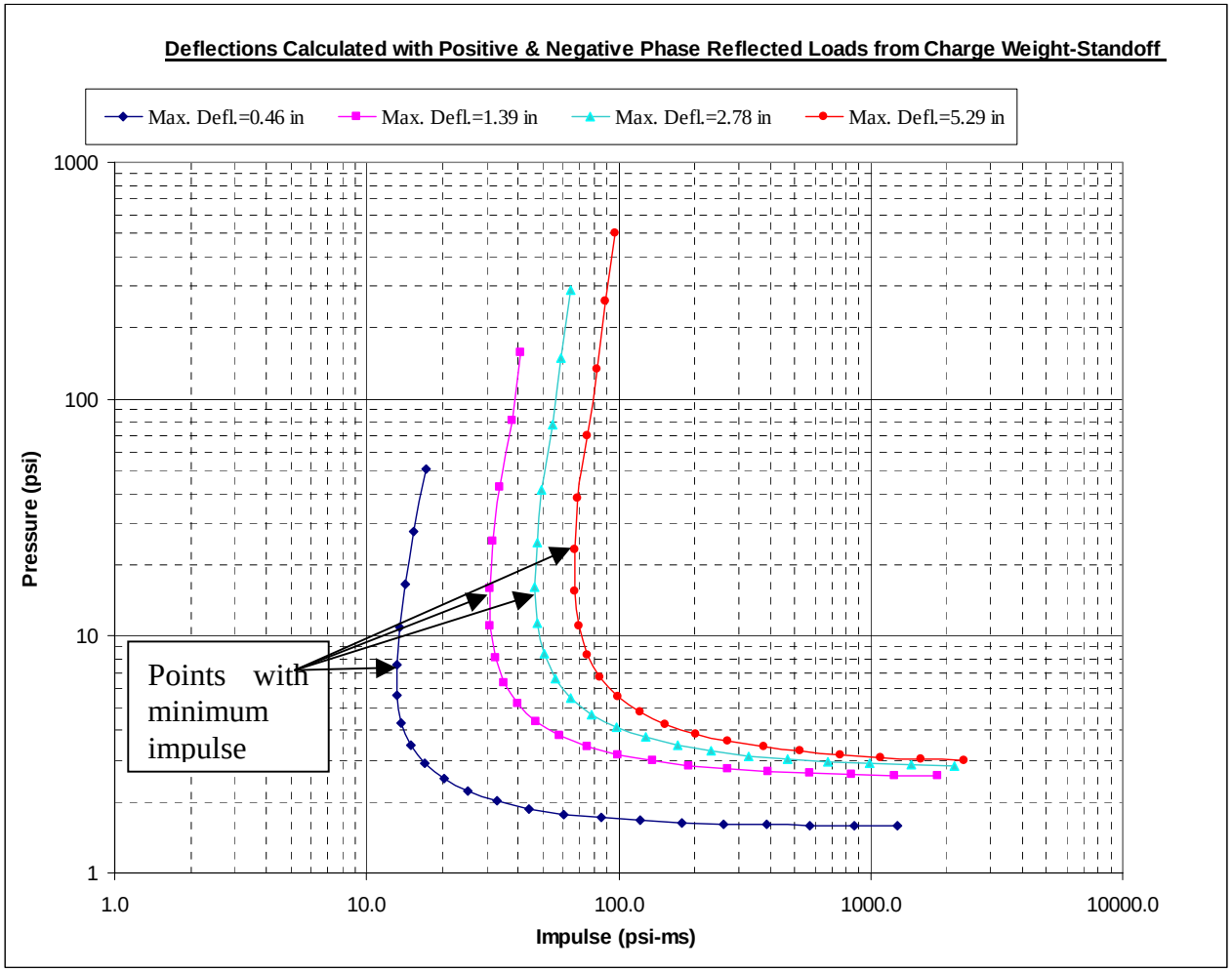

Figure 50. P-i Diagram Calculated Using SDOF Analyses for Corrugated Steel Panel

Figure 51 shows the unscaled P-i diagram generated by CEDAW for the same input corrugated steel component by unscaling the scaled P-i curves for this component type that are shown in Section 6.1. As discussed in the introductory part of Section 6.0, the unscaled P-i curves for each LOP of some component types, including corrugated steel panels, can be controlled by either ductility or support rotation criteria, whichever case causes lower blast loads to be associated with the given LOP. The applicable ductility or support rotation criteria from Table 3 that causes the controlling unscaled P-i curve for each LOP is calculated within the CEDAW workbook and these response parameters are used with the input component properties to determine the target deflections for each LOP used to calculate the comparable P-i curves in SBEDS. In the case

illustrated in Figure 51, the ductility ratio criteria for corrugated steel panels from Table 3 panels controlled all LOP except VLLOP.

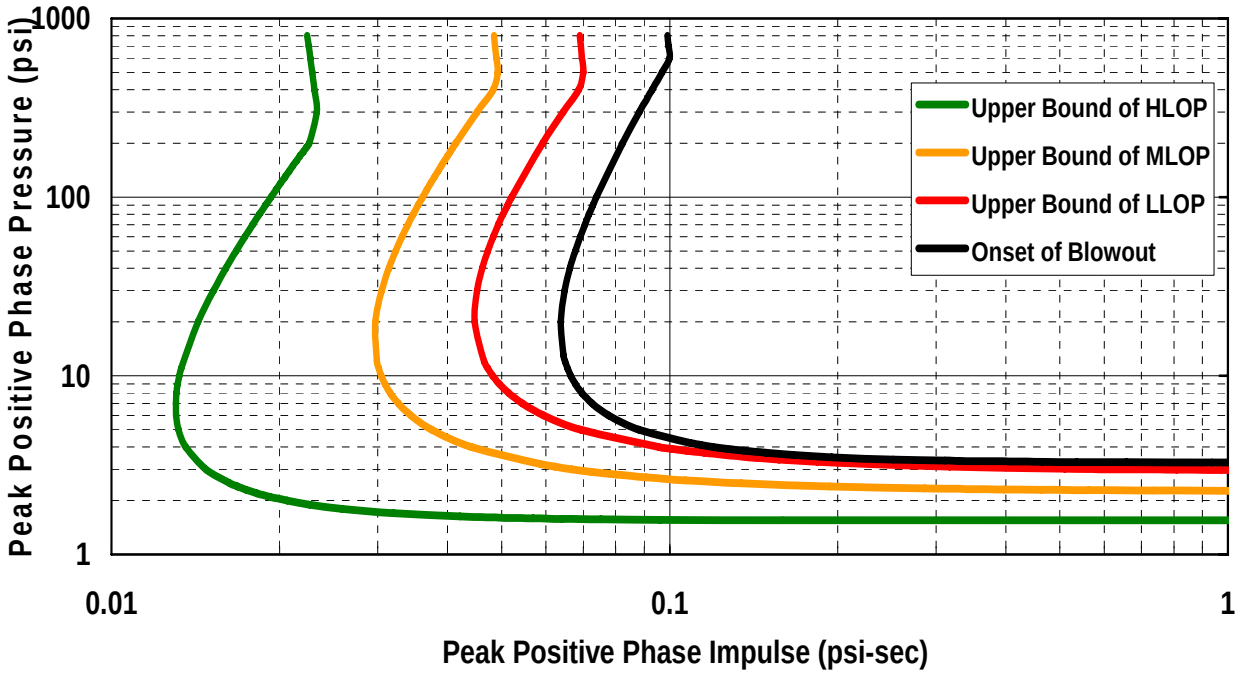

Figure 51. P-i Diagram Calculated with CEDAW for Corrugated Steel Panel

Comparable P-i diagrams for representative components of each component type were generated with iterative SDOF analyses in SBEDS and with CEDAW, such as those in Figure 50 and Figure 51. Both English and metric units cases were compared to check the capability of the CEDAW workbook to consistently calculate results using both units systems programmed into the workbook. P-i diagrams were generated for unreinforced masonry walls with different ratios of resistances from axial load arching and flexure because the CEDAW curve-fits for this component type are dependent on this ratio as discussed in Section 3.0 and Section 4.3. P-i diagrams were also generated for components spanning in both one and two directions for reinforced concrete slabs and unreinforced masonry walls, which are the two component types in CEDAW that can have both one-way and two-way spans.

The curves on the pairs of comparable P-i diagrams from SBEDS and CEDAW, such as those in Figure 50 and Figure 51, were compared at three points: 1) the pressure values at the pressure asymptote, 2) the pressure and impulse values at the point of minimum impulse, and 3) the impulse values at the same high pressure value - typically equal to 100 psi. These three points are illustrated in Figure 50. Comparisons at these three points showed that pressure and impulse values calculated with CEDAW are almost always within 15% of comparable values calculated directly with iterative SDOF-based calculations using SBEDS. This is least true for the pressure point on the minimum impulse point of the P-i diagrams, but this point is the most difficult to define since the P-i curves are relatively flat in this region. All comparisons were made by "eyeballing" points from printed P-i diagrams. The only general trend in the comparisons is for CEDAW to slightly overestimate the pressure value of the minimum impulse point.

Table 7 shows the averages and standard deviations of the ratios of impulses and pressures calculated at comparable points on the P-i curves from comparable analyses of twenty-five components covering the full range of component types, response modes, and unit systems. Typically, each component was compared for four different curves, representing HLOP through VLLOP. See Appendix K for more details on each compared component.

Table 7. Statistical Summary of Comparison of P-i Diagrams Calculated with CEDAW and SDOF Analyses

Statistical Parameter	Pressure Asymptote Comparison	Point of Minimum Impulse Comparison		High Pressure Value Comparison
	Pressure Ratio*	Impulse Ratio*	Pressure Ratio*	Impulse Ratio*
Average	0.98	1.10	1.01	0.99
Standard Deviation	0.09	0.17	0.09	0.08
* Ratio of CEDAW value/SDOF value				

7.2 Comparisons of Scaled P-i Curves for Similar Component Response

The process of creating scaled P-i curves based on SDOF analyses with a given constant component response level is described in Section 2.0 and illustrated in Figure 2. Ideally, scaled P-i curves developed from SDOF analyses for different components of the same component type, response level, and non-dimensional response level should be identical. It is important that the scaling is performed with Pbar and Ibar terms that were developed with a theoretically-based approach for the given response mode and non-dimensional response type (i.e., ductility ratio or support rotation) and that the blast load histories required to cause the given response level in the two components have the same basic shape. Any non-uniformity in the blast load shapes or simplifications and approximations involved in the theoretical development of the non-dimensional scaling terms will potentially cause differences between the scaled P-i curves.

Mathematical approximations in the development of the equations for the Pbar and Ibar scaling terms, which are used to create the scaled P-i curves, are described in Section 4.0. The approximations are most significant for the two most complex response modes of brittle flexure with arching from axial load, which is assumed for unreinforced masonry components, and ductile flexure with tension membrane response, which is assumed for light steel components. The Pbar and Ibar equations for these response modes include numerical terms that were back-calculated to cause the scaled P-i curves developed from SDOF analyses for different components with these response modes and identical response levels to be nearly the same. It is very possible that if components with somewhat different properties were used in the back-calculation process, somewhat different values would have been back-calculated for these numerical terms. Since this potential problem existed, an effort was made to base the back-calculations process on components with a relatively broad range of properties that were all considered within the range of "typical" properties for the given component type. However, the work described in this section was done after the Pbar and Ibar terms were developed and programmed into the CEDAW workbook and involved arbitrarily different component properties for the comparison of scaled P-i curves.

Figure 52 through Figure 56 show comparisons of scaled P-i diagrams for each of the different

Pbar and Ibar scaling terms used in CEDAW and described in Section 4.0. The diagrams are illustrative of the trends shown inAppendix L, which contains many more comparisons. The comparisons were made for components with a variety of spans, thicknesses, mass, strength and stiffness terms. The SDOF parameters and the response levels for each of the cases in these comparison analyses are shown in each figure and in Appendix L.

In each case, the scaling is done with the relevant Pbar and Ibar scaling equations for the response mode and response parameter type (i.e., ductility ratio or support rotation), as shown in Table 2. The trends noted in these comparisons are summarized in Table 8. Figure 55 and Figure 56 show scaled P-i curves for unreinforced masonry components responding in brittle flexural with arching from axial load. As described in Equation 2, the scaled P-i curve-fits for this case are a function of the peak resistance from axial load arching divided by the ultimate flexural resistance. As shown in the information boxes at the top of these figures, this ratio is different for each case and therefore there are different CEDAW scaled P-i curves representing the same response levels for each case in the figures. Ideally, the points in the figures representing from the SDOF analyses for all cases would lie along the CEDAW curves. As shown in Figure 55 and Figure 56, this is most true for ultimate flexural resistances (Ru) in the range of 0.7 psi to 2 psi, which is the range for most unreinforced walls, for the full range of resistances from axial load arching (Ra).

Case	Ductility Ratio	Ru (psi)	K (psi/in)	Mass (psi-ms^2/in)
Case 1	3	11.804	4.3467	1500
Case 2	3	4.8567	2.4839	1500
Case 3	3	2.1585	0.4906	1500
Case 4	3	1.1101	0.1854	1500

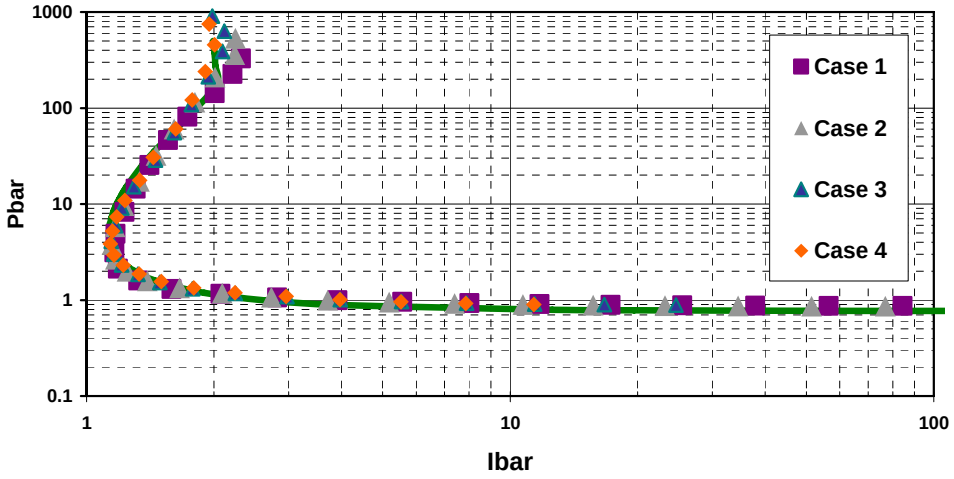

Figure 52. Comparison of Scaled P-i Curves Based on Ductility Ratio for Steel Beams with LOP Response

Case	Support Rotation	Ru (psi)	K (psi/in)	Mass (psi-ms^2/in)
Case 1	5	0.325	0.34483241	1336.787565
Case 2	5	0.7752	0.84187599	1336.787565
Case 3	5	1.3781	2.66074388	1336.787565
Case 4	5	7.3785	107.760127	2673.57513

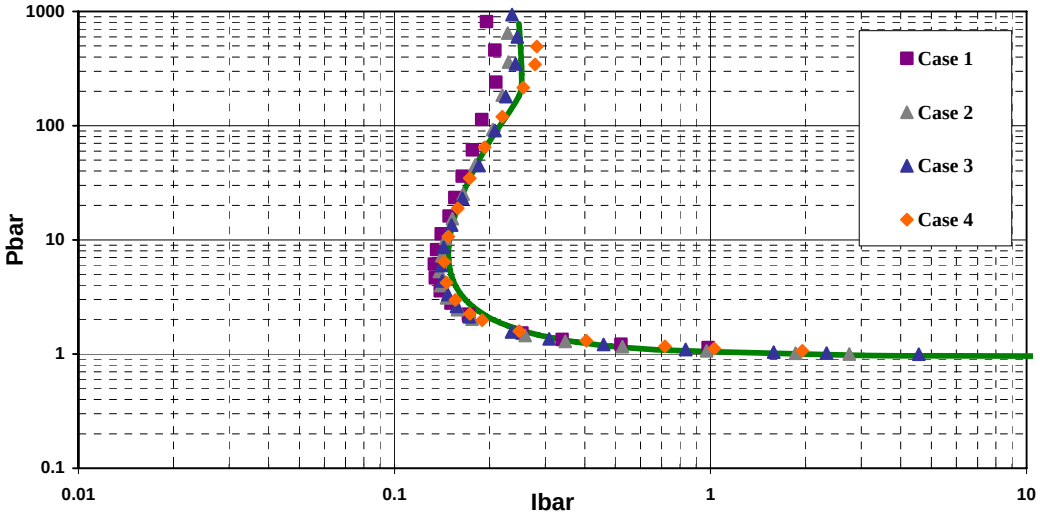

Figure 53. Comparison of Scaled P-i Curves Based on Support Rotation for Reinforced Concrete Slabs for MLOP Response (Uniform Load and Simple Supports)

Case	Support Rotation	Ru (psi)	K (psi/in)	Mass (psi-ms^2/in)	Ktm (psi/in)
Case 1	12	0.2666481	0.0693236	913.4283247	0.0463
Case 2	12	0.5605671	0.2019133	913.4283247	0.0463
Case 3	12	0.9965638	0.6381459	913.4283247	0.0823
Case 4	12	3.7707819	2.8362038	927.3172136	0.3292

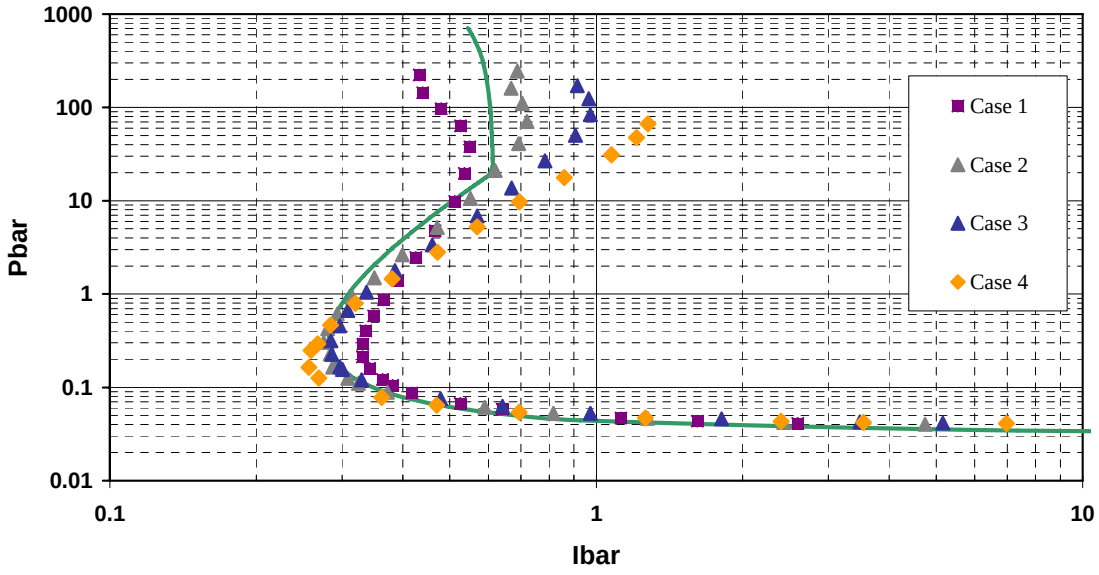

Figure 54. Comparison of Scaled P-i Curves For Cold-formed Beams with Significant Tension Membrane for LLOP Response

Case	Support Rotation	Ru (psi)	K (psi/in)	Mass psi-ms^2/in)	Ra/Ru
Case 1	4.00	0.82	18.89	665.66	0.08
Case 2	4.00	0.82	18.89	665.66	0.34
Case 3	4.00	0.82	18.89	665.66	0.60
Case 4	4.00	0.82	18.89	665.66	1.11

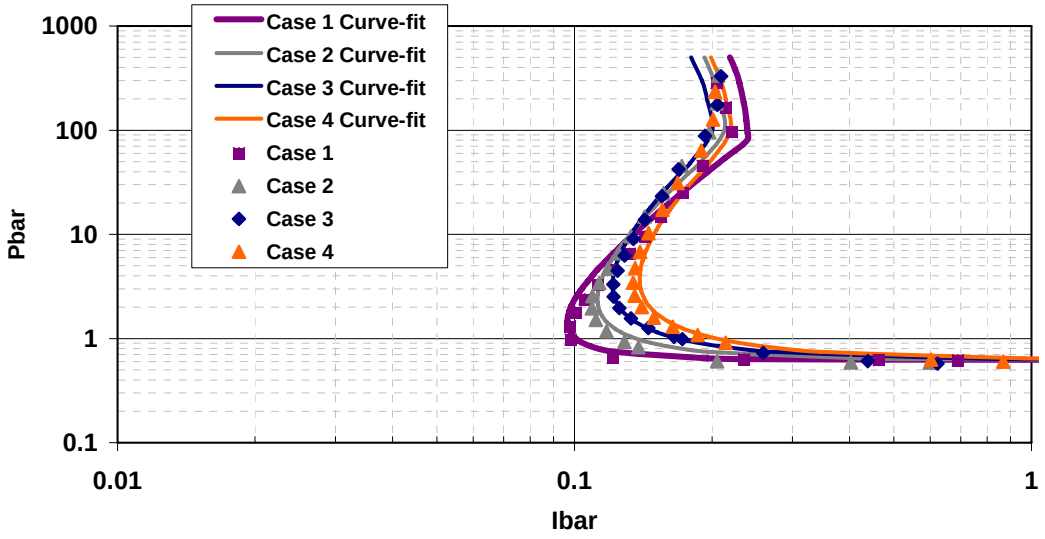

Figure 55. Comparison of Scaled P-i Curves Controlled for Unreinforced Masonry Wall with Constant Ultimate Resistance and Variable Axial Load for LLOP Response

Case	Support Rotation	Ru (psi)	K (psi/in)	Mass psi-ms^2/in)	Ra/Ru
Case 1	4.00	0.38	8.74	665.66	0.14
Case 2	4.00	0.82	18.89	665.66	0.34
Case 3	4.00	1.83	86.76	665.66	0.53
Case 4	4.00	3.00	223.41	665.66	0.95

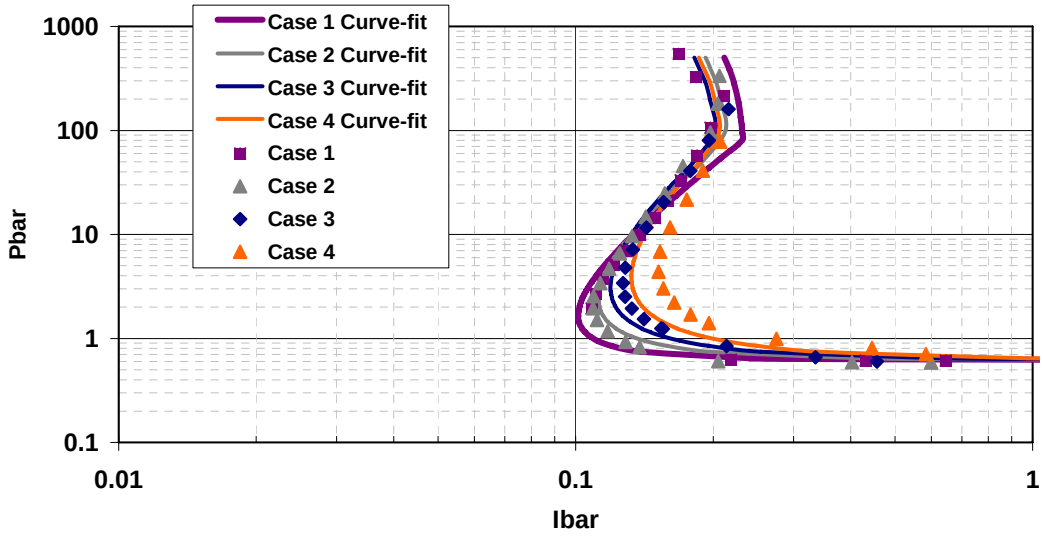

Figure 56. Comparison of Scaled P-i Curves Controlled for Unreinforced Masonry Wall with Variable Ultimate Resistance and Axial Load for LLOP Response

Table 8. Trends From Comparisons of Scaled P-i Curves

Response Mode	Response Parameter Type	Comparisons of Scaled P-i Curves for Different Components	Comment
Flexure	Ductility ratio	Very good agreement between scaled P-i curves except minor divergence at very high scaled Pbar values (>100).	Pbar and Ibar equations had no simplifying assumptions. Divergence at high Pbar probably due to dependence of short duration load shape on ultimate resistance (Ru).
Flexure	Support Rotation	Very good agreement between scaled P-i curves except some divergence at very high scaled Pbar values (>100).	Pbar and Ibar equations had only a few assumptions that were very good approximations for higher levels response (i.e., greater than HLOP). Same comment as above for Pbar divergence.
Flexure and tension membrane	Support Rotation	Very good agreement at low Pbar values. Up to 30% divergence in mid Pbar region (1 < Pbar < 10) and relatively large divergence in high Pbar region. Selected curve-fit is generally conservative.	Pbar and Ibar equations had significant approximations. The cases of Pbar < 10 covers the broad range of practical situations for light gauge steel beams and joists except for small explosions close-in to component (10-30 lbs at less than 20 ft standoff).
Brittle flexure with axial load arching	Support Rotation	Very good agreement for components with 0.7 psi < R_U < 2 psi and wide range of axial load. Up to 30%-40% divergence for significantly higher or lower resistance with axial load, particularly for very large resistance.	Pbar and Ibar equations had significant approximations. However, scaled curve-fits are accurate for cases with most typical ultimate resistance values for one-way and two-way unreinforced masonry walls (0.5 psi < R_U < 2 psi).

8.0 SUMMARY, CONCLUSIONS, AND RECOMMENDED FUTURE WORK

The CEDAW workbook generates pressure-impulse (P-i) diagrams and charge weight-standoff graphs that are used to determine the Level of Protection (LOP) provided by an input structural component loaded by blast from an input equivalent TNT charge weight and standoff. The P-i diagrams and charge weight-standoff graphs in CEDAW are generated by "unscaling" P-i curves defining regions of constant LOP response on scaled P-i diagrams for fourteen different common structural component types. The scaled P-i curves are made up of points defined by the positive phase peak pressures and impulses of blast loads with a full range of load durations that all cause a given response level in single-degree-of-freedom (SDOF) analyses of a representative component for the given structural component type, which are scaled with Pbar and Ibar equations to create generalized scaled blast loads that apply for all components of the given component type. The resistance-deflection relationships used in the SDOF analyses are consistent with response modes for each component type that are assumed to typically dominate blast load response of typical components for that component type, including flexural, tension membrane, concrete shear, and masonry arching response. The blast loads in the SDOF analyses were determined from a full range of charge weight-standoff combinations, starting with a short standoff distance and progressing to very large distances, that produced the given response levels considering both positive and negative phase loads. The Pbar and Ibar equations used to scale the blast loads from the SDOF analyses were developed from conservation of energy equations with some simplifying assumptions. The response levels in the SDOF analyses, which represent the response levels causing the upper and lower bounds of each LOP response level, were developed based primarily on available blast test data for each component type.

The most important steps in the development of the scaled P-i curves were the selection of the response levels for the SDOF analyses corresponding to the upper and lower ranges of each LOP for each component type (i.e., the response criteria) and the development of the Pbar and Ibar equations. The response criteria were determined using available scaled blast testing data and engineering judgment. Relevant data from blast tests where the blast loads, component properties, and LOP of the tested component were known, were scaled using the applicable Pbar and Ibar term scaling equations for the component type. These scaled data points were plotted against scaled P-i curves created with SDOF analyses using a range of different response levels expressed as ductility ratios or support rotations, depending on the non-dimensional response parameter type considered most applicable for the given component type. The response parameter values used for the SDOF analyses were varied until the corresponding scaled P-i curves defined approximate upper and lower boundaries for scaled data points with each LOP, considering the scatter in the data.

The Pbar and Ibar scaling equations were developed using a conservation of energy approach, where the strain energy from the dynamic response of a generic component was set equal to the work energy from a long duration blast load, which only involves the peak pressure of the blast load, and to the kinetic energy of a short duration blast load, which only involves the impulse of the blast load. These two energy equivalency equations representing the two extreme loading cases of very long duration and very short duration blast loads were each rearranged mathematically in the form of a non-dimensional load term (i.e., Pbar and Ibar) that is a function

of a non-dimensional response parameter (i.e., the ductility ratio of support rotation). The Pbar and Ibar terms, or equations were developed in this manner with two types of response parameters (i.e. ductility ratio or support rotation) and with strain energy terms corresponding to four response modes. The Pbar and Ibar terms associated with the response parameter type(s) and response mode considered the most applicable for each component type, based on available test data and commonly accepted blast analysis practice, were used to develop the scaled P-i curves for that component type. Tension membrane response was included in the strain energy equations used to develop Pbar and Ibar equations for light, cold-formed structural components and open web steel joist components well attached to framing components. Arching response from axial load was included in the strain energy equations used to develop the Pbar and Ibar equations for unreinforced masonry components. Concrete shear and connection shear response were included for the development of Pbar and Ibar equations for reinforced concrete and steel columns. Flexural response was assumed to occur with each of these response modes and to be the only dominant response mode for all other component types.

The development of the Pbar and Ibar term equations is discussed in Section 4.0. The P-i curves are fit through points defined by Pbar and Ibar values from SDOF analyses using curve-fit equations described in Section 3.0. The scaled P-i curves that form the best upper and lower bound limits for each LOP response of each component type, and the response levels in the SDOF analyses used to develop these scaled P-i curves (i.e., the response criteria for each LOP and component type), are discussed in Section 6.0. Detailed information on the available test data used to determine the response criteria, as discussed in Section 6.0, is provided in separate appendices for each component type. The accuracy of the Pbar and Ibar scaling terms is discussed for each component type in Section 7.2 and Appendix L by comparing scaled P-i curves developed for sets of different components with same component type, response mode, and response level. The scaled P-i curves for each set of components, which ideally would be identical, were typically within 20% of each other, especially for components that had the most typical properties for each component type.

The CEDAW workbook "unscales" the upper bound scaled P-i curves for each LOP for the component type of an input component. The Pbar and Ibar values of each point on the appropriate scaled P-i curves are "unscaled" into corresponding positive phase peak pressure and impulse values using the input component properties in the applicable Pbar and Ibar term equations. The workbook plots points based on these peak pressure and positive phase impulse values that are connected to create unscaled P-i curves for the upper bound of each LOP, which are only applicable for the input component. The CEDAW workbook also plots points defined by the charge weight and standoff causing the peak pressure and impulse of each point on the unscaled P-i curves for free-field and fully reflected conditions to create curves defining upper bound charge weight-standoff combinations for each LOP for the input component. Section 7.1 shows comparisons between unscaled P-i curves from the CEDAW workbook and P-i curves generated for the same component and response criteria with iterative SDOF-based analyses. A total of 100 comparisons for 25 components that included representative components for each component type and LOP showed that the approximate CEDAW curves and more exact curves calculated directly with iterative SDOF analyses were are almost always within 15%. Details of the comparisons are shown in Appendix K.

8.1 Recommended Future Work

The following tasks are recommended as future work to improve the CEDAW methodology and the application of this methodology to building blast assessment.

1. Perform testing to help define response criteria for each LOP for component types with very little or no available blast test data. These component types include metal stud walls, hot-rolled steel beams, reinforced concrete beams, light roof systems including open web steel joists, and two-way spanning reinforced concrete walls. More data for one-way reinforced concrete panels and wood walls are also needed to better define the response criteria for these component types.
2. Identify component types that typically respond together dynamically as systems, such as corrugated steel panels and lightweight steel girts/purlins, and develop scaled P-i curves for the overall system. In many cases, dynamic interactions between supported and supporting components of component systems acting together cause assumptions of SDOF based analyses to be inaccurate and overly conservative. Multi degree-of-freedom analyses, which have at least one degree-of-freedom representing each component in the system, or non-linear dynamic finite element analyses may be needed to develop these scaled P-i curves. Also, development of scaling terms that capture enough of the variables from the multi-component system to be effective, but are not too complicated and therefore impractical, will be necessary.
3. Perform more testing for all component types that can be used to define better response criteria associated with failure and post-failure component response, including the VLLOP response level and possibly an additional more severe response level. These response levels contribute most to injuries of building occupants. However, most blast component testing has focused on pre-failure component response.
4. Improve the component LOP descriptions to be more specific for each component type, or for given groups of component types, and include photographs illustrating different LOP response levels for different component types.
5. Establish a relationship between component LOP response levels and an overall building LOP. This relationship should consider the importance of given components to the overall building stability along with the LOP of the component. It should also describe the building damage and percentage of occupant injuries within the damage zone of the building, rather than for the building as a whole, and possibly provide information on the approximate size of the damage zone. This will help make the building LOP descriptions equally applicable for large and small buildings.

9.0 REFERENCES

ASCE Task Committee on Blast Resistant Design, *Design of Blast Resistant Buildings in Petrochemical Facilities*, American Society of Civil Engineers, N.Y., N.Y., 1997.

Bogozian, D.D., and Dunn, B., *"Analysis and Retrofit Designs for Lightweight Steel Roofs Exposed to Blast Loads,"* Report No. TR-00-02.2 Performed by Karagozian and Case for the U.S. Army Engineering Research and Development Center, July, 2000.

Colthorp, D.R., Vitayaudom, K.P., and Kiger, S.A., "*Semihardened Facility Design Criteria Improvement,*" Report No. ESL-TR-85-32 Performed by U.S. Army Waterways Experiment Station for Engineering and Services Laboratory at Tyndall AFB, September, 1985.

Departments of the Army, the Navy and the Air Force, *Structures to Resist the Effects of Accidental Explosions*, Department of the Army Technical Manual TM 5-1300, Department of the Navy Publication NAVFAC P-397, Department of the Air Force Manual AFM 88-22, November 1990.

Department of the Army, "*Design and Analysis of Hardened Structures to Conventional Weapons Effects* (DAHS CWE)," Army Technical Manual TM 5-855-1, November 1997.

Federal Emergency Management Agency (FEMA), "*The Oklahoma City Bombing,*" FEMA 277, August 1996.

Forsèn, R., "*Airblast Loading of Wall Panels,*" Swedish Defense Research Institute (FOA) Report C-20586-D6, October, 1985.

Forsèn, R., "*Increase of In-Plane Compressive Forces Due to Inertia in Wall Panels Subjected to Blast Loading,"* Swedish Defense Research Institute (FOA) Report C-20769-2.3,2.6, October, 1989.

Johnston, B. G., "*Damage to Commercial and Industrial Buildings Exposed to Nuclear Effects,*" Federal Civil Defense Administration, Report WT-1189, February, 1956.

Jones, Patricia, "*WAC: An Analysis Program for Dynamic Loading on Masonry and Reinforced Concrete Walls,*" Submitted to Faculty of Mississippi State University in Partial Fulfillment of the Requirement for the Degree of Master of Science in the Department of Civil Engineering, December, 1989.

Marchand, K. A., "*BAIT, BASS & RODS Testing Results,*" Prepared for the USAF Force Protection Battlelab by Applied Research Associates, Report within 12-CD set issued by The Technical Support Working Group (TSWG) and Defense Threat Reduction Agency (DTRA), April, 2002.

Nebuda, D. and Oswald, C.J.,"SBEDS (Single degree of freedom Blast Effects Design Spreadsheets)," Proceedings from the 31st DoD Explosives Safety Seminar, San Antonio, Texas, August, 2004.

Oswald, C.J., "*Facility And Component Explosive Damage Assessment Program (FACEDAP) User's Manual*," Prepared by Southwest Research Institute for the Department of the Army, Corps of Engineers, Omaha District, CEMRO-ED-ST, Contract No. DACA 45-91-D-0019, April, 1993.

Oswald, C. J., Lowak, M. J., Harrison, B.F., "*Handbook for Blast Capacity Upgrades of Metal Buildings,*" prepared for 1997 Technology Cooperative, Wilfred Baker Engineering, Inc., San Antonio, TX, 1998.

Plamondon, M.A. and Sheffield, C., "DIVINE BUFFALO 6 - Results of Structural Response and Window Experiments," Prepared for Defense Threat Reduction Agency by Applied Research Associates, Report No. ARA-LR-2.08-005, June 1999.

Salim, H.A., Dinan, R., Kiger, S.A., Townsend, P.T., and Shull, J., "*Blast Retrofit Wall Systems Using Cold-Formed Steel Studs,*" Presented at the 16th ASCE Engineering Mechanics Conference, University of Washington, July 16-18, 2003.

Stanley, M. and Osowski, J., "*COTS Blast Modeling and Visualization for Vulnerability Assessment*," Final Technical Report for Boeing-Autometric Inc., Contract No. 54145-41043, September 11, 2002.

Stea, W., Dobbs, N., Weissman, S., Price, P., and Caltagirone, J., "*Blast Capacity Evaluation of Pre-Engineered Building,*" US Army Armament Research and Development Command, Weapon Systems Laboratory, Contractor Report ARLCD-CR-79004, March, 1979.

Stea, W., Sock, F.E. and Caltagirone, J., "*Blast-Resistant Capacities of Cold-Formed Steel Panels,*" US Army Armament Research and Development Command, Weapon Systems Laboratory, Contractor Report ARLCD-CR-81001, May 1981.

SPAN32 Code Version 1.3, Sponsored by US Army Corps of Engineers and Defense Special Weapons Agency, POC Mr. W. F. Seipel, CEMRO-ED-SH, December, 2001.

Townsend, T, "*EWRP-7 Steel Stud Wall Overview,*" (Powerpoint presentation) Provided by the Protective Design Center at the U.S. Army Corps of Engineers, Omaha District.

Varma, R.K., Tomar, C.P.S., Parkash, S., and Sethi, V.S., "*Damage to Brick Masonry Wall Panels Under High Explosive Detonations,*" PVP-Vol. 351, Stuctures Under Extreme Loading Conditions, ASME, 1977.

Wesevich, J.W., Oswald, C. J., Edel, M.T., Lowak, M. J., Alaoui, S. S., "*Compile and Enhance Blast Related CMU Wall Test Database* (CMUDS)," Prepared for the Office of Special Technology by Wilfred Baker Engineering, Inc., Contract No. 41756-00-C-0900, September 6, 2002.

Wright, S.J., "*Scaled Testing and Analysis of Concrete Buildings and Components*," Naval Air Warfare Center Weapons Division Report No. NAWCWPNS TM 7554, April, 1993.

APPENDIX A.
DATA FROM SHOCK LOADING TESTS ON ONE-WAY SPANNING UNREINFORCED MASONRY WALLS

Table A-3 shows data from the CMUDS database (Wesevich et al, 2002) that was scaled using the $Pbar_{URM}$ and $Ibar_{URM}$ terms in Equation 10. These terms are called out as Pbar and Ibar values in Table A-3. Detailed information on tests in the CMUDS database are included in reports hot-linked to the CMUDS computer program distributed by TSWG and the U.S. Department of Defense. The Pbar and Ibar values in Table A-3 are plotted against scaled P-i curves in Section 6.8. All the data is for simply supported walls. Also, all the data only has self-weight axial loading from the wall above midspan, no additional axial loads were applied. The majority of the data is ungrouted CMU walls. The LOP were assigned to each data point using the relationship in Table A-1 between the CMUDS damage levels and component LOP. This relationship is based on the definitions of the CEDAW component LOP (Levels of Protection) in Table 1 and the CMUDS damage descriptions for unreinforced masonry without arching in column two in Table A-2.

Table A-1. Assumed Relationship Between CMUDS Damage Levels and CEDAW Component LOP

CMUDS Damage Level	LOP
1	MLOP
2	LLOP
3	VLLOP
4	Blowout

Table A-2. CMUDS Damage Levels Descriptions for Masonry

Damage Level	Unreinforced Without Arching	Unreinforced with Arching	Reinforced	Qualitative Response
1	Hairline cracks, no noticeable permanent deflections	Permanent deflections not exceeding 0.15h	Peak dynamic and residual support rotations not exceeding 7 and 1 degrees, respectively	Reusable
2	Wall is still standing, significant cracking with noticeable permanent deflections	Wall is still standing, permanent deflections exceed 0.15h	Peak dynamic and residual support rotations exceed 7 and 1 degrees, respectively	Replace
3	A major portion of the wall has fallen to the ground either immediately in front or behind the wall's original configuration	A major portion of the wall has fallen to the ground either immediately in front or behind the wall's original configuration	A major portion of the wall has fallen to the ground either immediately in front or behind the wall's original configuration	Collapse
4	Significant wall debris velocities are generated	Significant wall debris velocities are generated	Significant wall debris velocities are generated	Blowout

Table A-3. Data for One-Way Spanning Unreinforced Masonry Walls

Origin	Test No.	L (in)	B (in)	h (in)	fm (psi)	ft (psi)	ts (in)	W (psi)	Grout	Ieff (in^4)	S (in^3)	E (psi)	M (lb-in)	R_A (psi)	Ru (psi)	K (psi/in)	Mass ($psi-ms^2/in$)	R_A/Ru	P (psi)	I (psi-ms)	Pbar	ibar	LOP
EMRTC	97-2	84	16	7.63	2400.00	240.00	1.25	0.24	0%	406.4	127.5	2.40e6	30600	0.09	2.17	94	630	0.04	64.0	89	29.5	0.18	LLOP
EMRTC	1	93	16	5.625	2000	200	1	0.42	100%	237.3	84.4	2.00e6	16875	0.10	0.98	31	1080	0.10	270.0	257	276.8	0.41	VLLOP
EMRTC	2	93	16	5.625	2000	200	1	0.42	100%	237.3	84.4	2.00e6	16875	0.10	0.98	31	1080	0.10	38.0	31	39.0	0.05	MLOP
EMRTC	3	93	16	5.625	2000	200	1	0.42	100%	237.3	84.4	2.00e6	16875	0.10	0.98	31	1080	0.10	65.0	75	66.6	0.13	LLOP
EMRTC	4	93	16	5.625	2000	200	1	0.42	100%	237.3	84.4	2.00e6	16875	0.10	0.98	31	1080	0.10	80.0	134	82.0	0.23	LLOP
EMRTC	7	93	16	5.625	2000	200	1	0.42	100%	237.3	84.4	2.00e6	16875	0.10	0.98	31	1080	0.10	125.0	164	128.1	0.27	VLLOP
EMRTC	16	93	16	5.625	2000	200	1	0.42	100%	237.3	84.4	2.00e6	16875	0.10	0.98	31	1080	0.10	78.0	109	80.0	0.18	LLOP
EMRTC	17	93	16	5.625	2000	200	1	0.42	100%	237.3	84.4	2.00e6	16875	0.10	0.98	31	1080	0.10	225.0	252	230.6	0.40	Blowout
EMRTC	18	93	16	5.625	2000	200	1	0.42	100%	237.3	84.4	2.00e6	16875	0.10	0.98	31	1080	0.10	140.0	177	143.5	0.29	LLOP
ERDC	1	31	4	1.9	2300	230	0.4	0.08	0%	1.8	2.4	2.30e6	552	0.02	1.15	86	194	0.02	55.0	64	47.9	0.52	Blowout
ERDC	2	31	4	1.9	2300	230	0.4	0.08	0%	1.8	2.4	2.30e6	552	0.02	1.15	86	194	0.02	173.0	118	150.6	0.91	Blowout
ERDC	3	31	4	1.9	2300	230	0.4	0.08	0%	1.8	2.4	2.30e6	552	0.02	1.15	86	194	0.02	99.0	83	86.2	0.66	Blowout
ERDC	4	31	4	1.9	2300	230	0.4	0.08	0%	1.8	2.4	2.30e6	552	0.02	1.15	86	194	0.02	39.0	35	33.9	0.29	MLOP
ERDC	5	31	4	1.9	2300	230	0.4	0.14	100%	2.3	2.4	2.30e6	554	0.03	1.15	110	360	0.03	350.0	152	303.8	0.79	Blowout
ERDC	6	31	4	1.9	2300	230	0.4	0.14	100%	2.3	2.4	2.30e6	554	0.03	1.15	110	360	0.03	104.0	65	90.3	0.35	VLLOP
ERDC	7	31	4	1.9	2300	230	0.4	0.14	100%	2.3	2.4	2.30e6	554	0.03	1.15	110	360	0.03	201.0	104	174.5	0.55	Blowout
ERDC	8	31	4	1.9	2300	230	0.4	0.08	0%	1.8	2.4	2.30e6	552	0.02	1.15	86	194	0.02	52.0	44	45.3	0.36	VLLOP
ERDC	9	31	4	1.9	2300	230	0.4	0.14	100%	2.3	2.4	2.30e6	554	0.03	1.15	110	360	0.03	90.0	61	78.1	0.33	VLLOP
ERDC	21	31	4	1.9	2300	230	0.4	0.14	100%	2.3	2.4	2.30e6	554	0.03	1.15	110	360	0.03	63.0	42	54.7	0.23	MLOP
ERDC	23	31	4	1.9	2300	230	0.4	0.14	100%	2.3	2.4	2.30e6	554	0.03	1.15	110	360	0.03	44.0	28	38.2	0.16	LLOP
ERDC	27	31	4	1.9	2300	230	0.4	0.08	0%	1.8	2.4	2.30e6	552	0.02	1.15	86	194	0.02	41.0	35	35.7	0.29	LLOP
ERDC	39	31	4	1.9	2300	230	0.4	0.14	100%	2.3	2.4	2.30e6	554	0.03	1.15	110	360	0.03	29.0	23	25.2	0.13	MLOP
ERDC	41	31	4	1.9	2300	230	0.4	0.14	100%	2.3	2.4	2.30e6	554	0.03	1.15	110	360	0.03	44.0	32	38.2	0.18	MLOP
WBE	95-6	28	4	1.9	2000	200	0.4	0.08	0%	1.8	2.4	2.00e6	480	0.02	1.22	113	194	0.02	5.9	100	4.8	0.90	LLOP
WBE	95-7	28	4	1.9	2000	200	0.4	0.08	0%	1.8	2.4	2.00e6	480	0.02	1.22	113	194	0.02	4.6	23	3.8	0.21	VLLOP
WBE	95-8	28	4	1.9	2000	200	0.4	0.08	0%	1.8	2.4	2.00e6	480	0.02	1.22	113	194	0.02	3.1	40	2.5	0.37	Blowout
WBE	95-9	28	4	1.9	2000	200	0.4	0.08	0%	1.8	2.4	2.00e6	480	0.02	1.22	113	194	0.02	3.2	13	2.6	0.12	LLOP
WBE	95-11	28	4	1.9	2000	200	0.4	0.08	0%	1.8	2.4	2.00e6	480	0.02	1.22	113	194	0.02	4.3	20	3.5	0.18	LLOP
WBE	95-12	28	4	1.9	2000	200	0.4	0.08	0%	1.8	2.4	2.00e6	480	0.02	1.22	113	194	0.02	5.2	25	4.2	0.23	VLLOP
WBE	95-17	28	4	1.9	2000	200	0.4	0.08	0%	1.8	2.4	2.00e6	480	0.02	1.22	113	194	0.02	3.0	41	2.5	0.38	Blowout
WBE	95-18	28	4	1.9	2000	200	0.4	0.08	0%	1.8	2.4	2.00e6	480	0.02	1.22	113	194	0.02	1.4	17	1.1	0.16	LLOP
WBE	95-19	28	4	1.9	2000	200	0.4	0.08	0%	1.8	2.4	2.00e6	480	0.02	1.22	113	194	0.02	1.4	17	1.1	0.16	LLOP
WBE	95-20	28	4	1.9	2000	200	0.4	0.08	0%	1.8	2.4	2.00e6	480	0.02	1.22	113	194	0.02	1.5	18	1.2	0.17	VLLOP

Origin	Test No.	L (in)	B (in)	h (in)	fm (psi)	ft (psi)	ts (in)	W (psi)	Grout	Ieff (in^4)	S (in^3)	E (psi)	M (lb-in)	R_A (psi)	Ru (psi)	K (psi/in)	Mass ($psi-ms^2/in$)	R_A/Ru	P (psi)	I (psi-ms)	Pbar	ibar	LOP
WBE	95-21	28	4	1.9	2000	200	0.4	0.08	0%	1.8	2.4	2.00e6	480	0.02	1.22	113	194	0.02	3.1	15	2.5	0.14	LLOP
WBE	95-22	28	4	1.9	2000	200	0.4	0.08	0%	1.8	2.4	2.00e6	480	0.02	1.22	113	194	0.02	1.5	17	1.2	0.16	LLOP
WBE	95-23	28	4	1.9	2000	200	0.4	0.08	0%	1.8	2.4	2.00e6	480	0.02	1.22	113	194	0.02	3.0	12	2.5	0.11	LLOP
WBE	95-24	28	4	1.9	2000	200	0.4	0.08	0%	1.8	2.4	2.00e6	480	0.02	1.22	113	194	0.02	4.2	21	3.4	0.19	LLOP
WBE	95-26	28	4	1.9	2000	200	0.4	0.08	0%	1.8	2.4	2.00e6	480	0.02	1.22	113	194	0.02	1.5	15	1.2	0.14	VLLOP
WBE	95-27	28	4	1.9	2000	200	0.4	0.08	0%	1.8	2.4	2.00e6	480	0.02	1.22	113	194	0.02	3.5	36	2.9	0.33	Blowout
WBE	95-28	28	4	1.9	2000	200	0.4	0.08	0%	1.8	2.4	2.00e6	480	0.02	1.22	113	194	0.02	1.5	14	1.2	0.13	LLOP
WBE	95-29	28	4	1.9	2000	200	0.4	0.08	0%	1.8	2.4	2.00e6	480	0.02	1.22	113	194	0.02	1.5	16	1.2	0.15	LLOP
WBE	95-31	96	16	7.625	2000	200	1.25	0.22	0%	406.4	127.5	2.00e6	25500	0.07	1.38	46	576	0.05	2.1	31	1.5	0.08	MLOP
WBE	95-33	96	16	7.625	2000	200	1.25	0.22	0%	406.4	127.5	2.00e6	25500	0.07	1.38	46	576	0.05	4.2	77	3.0	0.19	VLLOP
WBE	95-35	96	16	7.625	2000	200	1.25	0.22	0%	406.4	127.5	2.00e6	25500	0.07	1.38	46	576	0.05	4.8	64	3.5	0.15	VLLOP
WBE	96-13	28	4	1.9	2000	200	0.4	0.10	50%	2.0	2.4	2.00e6	481	0.03	1.23	128	268	0.02	1.6	6	1.3	0.05	MLOP
WBE	96-13A	28	4	1.9	2000	200	0.4	0.10	50%	2.0	2.4	2.00e6	481	0.03	1.23	128	268	0.02	3.1	11	2.5	0.08	Blowout
WBE	96-14	96	16	7.625	2000	200	1.25	0.49	100%	591.1	155.0	2.00e6	31008	0.15	1.68	67	1259	0.09	3.6	50	2.1	0.07	MLOP
WBE	96-14A	96	16	7.625	2000	200	1.25	0.49	100%	591.1	155.0	2.00e6	31008	0.15	1.68	67	1259	0.09	6.0	95	3.6	0.13	MLOP
WBE	98-3	96	16	7.625	2000	200	1.25	0.22	0%	406.4	127.5	2.00e6	25500	0.07	1.38	46	576	0.05	2.1	60	1.5	0.15	VLLOP
WBE	98-4	96	16	7.625	2000	200	1.25	0.22	0%	406.4	127.5	2.00e6	25500	0.07	1.38	46	576	0.05	1.9	60	1.4	0.15	VLLOP
WBE	00-2	96	16	5.625	1720	200	1	0.18	0%	171.1	74.0	1.72e6	14800	0.04	0.80	17	468	0.05	1.0	15	1.2	0.06	MLOP
WBE	00-1	96	16	5.625	1720	200	1	0.18	0%	171.1	74.0	1.72e6	14800	0.04	0.80	17	468	0.05	0.3	11	0.4	0.04	MLOP
WBE	00-2A	96	16	5.625	1720	200	1	0.18	0%	171.1	74.0	1.72e6	14800	0.04	0.80	17	468	0.05	2.3	14	2.9	0.05	VLLOP
WBE	01-1	96	16	5.625	1970	200	1	0.18	0%	171.1	74.0	1.97e6	14800	0.04	0.80	19	455	0.05	4.1	34	5.1	0.12	VLLOP
WBE	01-2	96	16	5.625	1970	200	1	0.18	0%	171.1	74.0	1.97e6	14800	0.04	0.80	19	455	0.05	3.4	24	4.2	0.08	LLOP
WBE	02-15	96	16	5.625	1970	200	1	0.18	0%	171.1	74.0	1.97e6	14800	0.04	0.80	19	455	0.05	3.7	27	4.5	0.09	VLLOP
WBE	02-16	96	16	5.625	1970	200	1	0.18	0%	171.1	74.0	1.97e6	14800	0.04	0.80	19	455	0.05	3.3	21	4.0	0.07	LLOP
WBE	02-17	96	16	5.625	1970	200	1	0.18	0%	171.1	74.0	1.97e6	14800	0.04	0.80	19	455	0.05	4.1	41	5.0	0.14	VLLOP
WBE	02-18	96	16	5.625	1970	200	1	0.18	0%	171.1	74.0	1.97e6	14800	0.04	0.80	19	455	0.05	1.3	39	1.6	0.14	VLLOP
WBE	02-19	96	16	5.625	1970	200	1	0.18	0%	171.1	74.0	1.97e6	14800	0.04	0.80	19	455	0.05	0.6	19	0.7	0.07	LLOP
WBE	02-20	96	16	5.625	1970	200	1	0.18	0%	171.1	74.0	1.97e6	14800	0.04	0.80	19	455	0.05	8.5	59	10.6	0.19	VLLOP
WBE	02-21	46	16	5.625	1970	200	1	0.18	0%	171.1	74.0	1.97e6	14800	0.09	5.25	753	455	0.02	2.4	75	0.5	0.15	LLOP
WBE	02-22	46	16	5.625	1970	200	1	0.18	0%	171.1	74.0	1.97e6	14800	0.09	5.25	753	455	0.02	4.0	117	0.8	0.25	Blowout
DB2	2	144	16	5.625	2000	200	1	0.22	100%	237.3	84.4	2.00e6	16875	0.03	0.61	11	558	0.06	8.0	60	13.1	0.16	VLLOP
URS *	11	102	16	7.62	2387	238.7	n/a	0.56	n/a	589.9	154.8	2.39e6	36960	0.17	1.78	63	1439	0.09	3.0	240	1.7	0.30	Blowout
URS	12	102	16	7.62	2387	238.7	n/a	0.56	n/a	589.9	154.8	2.39e6	36960	0.17	1.78	63	1439	0.09	3.4	272	1.9	0.34	Blowout
URS	13	102	16	7.62	2387	238.7	n/a	0.56	n/a	589.9	154.8	2.39e6	36960	0.17	1.78	63	1439	0.09	3.4	272	1.9	0.34	Blowout
URS	14	102	16	7.62	2387	238.7	n/a	0.56	n/a	589.9	154.8	2.39e6	36960	0.17	1.78	63	1439	0.09	3.6	288	2.0	0.36	Blowout

Origin	Test No.	L (in)	B (in)	h (in)	fm (psi)	ft (psi)	ts (in)	W (psi)	Grout	Ieff (in^4)	S (in^3)	E (psi)	M (lb-in)	R_A (psi)	Ru (psi)	K (psi/in)	Mass ($psi\text{-}ms^2/in$)	R_A/Ru	P (psi)	I (psi-ms)	Pbar	ibar	LOP
URS	15	102	16	7.62	2387	238.7	n/a	0.56	n/a	589.9	154.8	2.39e6	36960	0.17	1.78	63	1439	0.09	3.6	288	2.0	0.36	Blowout
URS	16	102	16	7.62	2387	238.7	n/a	0.56	n/a	589.9	154.8	2.39e6	36960	0.17	1.78	63	1439	0.09	3.4	272	1.9	0.34	VLLOP
URS	17	102	16	7.62	2387	238.7	n/a	0.56	n/a	589.9	154.8	2.39e6	36960	0.17	1.78	63	1439	0.09	10.0	800	5.6	0.98	Blowout
URS	18	102	16	7.62	2387	238.7	n/a	0.56	n/a	589.9	154.8	2.39e6	36960	0.17	1.78	63	1439	0.09	10.0	800	5.6	0.98	Blowout
URS	19	102	16	7.62	2387	238.7	n/a	0.56	n/a	589.9	154.8	2.39e6	36960	0.17	1.78	63	1439	0.09	10.1	808	5.7	0.99	Blowout
URS	20	102	16	7.62	2387	238.7	n/a	0.56	n/a	589.9	154.8	2.39e6	36960	0.17	1.78	63	1439	0.09	10.0	800	5.6	0.98	Blowout
URS	50	102	16	11.62	2387	238.7	n/a	0.83	n/a	2092.0	360.1	2.39e6	85948	0.38	4.13	222	2159	0.09	4.0	800	1.0	0.51	Blowout
URS	51	102	16	11.62	2387	238.7	n/a	0.83	n/a	2092.0	360.1	2.39e6	85948	0.38	4.13	222	2159	0.09	4.3	800	1.0	0.51	Blowout
URS	52a	102	16	11.62	2387	238.7	n/a	0.83	n/a	2092.0	360.1	2.39e6	85948	0.38	4.13	222	2159	0.09	1.5	800	0.4	0.49	MLOP
URS	52b	102	16	11.62	2387	238.7	n/a	0.83	n/a	2092.0	360.1	2.39e6	85948	0.38	4.13	222	2159	0.09	1.5	800	0.4	0.49	MLOP
URS	52c	102	16	11.62	2387	238.7	n/a	0.83	n/a	2092.0	360.1	2.39e6	85948	0.38	4.13	222	2159	0.09	1.5	800	0.4	0.49	MLOP
URS	52d	102	16	11.62	2387	238.7	n/a	0.83	n/a	2092.0	360.1	2.39e6	85948	0.38	4.13	222	2159	0.09	4.2	800	1.0	0.51	Blowout
* All URS tests were conducted on brick walls. Other tests were on CMU walls.																							

APPENDIX B.
DATA FROM SHOCK LOADING TESTS ON TWO-WAY SPANNING UNREINFORCED MASONRY WALLS

Table B-3 shows data from two-way spanning unreinforced masonry walls conducted by the Indian Ministry of Defense (MOD) tests with high explosive loading (Varma et al, 1997) and by Wilfred Baker Engineering, Inc. in a shock tube (Wesevich et al, 2002) that was scaled using the $Pbar_{URM}$ and $Ibar_{URM}$ terms in Equation 10. These terms are called out as Pbar and ibar in Table B-3. The Pbar and Ibar values in Table B-3 are plotted against scaled P-i curves in Section 6.8. All the data is for walls simply supported on four sides. Also, all the data only has self-weight axial loading from the wall above midspan, no additional axial loads were applied. The majority of the data is brick walls, with some ungrouted CMU walls. All the brick walls greater than 9 inches thick were multi-wythe walls that were assumed to act compositely as a single wall. The brick walls were attached to a strong surrounding concrete frame with dowels, grooved connections in the brick fitting into recesses in the frame, and plain bonding. The different attachments to the frame did not seem to matter except for a relatively small difference at the lowest damage level. The LOP were assigned to each data point based on the relationship below between the damage levels reported by the MOD and CEDAW component LOP response levels. See Table 1 for definitions of CEDAW component LOP (Levels of Protection). The blast loads in Table B-3 for the MOD tests are based on measured TNT blast loads. Torpex was used for some tests, but no information on blast loads from this explosive was available and these tests are not included in Table B-3.

Table B-1 Assumed Relationship Between CMUDS Damage Levels and LOP

CMUDS Damage Level	LOP
1	MLOP
2	LLOP
3	VLLOP
4	Blowout

Table B-2 Assumed Relationship Between MOD Damage Levels and LOP

MOD Damage Level	MOD Damage Level Description	LOP
D	Superficial damage such as hairline cracks and general chipping of the mortar. Support rotations up to 1.5 degrees.	MLOP
C,B	Noticeable cracks in joints to major dislocation of brick/mortar. Major cracks in reinforced concrete frame. Support rotations up to 4.5 degrees.	LLOP
A	Total collapse of wall, permanent deformation of reinforced concrete frame.	VLLOP

Table B-3. Data for Two-Way Spanning Unreinforced Masonry Walls

Origin	Test No.	Lx (in)	Ly (in)	h (in)	fm (psi)	ft (psi)	ts (in)	W psi)	Wall Type	Ieff in^4/in)	S in^3/in)	E (psi)	M (lb-in/in)	R_A (psi)	Ru (psi)	K (psi/in)	Mass (psi-ms^2/in)	R_A/Ru	P (psi)	I (psi-ms)	Pbar	ibar	Max. Defl. (inch)	LOP
WBE 1995	1	28	28	2	2000	200	0.35	0.08	CMU	0.48	0.58	2.0e06	116	0.02	3.5	391	194	0.006	5.2	27	1.5	0.17		MLOP
	2	28	28	2	2000	200	0.35	0.08	CMU	0.48	0.58	2.0e06	116	0.02	3.5	391	194	0.006	8.2	32	2.3	0.21		LLOP
	3	28	28	2	2000	200	0.35	0.08	CMU	0.48	0.58	2.0e06	116	0.02	3.5	391	194	0.006	7.1	35	2.0	0.22		LLOP
	4	28	28	2	2000	200	0.35	0.08	CMU	0.48	0.58	2.0e06	116	0.02	3.5	391	194	0.006	7.2	38	2.0	0.24		VLLOP
	5	28	28	2	2000	200	0.35	0.08	CMU	0.48	0.58	2.0e06	116	0.02	3.5	391	194	0.006	4.2	19	1.2	0.12		LLOP
	30	28	28	2	2000	200	0.35	0.08	CMU	0.48	0.58	2.0e06	116	0.02	3.5	391	194	0.006	3.2	30	0.9	0.19		LLOP
Indian Ministry of Defense (MOD)	1	117	117	9	1775	178		0.63	brick	61.87	13.67	1.8e06	2426	0.19	4.3	148	2426	0.046	188.5	162	44.3	0.15	5.0	LLOP
	2	117	117	9	1775	178		0.63	brick	61.87	13.67	1.8e06	2426	0.19	4.3	148	2426	0.046	145.0	216	34.1	0.20		LLOP
	3	117	117	9	1775	178		0.63	brick	61.87	13.67	1.8e06	2426	0.19	4.3	148	2426	0.046	188.5	232	44.3	0.21		LLOP
	4	117	117	9	1775	178		0.63	brick	61.87	13.67	1.8e06	2426	0.19	4.3	148	2426	0.046	266.9	281	62.8	0.26		VLLOP
	5	117	117	9	1775	178		0.63	brick	61.87	13.67	1.8e06	2426	0.19	4.3	148	2426	0.046	124.7	244	29.3	0.22		LLOP
	6	117	117	9	1775	178		0.63	brick	61.87	13.67	1.8e06	2426	0.19	4.3	148	2426	0.046	210.3	256	49.5	0.23		LLOP
	7	117	117	9	1775	178		0.63	brick	61.87	13.67	1.8e06	2426	0.19	4.3	148	2426	0.046	291.5	282	68.5	0.26		VLLOP
	8	117	117	9	1775	178		0.63	brick	61.87	13.67	1.8e06	2426	0.19	4.3	148	2426	0.046	304.6	226	71.6	0.21		LLOP
	9	117	117	9	1775	178		0.63	brick	61.87	13.67	1.8e06	2426	0.19	4.3	148	2426	0.046	266.9	281	62.8	0.26		VLLOP
	11	117	117	13.6	1775	178		0.95	brick	205	30.38	1.8e06	3634	0.29	9.5	489	5392	0.046	414.8	324	43.9	0.18	3.7	LLOP
	12	117	117	13.6	1775	178		0.95	brick	205	30.38	1.8e06	3634	0.29	9.5	489	5392	0.046	58.0	113	6.1	0.05	0.9	MLOP
	13	117	117	13.6	1775	178		0.95	brick	205	30.38	1.8e06	3634	0.29	9.5	489	5392	0.046	121.0	143	12.8	0.07	1.6	MLOP
	14	117	117	13.6	1775	178		0.95	brick	205	30.38	1.8e06	3634	0.29	9.5	489	5392	0.046	132.0	164	14.0	0.08	1.9	MLOP
	15	117	117	13.6	1775	178		0.95	brick	205	30.38	1.8e06	3634	0.29	9.5	489	5392	0.046	344.6	221	36.5	0.12	4.6	LLOP
	16	117	117	13.6	1775	178		0.95	brick	205	30.38	1.8e06	3634	0.29	9.5	489	5392	0.046	741.7	438	78.5	0.26		VLLOP
	17	117	117	13.6	1775	178		0.95	brick	205	30.38	1.8e06	3634	0.29	9.5	489	5392	0.046	414.8	324	43.9	0.18	4.1	LLOP
	19	117	117	13.6	1775	178		0.95	brick	205	30.38	1.8e06	3634	0.29	9.5	489	5392	0.046	753.3	445	79.7	0.26		VLLOP
	20	117	117	13.6	1775	178		0.95	brick	205	30.38	1.8e06	3634	0.29	9.5	489	5392	0.046	111.7	176	11.8	0.09	1.0	LLOP

Origin	Test No.	Lx (in)	Ly (in)	h (in)	fm (psi)	ft (psi)	ts (in)	W psi)	Wall Type	Ieff in^4/in)	S in^3/in)	E (psi)	M (lb-in/in)	R_A (psi)	Ru (psi)	K (psi/in)	Mass (psi-ms^2/in)	R_A/Ru	P (psi)	I (psi-ms)	Pbar	ibar	Max. Defl. (inch)	LOP
	22	117	117	13.6	1775	178		0.95	brick	205	30.38	1.8e06	3634	0.29	9.5	489	5392	0.046	752.0	444	79.6	0.26		VLLOP
	23	117	117	13.6	1775	178		0.95	brick	205	30.38	1.8e06	3634	0.29	9.5	489	5392	0.046	739.7	438	78.3	0.26		VLLOP
	24	117	117	18	1775	178		1.26	brick	486	54	1.8e06	4846	0.39	17	1160	9585	0.046	480.2	345	28.6	0.13	1.2	LLOP
	25	117	117	18	1775	178		1.26	brick	486	54	1.8e06	4846	0.39	17	1160	9585	0.046	480.2	345	28.6	0.13	1.2	LLOP
	28	117	117	18	1775	178		1.26	brick	486	54	1.8e06	4846	0.39	17	1160	9585	0.046	183.3	185	10.9	0.06	1.6	LLOP
	30	117	117	18	1775	178		1.26	brick	486	54	1.8e06	4846	0.39	17	1160	9585	0.046	473.1	377	28.2	0.14	3.6	LLOP
Indian Ministry of Defense	31	117	117	18	1775	178		1.26	brick	486	54	1.8e06	4846	0.39	17	1160	9585	0.046	353.9	335	21.1	0.12		LLOP
	32	117	117	18	1775	178		1.26	brick	486	54	1.8e06	4846	0.39	17	1160	9585	0.046	480.2	345	28.6	0.13	1.2	LLOP
	33	117	117	18	1775	178		1.26	brick	486	54	1.8e06	4846	0.39	17	1160	9585	0.046	480.2	345	28.6	0.13	2.3	LLOP

APPENDIX C.
DATA FROM SHOCK LOADING TESTS ON ONE-WAY SPANNING REINFORCED MASONRY WALLS

Table C-3 shows data from the CMUDS database (Wesevich et al, 2002) that was scaled using the Pbar1 and Ibar2 terms in Equation 10. These terms are called out as Pbar and Ibar in Table C-3. Detailed information on tests in the CMUDS database are included in reports hot-linked to the CMUDS computer program distributed by TSWG in the U.S. Department of Defense. The Pbar and Ibar values in Table C-3 are plotted against scaled P-i curves in Section 6.6. All the data is for simply supported walls. All the data is for full-scale reinforced CMU walls reinforced with rebar with a minimum static yield strength of 60,000 psi and an assumed dynamic yield strength of 77,000 psi. The LOP were assigned to each data point using the relationship in Table C-1 between the CMUDS damage levels and LOP. This relationship is based on the CEDAW component LOP descriptions in Table 1 and the CMUDS damage level descriptions for reinforced masonry in column 4 of Table C-2.

Table C-1 Assumed Relationship Between CMUDS Damage Levels and LOP

CMUDS Damage Level	LOP
1	MLOP
2	LLOP
3	VLLOP
4	Blowout

Table C-2. CMUDS Damage Levels Descriptions for Masonry

Damage Level	Unreinforced Without Arching	Unreinforced with Arching	Reinforced	Qualitative Response
1	Hairline cracks, no noticeable permanent deflections	Permanent deflections not exceeding 0.15h	Peak dynamic and residual support rotations not exceeding 7 and 1 degrees, respectively	Reusable
2	Wall is still standing, significant cracking with noticeable permanent deflections	Wall is still standing, permanent deflections exceed 0.15h	Peak dynamic and residual support rotations exceed 7 and 1 degrees, respectively	Replace
3	A major portion of the wall has fallen to the ground either immediately in front or behind the wall's original configuration	A major portion of the wall has fallen to the ground either immediately in front or behind the wall's original configuration	A major portion of the wall has fallen to the ground either immediately in front or behind the wall's original configuration	Collapse
4	Significant wall debris velocities are generated	Significant wall debris velocities are generated	Significant wall debris velocities are generated	Blowout

Table C-3. Data for One-Way Spanning Reinforced CMU Walls

Origin	Test No.	L (inch)	Rebar Spacing (inch)	Thick (inch)	f'm (psi)	d (inch)	steel ratio	W psi	I (in^4)	E psi	M* in-lb	Supports	Ru (psi)	K (psi/in)	Mass (psi-ms^2/in)	P (psi)	I (psi-ms)	Pbar	ibar	Max. Defl. (inch	Theta (deg)	LOP
EMRTC	6	93	32	5.6	2.0e3	2.8	0.002	0.42	252	2.0e6	4.1e4	Simple	1.2	16.2	1080	56	86	47	0.112	1.80	2.15	MLOP
EMRTC	8	93	32	5.6	2.0e3	2.8	0.002	0.42	252	2.0e6	4.1e4	Simple	1.2	16.2	1080	115	148	97	0.188	5.80	6.89	MLOP
EMRTC	9	93	32	5.6	2.0e3	2.8	0.002	0.42	252	2.0e6	4.1e4	Simple	1.2	16.2	1080	200	261	169	0.324	9.80	11.54	LLOP
EMRTC	10	93	32	5.6	2.0e3	2.8	0.002	0.42	252	2.0e6	4.1e4	Simple	1.2	16.2	1080	150	178	127	0.223	7.30	8.65	LLOP
EMRTC	11	93	32	5.6	2.0e3	2.8	0.002	0.42	252	2.0e6	4.1e4	Simple	1.2	16.2	1080	225	248	190	0.307	14.10	16.37	LLOP
EMRTC	12	93	32	5.6	2.0e3	2.8	0.002	0.42	252	2.0e6	4.1e4	Simple	1.2	16.2	1080	330	319	279	0.389			Blowout
EMRTC	13	93	32	5.6	2.0e3	2.8	0.002	0.42	252	2.0e6	4.1e4	Simple	1.2	16.2	1080	92	151	78	0.193	5.90	7.01	MLOP
EMRTC	14	93	32	5.6	2.0e3	2.8	0.002	0.42	252	2.0e6	4.1e4	Simple	1.2	16.2	1080	132	156	112	0.197	6.30	7.48	LLOP
EMRTC	15	93	32	5.6	2.0e3	2.8	0.002	0.42	252	2.0e6	4.1e4	Simple	1.2	16.2	1080	195	223	165	0.277	9.60	11.31	LLOP
EMRTC	19	93	32	5.6	2.0e3	2.8	0.002	0.42	252	2.0e6	4.1e4	Simple	1.2	16.2	1080	210	233	177	0.289	7.30	8.65	LLOP
EMRTC	20	93	32	5.6	2.0e3	2.8	0.002	0.42	252	2.0e6	4.1e4	Simple	1.2	16.2	1080	250	282	211	0.347	13.20	15.38	LLOP
EMRTC	21	93	32	5.6	2.0e3	2.8	0.002	0.42	252	2.0e6	4.1e4	Simple	1.2	16.2	1080	430	375	363	0.453			Blowout
EMRTC	24	93	8	5.6	2.0e3	2.8	0.009	0.42	63	2.0e6	3.5e4	Simple	4.0	16.2	1080	225	218	56	0.192	5.80	6.89	MLOP
EMRTC	25	93	8	5.6	2.0e3	2.8	0.009	0.42	63	2.0e6	3.5e4	Simple	4.0	16.2	1080	135	159	34	0.138	2.80	3.34	MLOP
EMRTC	26	93	8	5.6	2.0e3	2.8	0.009	0.42	63	2.0e6	3.5e4	Simple	4.0	16.2	1080	285	260	71	0.232	2.80	3.34	LLOP
DTRA	DB2	144	32	5.6	2.0e3	3.0	0.002	0.39	252	2.0e6	4.5e4	Fixed-Simple	0.8	5.8	1012	8	60	10	0.080	1.00	1.19	MLOP
DTRA	DB3	144	32	5.6	2.0e3	3.0	0.002	0.39	252	2.0e6	4.5e4	Fixed-Simple	0.8	5.8	1012	57	165	71	0.195			VLLOP
DTRA	DB12	144	24	7.6	2.0e3	4.0	0.002	0.53	470	2.0e6	5.9e4	Fixed-Simple	1.4	14.6	1372	45	270	31	0.239			VLLOP
ERDC	10	32	6	1.9	2.0e3	1.0	0.002	0.09	2	2.0e6	7.2e2	Fixed-Simple	1.4	92.6	233	163	101	115	0.447			Blowout
ERDC	11	32	6	1.9	2.0e3	1.0	0.002	0.09	2	2.0e6	7.2e2	Fixed-Simple	1.4	92.6	233	96	80	68	0.359			VLLOP
ERDC	12	32	6	1.9	2.0e3	1.0	0.002	0.09	2	2.0e6	7.2e2	Fixed-Simple	1.4	92.6	233	235	148	166	0.649			Blowout

Origin	Test No.	L (inch)	Rebar Spacing (inch)	Thick (inch)	f'm (psi)	d (inch)	steel ratio	W psi	I (in^4)	E psi	M* in-lb	Supports	Ru (psi)	K (psi/in)	Mass (psi-ms^2/in)	P (psi)	I (psi-ms)	Pbar	ibar	Max. Defl. (inch	Theta (deg)	LOP
ERDC	13	32	6	1.9	2.0e3	1.0	0.002	0.13	2	2.0e6	7.2e2	Fixed-Simple	1.4	92.6	342	281	130	199	0.468			Blowout
ERDC	14	32	6	1.9	2.0e3	1.0	0.002	0.13	2	2.0e6	7.2e2	Fixed-Simple	1.4	92.6	342	210	117	149	0.425			Blowout
ERDC	15	32	6	1.9	2.0e3	1.0	0.002	0.13	2	2.0e6	7.2e2	Fixed-Simple	1.4	92.6	342	346	166	245	0.595			Blowout
ERDC	16	32	6	1.9	2.0e3	1.0	0.002	0.13	2	2.0e6	7.2e2	Fixed-Simple	1.4	92.6	342	158	99	112	0.362			VLLOP
ERDC	17	32	6	1.9	2.0e3	1.0	0.002	0.09	2	2.0e6	7.2e2	Fixed-Simple	1.4	92.6	233	153	115	108	0.509			Blowout
ERDC	18	32	6	1.9	2.0e3	1.0	0.002	0.09	2	2.0e6	7.2e2	Fixed-Simple	1.4	92.6	233	268	133	190	0.581			Blowout
ERDC	19	32	6	1.9	2.0e3	1.0	0.002	0.09	2	2.0e6	7.2e2	Fixed-Simple	1.4	92.6	233	95	72	67.2	0.323			LLOP
ERDC	22	32	6	1.9	2.0e3	1.0	0.002	0.13	2	2.0e6	7.2e2	Fixed-Simple	1.4	92.6	342	118	65	83.5	0.239			VLLOP
ERDC	25	32	6	1.9	2.0e3	1.0	0.002	0.13	2	2.0e6	7.2e2	Fixed-Simple	1.4	92.6	342	78	64	55.2	0.238			LLOP
ERDC	26	32	6	1.9	2.0e3	1.0	0.002	0.13	2	2.0e6	7.2e2	Fixed-Simple	1.4	92.6	342	83	52	58.7	0.193			LLOP
ERDC	31	32	6	1.9	2.0e3	1.0	0.002	0.13	2	2.0e6	7.2e2	Fixed-Simple	1.4	92.6	342	48	40	34.0	0.151			MLOP
ERDC	35	32	6	1.9	2.0e3	1.0	0.002	0.13	2	2.0e6	7.2e2	Fixed-Simple	1.4	92.6	342	71	51	50.3	0.190			LLOP
ERDC	36	32	6	1.9	2.0e3	1.0	0.002	0.13	2	2.0e6	7.2e2	Fixed-Simple	1.4	92.6	342	50	43	35.4	0.162			MLOP
ERDC	37	32	6	1.9	2.0e3	1.0	0.002	0.13	2	2.0e6	7.2e2	Fixed-Simple	1.4	92.6	342	60	43	42.5	0.161			MLOP
ERDC	38	32	6	1.9	2.0e3	1.0	0.002	0.13	2	2.0e6	7.2e2	Fixed-Simple	1.4	92.6	342	76	63	53.8	0.235			LLOP
ERDC	40	32	6	1.9	2.0e3	1.0	0.002	0.13	2	2.0e6	7.2e2	Fixed-Simple	1.4	92.6	342	87	56	61.6	0.208			LLOP
ERDC	42	32	6	1.9	2.0e3	1.0	0.002	0.13	2	2.0e6	7.2e2	Fixed-Simple	1.4	92.6	342	69	43	48.8	0.161			MLOP
ERDC	43	32	6	1.9	2.0e3	1.0	0.002	0.13	2	2.0e6	7.2e2	Fixed-	1.4	92.6	342	97	48	68.7	0.178			MLOP

Origin	Test No.	L (inch)	Rebar Spacing (inch)	Thick (inch)	f'm (psi)	d (inch)	steel ratio	W psi	I (in^4)	E psi	M* in-lb	Supports	Ru (psi)	K (psi/in)	Mass (psi-ms^2/in)	P (psi)	I (psi-ms)	Pbar	ibar	Max. Defl. (inch	Theta (deg)	LOP
												Simple										
WBE	00-3	97	24	5.6	2.0e3	2.8	0.002	0.29	189	2.0e6	2.3e4	Simple	0.8	13.5	756	1.9	50	2.4	0.104			MLOP
WBE	00-3A	97	24	5.6	2.0e3	2.8	0.002	0.29	189	2.0e6	2.3e4	Simple	0.8	13.5	756	1.9	50	2.4	0.104			MLOP
WBE	00-4	97	24	5.6	2.0e3	2.8	0.002	0.29	189	2.0e6	2.3e4	Simple	0.8	13.5	756	2	58	2.5	0.120			MLOP
WBE	00-4A	97	24	5.6	2.0e3	2.8	0.002	0.29	189	2.0e6	2.3e4	Simple	0.8	13.5	756	1.9	48	2.4	0.100			MLOP
WBE	00-4B	97	24	5.6	2.0e3	2.8	0.002	0.29	189	2.0e6	2.3e4	Simple	0.8	13.5	756	3.5	75	4.4	0.150			MLOP
WBE	00-5	97	24	5.6	2.0e3	2.8	0.002	0.29	189	2.0e6	2.3e4	Simple	0.8	13.5	756	0.6	17	0.7	0.038			MLOP
WBE	00-5A	97	24	5.6	2.0e3	2.8	0.002	0.29	189	2.0e6	2.3e4	Simple	0.8	13.5	756	2.4	17	3.0	0.035			MLOP
WBE	00-5B	97	24	5.6	2.0e3	2.8	0.002	0.29	189	2.0e6	2.3e4	Simple	0.8	13.5	756	3.1	18	3.9	0.036			MLOP
WBE	00-5C	97	24	5.6	2.0e3	2.8	0.002	0.29	189	2.0e6	2.3e4	Simple	0.8	13.5	756	1.8	30	2.2	0.062			MLOP
WBE	00-6	97	24	5.6	2.0e3	2.8	0.002	0.29	189	2.0e6	2.3e4	Simple	0.8	13.5	756	4.5	108	5.6	0.212			LLOP
WBE	00-7	97	24	5.6	2.0e3	2.8	0.002	0.29	189	2.0e6	2.3e4	Simple	0.8	13.5	756	5.2	24	6.5	0.047			MLOP
WBE	00-7A	97	24	5.6	2.0e3	2.8	0.002	0.29	189	2.0e6	2.3e4	Simple	0.8	13.5	756	8.1	67	10.1	0.127			LLOP
WBE	00-8	97	16	5.6	2.0e3	2.8	0.007	0.29	126	2.0e6	5.7e4	Simple	3.0	13.5	756	4	48	1.3	0.050			MLOP
WBE	00-8A	97	16	5.6	2.0e3	2.8	0.007	0.39	126	2.0e6	5.7e4	Simple	3.0	13.5	1012	4.5	55	1.5	0.050			MLOP
WBE	00-8B	97	16	5.6	2.0e3	2.8	0.007	0.39	126	2.0e6	5.7e4	Simple	3.0	13.5	1012	6.5	90	2.2	0.082			MLOP
WBE	00-9	97	16	5.6	2.0e3	2.8	0.007	0.39	126	2.0e6	5.7e4	Simple	3.0	13.5	1012	3.5	94	1.2	0.084			MLOP
WBE	00-9A	97	16	5.6	2.0e3	2.8	0.007	0.39	126	2.0e6	5.7e4	Simple	3.0	13.5	1012	6.8	162	2.3	0.147			LLOP
WBE	01-3	96	22	5.6	2.0e3	2.8	0.002	0.25	164	2.0e6	2.3e4	Simple	0.9	13.3	648	10.5	107	11.5	0.207			VLLOP
WBE	01-4	96	22	5.6	2.0e3	2.8	0.002	0.25	164	2.0e6	2.3e4	Simple	0.9	13.3	648	10.3	206	11.2	0.398			Blowout
WBE	01-5	96	22	5.6	2.0e3	2.8	0.002	0.25	164	2.0e6	2.3e4	Simple	0.9	13.3	648	10	79	10.9	0.153			LLOP
WBE	01-6	96	22	5.6	2.0e3	2.8	0.002	0.25	164	2.0e6	2.3e4	Simple	0.9	13.3	648	3.4	106	3.7	0.218			LLOP
WBE	01-7	96	22	5.6	2.0e3	2.8	0.002	0.25	164	2.0e6	2.3e4	Simple	0.9	13.3	648	3.4	73	3.7	0.150			MLOP
WBE	01-7A	96	22	5.6	2.0e3	2.8	0.002	0.25	164	2.0e6	2.3e4	Simple	0.9	13.3	648	3.5	72	3.8	0.148			LLOP
WBE	01-8	96	22	5.6	2.0e3	2.8	0.002	0.25	164	2.0e6	2.3e4	Simple	0.9	13.3	648	17.5	118	19.1	0.221			LLOP
WBE	01-9	96	22	5.6	2.0e3	2.8	0.002	0.25	164	2.0e6	2.3e4	Simple	0.9	13.3	648	14.9	100	16.3	0.189			LLOP
WBE	01-11	96	14.667	5.6	2.0e3	2.8	0.010	0.29	110	2.0e6	6.8e4	Simple	4.0	13.3	744	17.3	119	4.3	0.113			MLOP
WBE	01-11A	96	14.7	5.6	2.0e3	2.8	0.010	0.29	110	2.0e6	6.8e4	Simple	4.0	13.3	744	18	123	4.5	0.117			MLOP

Origin	Test No.	L (inch)	Rebar Spacing (inch)	Thick (inch)	f'm (psi)	d (inch)	steel ratio	W psi	I (in^4)	E psi	M* in-lb	Supports	Ru (psi)	K (psi/in)	Mass (psi-ms^2/in)	P (psi)	I (psi-ms)	Pbar	ibar	Max. Defl. (inch	Theta (deg)	LOP
WBE	01-12	96	14.667	5.6	2.0e3	2.8	0.010	0.29	110	2.0e6	6.8e4	Simple	4.0	13.3	744	10.1	138	2.5	0.128			MLOP
WBE	01-13	96	14.7	5.6	2.0e3	2.8	0.005	0.29	110	2.0e6	3.8e4	Simple	2.3	13.3	744	6.7	178	3.0	0.221			LLOP
WBE	01-14	96	14.7	5.6	2.0e3	2.8	0.005	0.29	110	2.0e6	3.8e4	Simple	2.3	13.3	744	27	275	11.9	0.343			Blowout
WBE	01-23	46	22	5.6	2.0e3	2.8	0.002	0.25	164	2.0e6	2.3e4	Fixed-Simple	6.0	526.1	648	7.3	216	1.2	0.240			MLOP
WBE	01-24	96	14.7	5.6	2.0e3	2.8	0.005	0.29	110	2.0e6	3.8e4	Simple	2.3	13.3	744	4.6	137	2.0	0.169			LLOP
WBE	04-1	96	88	5.6	2.0e3	2.8	0.002	0.25	609	2.0e6	9.2e4	Simple	0.9	12.5	645	5	30	5.5	0.061	1.25	1.19	MLOP
WBE	04-1A	96	88	5.6	2.0e3	2.8	0.002	0.25	31	2.0e6	9.2e4	Simple	0.9	0.6	645	7.8	68	8.6	0.134	6.00	1.19	LLOP
WBE	04-2	96	88	5.6	2.0e3	2.8	0.007	0.39	704	2.0e6	3.2e5	Simple	3.2	14.5	1012	4	52	1.3	0.046	0.63	1.19	MLOP
WBE	04-2A	96	88	5.6	2.0e3	2.8	0.007	0.39	98	2.0e6	3.2e5	Simple	3.2	2.0	1012	6.6	85	2.1	0.076	1.50	1.19	MLOP
WBE	04-2B	96	88	5.6	2.0e3	2.8	0.007	0.39	98	2.0e6	3.2e5	Simple	3.2	2.0	1012	9.9	119	3.1	0.107	3.25	1.19	LLOP
WBE	04-3	96	88	5.6	2.0e3	2.8	0.009	0.39	713	2.0e6	3.8e5	Simple	3.8	14.7	1012	9.8	131	2.6	0.107	2.88	1.19	LLOP
WBE	04-3A	96	88	5.6	2.0e3	2.8	0.009	0.39	117	2.0e6	3.8e5	Simple	3.8	2.4	1012	10.2	122	2.7	0.100	4.75	1.19	LLOP
WBE	04-4	96	88	5.6	2.0e3	2.8	0.005	0.29	647	2.0e6	2.3e5	Simple	2.3	13.3	750	7	201	3.1	0.247	10.35	1.19	LLOP
WBE	04-5	96	88	5.6	2.0e3	2.8	0.009	0.39	713	2.0e6	3.8e5	Simple	3.8	14.7	1012	22	291	5.8	0.246			VLLOP
WBE	04-6	96	88	7.6	2.0e3	3.8	0.002	0.40	1507	2.0e6	1.9e5	Simple	1.8	31.0	1032	2.9	127	1.6	0.149	1.25	1.19	MLOP
WBE	04-6A	96	88	7.6	2.0e3	3.8	0.002	0.40	84	2.0e6	1.9e5	Simple	1.8	1.7	1032	5.3	251	2.9	0.293			VLLOP
WBE	04-7	96	88	7.6	2.0e3	3.8	0.004	0.40	1535	2.0e6	3.3e5	Simple	3.2	31.6	1032	4.5	212	1.4	0.184	1.63	1.19	MLOP
WBE	04-7A	96	88	7.6	2.0e3	3.8	0.004	0.40	141	2.0e6	3.3e5	Simple	3.2	2.9	1032	6.4	296	2.0	0.259	13.33	1.19	LLOP
WBE	04-9	96	88	7.6	2.0e3	3.8	0.002	0.35	1449	2.0e6	2.2e5	Simple	2.2	29.8	896	3.8	163	1.7	0.186	3.50	1.19	MLOP
WBE	04-9A	96	88	7.6	2.0e3	3.8	0.002	0.35	100	2.0e6	2.2e5	Simple	2.2	2.1	896	4.5	200	2.0	0.229	9.92	1.19	LLOP
WBE	04-10	96	88	7.6	2.0e3	3.8	0.002	0.35	1449	2.0e6	2.2e5	Simple	2.2	29.8	896	4.6	216	2.1	0.247	6.71	1.19	LLOP
WBE	04-10A	96	88	7.6	2.0e3	3.8	0.002	0.35	100	2.0e6	2.2e5	Simple	2.2	2.1	896	4.6	218	2.1	0.249	8.46	1.19	LLOP
WBE	04-11	96	88	7.6	2.0e3	3.8	0.004	0.40	1535	2.0e6	3.3e5	Simple	3.2	31.6	1032	6.5	345	2.0	0.302	7.13	1.19	LLOP
WBE	04-12	96	88	7.6	2.0e3	3.8	0.004	0.40	1535	2.0e6	3.3e5	Simple	3.2	31.6	1032	5.7	310	1.8	0.270	6.25	1.19	LLOP

* All walls reinforced with rebar with a minimum static yield strength of 60,000 psi and an assumed dynamic yield strength of 77,000 psi.

APPENDIX D.
DATA FROM SHOCK LOADING TESTS ON ONE-WAY SPANNING REINFORCED CONCRETE WALLS

Table D-1 shows data from one-way spanning reinforced concrete slabs conducted during three test programs as shown in the table, which were scaled using the Pbar1and Ibar2 terms in Equation 10. These terms are referred to as Pbar and Ibar in Table D-1. The Pbar and Ibar values in Table D-1 are plotted against scaled P-i curves in Section 6.5. The data from *Scaled Testing and Analysis of Building Component* (Wright, 1993) was conducted at one-quarter scale with high explosive cylindrical charges. Measured blast loads are shown in Table D-1. The LOP was based on reported damage and photographs and the definitions for the component LOP in Table 1. The data in Table D-1 was converted into equivalent full-scale values. This caused all the dimensional data to be increased by the inverse of the scale factor raised to the same power as the dimensional units and the impulse to the increased by the inverse of the scale factor. It caused no change in the concrete and reinforcing steel material yield strength, mass density, and modulus values.

The data from *Airblast Loading on Wall Panels* (Forsèn, 1985) is from full-scale high explosive tests on wall panels. Measured blast loads from the same blast loading configurations that is reported by Forsèn (1989) are shown in Table D-1. Reinforcing data and concrete strength information was obtained by private communication with Mr. Forsèn based on information in a more detailed Swedish version of the referenced test report. LOP values were assigned to the test data based on the reported maximum deflection and an failure deflection of 150 mm for the test walls, corresponding to 7 degrees support rotation, estimated by the researchers based on their observations of the tested wall panels.

The data from *WES Semi –Hardened Facility Design Criteria Tests* (Colthorp et al, 1985) is from tests on the wall of a box culvert type structure with two opposite sides open and one-way spanning wall, roof, and floor slabs that was subject to blast loads and fragments from a close-in fragmenting explosive. All tests were exposed to the same explosive loading, which was spatially non-uniform. An equivalent, spatially uniform blast load that included the measured impulse of the fragments was developed by the researchers is shown in Table D-1. The researchers reported that this equivalent uniform blast load caused deflections from SDOF analyses of the wall response to approximately match measured wall deflections. Tests were also conducted that investigated mitigation concepts to decrease wall damage, but these tests are not included in Table D-1. The tested wall slabs correspond to a one-half scale model of a relatively thick, heavily reinforced concrete wall. The data in Table D-1 is shown in terms of the actual measured and tested dimensions. The Ibar and Pbar terms are scale independent since they are dimensionless.

Table D-1. Data for One-Way Spanning Reinforced Concrete Slabs

Test Series	Test No.	L	Thick (inch)	Depth (inch)	f'dc (psi)	fdy (psi)	Reinf. Ratio (%)	Reinf. Index	Support	Weight (psi)	Ieff (in^4/in)	E (psi)	M (lb-in/in)	Ru (psi)	K (psi/in)	Mass (psi-ms^2/in)	P (psi)	I (psi-ms)	Pbar	Ibar	Max. Defl. (inch)	Theta (deg)	LOP
Scaled Testing, Analysis of Building Components	F1	250	7.9	6.7	8000	8.5e4	0.66	0.069	Simple	0.68	20.3	5.1e6	2.4e4	3.0	2.0	1753	42	212	13.8	0.09	5.2	2.4	LLOP
	F3	250	7.9	6.7	8000	8.5e4	0.66	0.069	Simple	0.68	20.3	5.1e6	2.4e4	3.0	2.0	1753	15	140	4.9	0.06	2.5	1.2	MLOP
	F4	250	7.9	6.7	8000	8.5e4	0.66	0.069	Simple	0.68	20.3	5.1e6	2.4e4	3.0	2.0	1753	7	72	2.3	0.03	0.8	0.4	MLOP
	F5	250	7.9	6.7	8000	8.5e4	0.66	0.069	Simple	0.68	20.3	5.1e6	2.4e4	3.0	2.0	1753	166	350	54.4	0.16	7.9	3.6	LLOP
	F6	250	7.9	6.7	8000	8.5e4	0.66	0.069	Simple	0.68	20.3	5.1e6	2.4e4	3.0	2.0	1753	4	32	1.1	0.01	0.3	0.1	HLOP
	P1-shot 1	250	5.3	4.5	8000	8.5e4	0.66	0.069	Simple	0.46	6.2	5.1e6	6.8e3	0.9	0.6	1183	15	72	16.6	0.06	2.4	1.1	MLOP
	P1-shot 2	250	5.3	4.5	8000	8.5e4	0.66	0.069	Simple	0.46	6.2	5.1e6	6.8e3	0.9	0.6	1183	167	350	192	0.27	13.4	6.1	VLLOP
	P2	250	5.3	4.5	8000	8.5e4	0.66	0.069	Simple	0.46	6.2	5.1e6	6.8e3	0.9	0.6	1183	8	76	9.6	0.07	2.4	1.1	MLOP
	P3	250	5.3	4.5	8000	8.5e4	0.66	0.069	Simple	0.46	6.2	5.1e6	6.8e3	0.9	0.6	1183	56	224	64.3	0.18	11.8	5.4	LLOP
	P5	250	5.3	4.5	8000	8.5e4	0.66	0.069	Simple	0.46	6.2	5.1e6	6.8e3	0.9	0.6	1183	15	124	16.9	0.11	4.9	2.2	MLOP
	P6	250	5.3	4.5	8000	8.5e4	0.66	0.069	Simple	0.46	6.2	5.1e6	6.8e3	0.9	0.6	1183	3	36	3.4	0.03	0.6	0.3	HLOP
Airblast Loading on Wall Panels	150-1	94	5.9	5.0	6000	7.7e4	0.21	0.027	Simple	0.51	8.6	4.4e6	3.9e3	3.6	37.4	1316	62	116	17.5	0.09	1.8	2.2	MLOP
	150-2	94	5.9	5.0	6000	7.7e4	0.21	0.027	Simple	0.51	8.6	4.4e6	3.9e3	3.6	37.5	1317	234	227	65.6	0.19	4.5	5.4	LLOP
	200-1	94	7.9	7.0	4400	7.7e4	0.26	0.041	Simple	0.68	20.3	3.8e6	8.7e3	7.9	75.7	1753	1008	528	128	0.31	3.9	4.7	LLOP
	200-2	94	7.9	7.0	4400	7.7e4	0.26	0.041	Simple	0.68	20.3	3.8e6	8.7e33	7.9	75.7	1753	1008	528	128	0.31	3.6	4.4	LLOP
	200-3	94	7.9	7.0	4400	7.7e4	0.26	0.041	Simple	0.68	20.3	3.8e6	8.7e3	7.9	75.7	1753	1008	528	128	0.31	3.8	4.6	LLOP
	200-4	94	7.9	7.0	4400	7.7e4	0.26	0.041	Simple	0.68	20.3	3.8e6	8.7e3	7.9	75.7	1753	219	227	27.8	0.12	2.1	2.5	MLOP
	200-5	94	7.9	7.0	4400	7.7e4	0.26	0.041	Simple	0.68	20.3	3.8e6	8.7e3	7.9	75.7	1753	529	311	67.2	0.17	2.2	2.6	MLOP
	200-6	94	7.9	7.0	4400	7.7e4	0.26	0.041	Simple	0.68	20.3	3.8e6	8.7e3	7.9	75.7	1753	1008	528	128	0.31	3.1	3.8	LLOP
	200-7	94	7.9	7.0	4400	7.7e4	0.26	0.041	Simple	0.68	20.3	3.8e6	8.7e3	7.9	75.7	1753	1008	528	128	0.31	3.0	3.7	LLOP
	200-8	94	7.9	7.0	4400	7.7e4	0.26	0.041	Simple	0.68	20.3	3.8e6	8.7e3	7.9	75.7	1753	1008	528	128	0.31	3.1	3.7	LLOP
	200-9	94	7.9	7.0	4400	7.7e4	0.26	0.041	Simple	0.68	20.3	3.8e6	8.7e3	7.9	75.7	1753	1008	528	128	0.31	3.7	4.5	LLOP
WES Semi - Hardened Facility Design Criteria Tests	Test I-1	65	12.8	11.0	6000	8.5e4	1.00	0.141	Fixed	1.10	87.3	4.4e6	9.5e4	360	6644	2851	2960	916	8.2	0.07	0.6	1.0	MLOP
	Test I-2	65	12.8	11.0	6000	8.5e4	0.50	0.071	Fixed	1.10	87.3	4.4e6	5.0e4	188	6644	2851	2960	916	15.7	0.10	1.0	1.8	MLOP
	Test I-3	65	12.8	11.0	6000	8.5e4	0.50	0.071	Fixed	1.10	87.3	4.4e6	5.0e4	188	6644	2851	2960	916	15.7	0.10	3.0	5.3	LLOP
	Test I-4	65	12.8	11.0	6000	8.5e4	0.25	0.035	Fixed	1.10	87.3	4.4e6	2.5e4	96	6644	2851	2960	916	30.8	0.16	2.2	4.0	LLOP
	Test I-6	65	12.8	11.0	6000	8.5e4	0.25	0.035	Fixed	1.10	87.3	4.4e6	2.5e4	96	6644	2851	2960	916	30.8	0.16	1.5	2.6	MLOP

APPENDIX E.
DATA FROM SHOCK LOADING TESTS ON COLD-FORMED GIRTS WITH TENSION MEMBRANE

Table E-1 shows data from girts and purlins with significant tension membrane conducted during several test programs as shown in the table that was scaled using the $Pbar_{TM}$ and $Ibar_{TM}$ terms in Equation 10. These terms are referred to as Pbar and Ibar in Table E-1. The Pbar and Ibar values in Table E-1 are plotted against scaled P-i curves in Section 6.2. The data from Operation Teapot (O.T. in Table E-1), as reported by Johnson (1956), was from a small pre-engineered building with aluminum siding and cold-formed girts that was tested with very long duration blast loads simulating nuclear explosions. Tests were conducted with a 15000 ft and 6800 ft standoff, including one unplanned test. The maximum tensile force in the girts is based on an estimated connection capacity of 10 kips reported by the researchers. Free-field blast loads were measured that were converted to reflected blast loads. The roof was assumed to have a reflected blast load since it had approximately a 60 degree angle of incidence and the free-field pressure was very low (one the order of 1 to 2 psi). The LOP levels were based on photographs of the tested buildings and reported maximum permanent deflections. Estimated maximum permanent deflections from failed girts at failure are shown for the Blowout cases in Table E-1.

The Coop Data in Table E-1 (Oswald et al, 1998) is from a proprietary study performed by Wilfred Baker Engineering, Inc. (WBE) for the 1997 Petrochemical Technology Cooperative (Coop). As part of the study, a series of tests were performed in WBE's large shock tube on 8 ft by 8 ft wall systems with corrugated steel panels supported by cold-formed steel girts. The girts were approximately one-half scale, consisting of 4 inch deep sections with 16 gauge thickness spanning 8 ft, that supported panels spanning 4 ft. The data from these tests in Table E-1 are shown in terms of the actual measured and tested dimensions. The maximum tension forces in Table E-1 are based on the lower of the ultimate bolt shear capacity or the ultimate bearing capacity of the girts. In some cases, a nested section was screwed to the girts at the connection to increase the girt bearing capacity. A325 bolts were used in most of the tests, although these were upgraded to A490 bolts in the last tests. The blast loads in Table E-1 are reflected loads that were measured in the shock tube. The LOP levels were based on photographs of the tested walls and measured maximum girt deflections. The test report is an appendix of a larger document on blast capacity upgrades to metal buildings that is not in the public domain. The Coop has agreed to share only the test data with the U.S. government.

The data from *Blast Capacity Evaluation of Pre-Engineered Building* (Stea et al, 1979), which is abbreviated as (BCEPB) in Table E-1, was from a pre-engineered building that was subject to high explosive loads from a 2000 lb explosion at a relatively large standoff. The same building was tested in six tests, which all caused relatively limited damage that was repaired as necessary between tests. Failure of girt connection bolts and widening of bolt holes in the girts was reported. The maximum tension force in the girts was assumed equal to 10 kips for Tests 1 through 4, equal to the ultimate shear strength of two 0.5 inch diameter A307 bolts, based on the reported use of standard, low strength bolts in the building. In Tests 5 and 6, these bolts were replaced with high strength bolts. The maximum tension force in the girts was assumed equal to 20 kips for these bolts, equal to the shear capacity of two 0.5 inch A325 bolts. This load is also approximately equal to the ultimate bearing capacity of 0.14 inch thick girts. The measured reflected blast loads are shown in Table E-1. The LOP levels were based on photographs of the tested walls and reported maximum dynamic girt deflections.

The AFRL BREW-1 tests (Salim et al, 1996) were conducted at Tyndall AFB with high explosive loading applied to test walls with 600S162-43 steel studs (6" deep 18 gauge studs) bolted to a concrete frame supporting lightweight External Insulation and Finish (EIFS) and 4 inch brick wall panels. The studs were anchored to develop the full tensile capacity of their cross sections. The studs had 1.9 inch wide utility hole openings in their web, which caused a minimum calculated cross sectional area of 0.35 in^2. The measured reflected blast loads are shown in Table E-1. The wall with EIFS, which had significantly less mass, failed at an estimated deflection of 14 inches. The LOP levels were based on photographs of the tested walls and reported maximum dynamic girt deflections.

The ERDC EWRP-7 Tests (Townsend) were similar to the AFRL BREW tests. However, back-to-back steel studs and 2 inch granite façade were used in the Outboard and Inboard Test Walls in Table E-1. Both of these test walls had strengthened windows with a muntin frame system. The blast resistant windows were assumed to transfer load into the continuous studs around the window. The Army Inboard Tests included one test with back-to-back studs and one test with single studs and a 1.25 inch granite façade. All studs were assumed to be 600S162-43 steel studs (6" deep 18 gauge studs) with standard utility hole openings based on available information that were very well connected to framing so that their maximum tension force was controlled by their minimum cross sectional area. The measured reflected blast loads are shown in Table E-1. The LOP levels were based on photographs of the tested walls and reported maximum girt dynamic deflections.

Table E-1. Data for Cold-Formed Steel Girts and Purlins with Significant Tension Membrane

Test Series/ Component[1, 2]	L (in)	B (in)	fdy (psi)	E (psi)	Z (in^3)	I (in^4)	A (in^2)	Self Weight (lb/in)	Supp Weight (psi)	Support	M (lb-in)	Max Tension Force (lbs)	Ru (psi)	K (psi/in)	Mass (psi-ms^2/in)	Ktm (psi/in)	P (psi)	I (psi-ms)	Pbar	Ibar	Max. Defl. (in)	Theta (deg)	LOP
O.T. Reflected Girt Planned Test @6800 ft	142	40	6.5e4	2.9e7	0.95	1.50	0.72	0.20	0.01	Simple	6.2e4	1.0e4	0.62	0.21	31	0.10	5.9	180	0.37	1.71	17.0	13.5	Blowout
O.T. Reflected Girt Planned Test @15000 ft	142	40	6.5e4	2.9e7	0.95	1.50	0.72	0.20	0.01	Simple	6.2e4	1.0e4	0.62	0.21	31	0.10	2.5	75	0.13	0.69	16.0	12.7	Blowout
O.T. Reflected Purlin Planned Test @6800 ft	142	42	6.5e4	2.9e7	2.20	6.25	0.94	0.27	0.01	Simple	1.4e5	1.0e4	1.36	0.82	34	0.09	2.9	180	0.12	0.99		0.0	Blowout
O.T. Reflected Girt Unplanned Test@ 6800	142	40	6.5e4	2.9e7	0.95	1.50	0.72	0.20	0.01	Simple	6.2e4	1.0e4	0.62	0.21	31	0.10	1.5	26	0.06	0.23	7.5	6.0	LLOP
1997 Coop Test 7	96	45	7.5e4	2.9e7	0.72	1.54	0.61	0.17	0.02	Simple	5.4e4	1.2e4	1.04	0.90	60	0.24	5.5	95	0.20	0.56	12.0	14.0	VLLOP
1997 Coop Test 12	96	45	7.5e4	2.9e7	0.72	1.54	0.61	0.17	0.01	Simple	5.4e4	1.2e4	1.04	0.90	33	0.24	2.5	42	0.06	0.30	8.0	9.5	VLLOP
1997 Coop Test 13	96	45	7.5e4	2.9e7	0.72	1.54	0.61	0.17	0.01	Simple	5.4e4	1.9e4	1.04	0.90	37	0.37	4.7	69	0.10	0.47	14.4	16.7	VLLOP
1997 Coop Test 4	96	45	7.5e4	2.9e7	0.72	1.54	0.61	0.17	0.03	Simple	5.4e4	1.2e4	1.04	0.90	89	0.24	5.9	80	0.22	0.39	11.0	12.9	VLLOP
1997 Coop Test 5	96	45	7.5e4	2.9e7	0.72	1.54	0.61	0.17	0.03	Simple	5.4e4	1.2e4	1.04	0.90	89	0.24	7.8	84	0.30	0.43	16.0	18.4	VLLOP
1997 Coop Test 6	96	45	7.5e4	2.9e7	0.72	1.54	0.61	0.17	0.01	Simple	5.4e4	1.2e4	1.04	0.90	37	0.24	4.2	55	0.14	0.40	13.0	15.2	VLLOP
1997 Coop Test 10	96	45	7.5e4	2.9e7	0.72	1.54	0.61	0.17	0.01	Simple	5.4e4	1.2e4	1.04	0.90	30	0.24	3.1	43	0.09	0.34	7.0	8.3	LLOP
1997 Coop Test 11	96	45	7.5e4	2.9e7	0.72	1.54	0.61	0.17	0.02	Simple	5.4e4	1.2e4	1.04	0.90	55	0.24	4.2	72	0.14	0.43	11.0	12.9	LLOP
1997 Coop Test 14	96	45	7.5e4	2.9e7	2.69	9.35	1.60	0.45	0.02	Simple	2.0e5	2.1e4	3.87	5.46	71	0.41	8.2	137	0.11	0.32	7.5	8.9	LLOP
1997 Coop Test 15	96	45	7.5e4	2.9e7	1.76	6.18	1.14	0.32	0.02	Simple	1.3e5	3.1e4	2.53	3.61	64	0.59	5.0	100	0.04	0.25	5.6	6.7	LLOP
BCEPB Test No.3 Reflected Girt	240	49	7.2e4	2.9e7	6.74	37.3	2.00	8.97	0.01	Simple	4.9e5	1.0e4	1.38	0.51	496	0.03	1.4	25	0.01	0.02	2.8	1.3	MLOP
BCEPB Test No.4 Reflected Girt	240	49	7.2e4	2.9e7	6.74	37.3	2.00	8.97	0.01	Simple	4.9e5	1.0e4	1.38	0.51	496	0.03	2.1	32	0.11	0.04	4.4	2.1	MLOP
BCEPB Test No.5 Reflected Girt	240	49	7.2e4	2.9e7	6.74	37.3	2.00	8.97	0.01	Simple	4.9e5	2.0e4	1.38	0.51	496	0.06	2.5	44	0.08	0.05	4.8	2.3	MLOP
BCEPB Test No.6 Reflected Girt	240	49	7.2e4	2.9e7	6.74	37.3	2.00	8.97	0.01	Simple	4.9e5	2.0e4	1.38	0.51	496	0.06	2.4	42	0.08	0.04	4.9	2.3	MLOP
URS Shock Tube Metal panel walls	120	45	7.1e4	2.9e7	0.70	0.43	2.13	0.58	0.01	Simple	5.0e4	1.0e4	0.61	0.10	70	0.12	4.2	210	0.24	1.44			Blowout
ERDC EWRP-7 Tests Outboard Stud Wall	129	16	4.7e4	2.9e7	1.53	4.62	0.71	0.25	0.23	Simple	7.3e4	3.4e4	2.18	2.33	643	1.01	35.0	212	0.25	0.20	7.6	6.7	LLOP

Test Series/ Component[1, 2]	L (in)	B (in)	fdy (psi)	E (psi)	Z (in^3)	I (in^4)	A (in^2)	Self Weight (lb/in)	Supp Weight (psi)	Support	M (lb-in)	Max Tension Force (lbs)	Ru (psi)	K (psi/in)	Mass (psi-ms^2/in)	Ktm (psi/in)	P (psi)	I (psi-ms)	Pbar	Ibar	Max. Defl. (in)	Theta (deg)	LOP
ERDC EWRP-7 Tests Army Inboard Stud Wall	110	16	4.7e4	2.9e7	1.53	4.62	0.71	0.25	0.15	Simple	7.3e4	3.4e4	3.00	4.40	422	1.39	34.0	219	0.20	0.22	8.5	8.8	LLOP
ERDC EWRP-7 Tests Army Inboard Stud Wall	110	16	4.7e4	2.9e7	0.77	2.32	0.36	0.13	0.15	Simple	3.6e4	1.7e4	1.50	2.21	402	0.70	34.0	219	0.42	0.38	7.2	7.5	VLLOP
AFRL BREW -1 Tests Single Stud w/ Brick	144	16	4.7e4	2.9e7	0.76	2.32	0.35	0.16	0.28	Simple	3.6e4	1.6e4	0.87	0.75	746	0.40	33.0	200	0.56	0.30	6.8	5.4	LLOP
AFRL BREW -1 Tests Single Stud w/ EIFS	144	16	4.7e4	2.9e7	0.76	2.32	0.35	0.16	0.01	Simple	3.6e4	1.6e4	0.87	0.75	52	0.40	33.0	200	0.56	1.14			Blowout

Note 1: BCEPB refers to the Blast Capacity Evaluation of Pre-Engineered Building test series
Note 2: O.T. refers to Operation Teapot test series

APPENDIX F.
DATA FROM SHOCK LOADING TESTS ON OPEN WEB STEEL JOISTS

Table F-1 shows data from open web steel joists with significant tension membrane conducted during a test program performed at Tyndall AFB (Bogozian and Dunn, 2000) that was scaled using the $Pbar_{TM}$ and $Ibar_{TM}$ terms in Equation 10. These terms are called out as Pbar and Ibar in Table F-1. The Pbar and Ibar values in Table F-1 are plotted against scaled P-i curves in Section 6.7.

The tests were conducted on a roof with corrugated steel panels supported by cold-formed girts that spanned across the open web steel joists. The joists only had typical bracing for the tension flange, which buckled during rebound. See Section 6.7 for discussion of tension membrane forces that developed in the joists during the tests. The joists were welded to embedded plates in a support structure with 12 inch concrete walls. The measured side-on blast loads at the center of the roof are shown in Table F-1. The joists actually had a spatially non-uniform blast load along their span since the blast wave swept across the roof and did not apply the same load at all points along the joist spans. However, the charge standoffs used in the tests were in the 100 ft to 200 ft range compared to the 20 ft span length, so the use of the midspan load as an equivalent uniform load was considered to be an acceptable approximation for analyzing the data. The joist in the last test was upgraded so that it had a reported 50% increase in strength. This factor was used to determine the stiffness and ultimate resistance reported in Table F-1.

Table F-1. Data for Open Web Steel Joists

Test	L (in)	B (in)	Allowable Load Capacity (lb/ft)	Load Causing L/360 (lb/ft)	Self Weight (lb/ft^2)	Supported Weight (lb/ft^2)	Max Tension Force (lbs)	Ru (psi)	K (psi/in)	Mass ($psi\text{-}ms^2/in$)	Ktm (psi/in)	Max Defl (in)	Theta (deg)	mu	P (psi)	I (psi-ms)	Pbar	Ibar	LOP
Test 1 12K1 Joist	240	48	240	142	1.8	2.0	9000	0.88	0.37	67	0.026	4.7	2.2	2.0	2.1	26	0.19	0.10	MLOP
Test 2 12K1 Joist	240	48	240	142	1.8	2.0	9000	0.88	0.37	67	0.026	5.6	2.7	2.3	2.8	37	0.31	0.14	MLOP
Test 3 12K1 Joist	240	48	240	142	1.8	2.0	9000	0.88	0.37	67	0.026	7.7	3.7	3.2	4.4	43	0.56	0.16	LLOP
Test 4 Upgraded Joist	240	48	360	213	2.2	3.8	30000	1.33	0.55	108	0.087	9.1	4.3	3.8	6	65	0.22	0.14	LLOP

APPENDIX G.
DATA FROM SHOCK LOADING TESTS ON CORRUGATED STEEL PANELS

Table G-1 shows data from corrugated steel panels without significant tension membrane conducted during several test programs as noted in the table scaled using the Pbar1 (for ductility ratio and support rotation criteria), Ibar1 (for ductility ratio criteria), and Ibar2 (for support rotation criteria) terms in Equation 10. These terms are called out as Pbar and Ibar in Table G-1. The Pbar and Ibar values in Table G-1 for the cases where the panel response is controlled by ductility ratio and by support rotation criteria are each plotted against scaled P-i curves with Pbar and Ibar terms based on the same response criteria type in Section 6.1.

The data from *Blast Capacity Evaluation of Pre-Engineered Building* (Stea et al, 1979), which is abbreviated as (BCEPB) in Table G-1, was from a pre-engineered building that was subject to high explosive loads. The same building was subjected to six tests, which all caused relatively minor damage, and was repaired as necessary between tests. The panels were connected to cold-formed steel girts that were somewhat heavier than is typical, with somewhat reduced span lengths (3 ft to 4 ft). No tension membrane was assumed because the panels were connected to the slab with a small tube section that had "pig-tails" embedded in the concrete, which did not provide very much restraint necessary to develop tensile force in the panels. Also, the eave strut at the top of the wall had a relatively low flexural capacity against in-plane tension loading from the wall panels. Finally, the measured support rotations were relatively small. Tension membrane effects become much more pronounced at support rotations greater than approximately 4 degrees. This is based in part of data presented later in this appendix in Table G-2 where tension membrane effects were clearly noted in the observed panel response. The blast loads are based on measured reflected blast loads from 2000 lbs of high explosive at relatively large standoffs. The LOP were assigned to the test data based on photographs, descriptions of the damage, and the maximum measured panel deflections.

Data is also shown in Table G-1 from *Blast-Resistant Capacities of Cold-Formed Metal Panels* (BCCSP). High explosive loads were applied to test panels attached to support frames constructed from steel beams and a heavy wood and plywood frame. Relatively strong panels were tested that would be suitable for a blast resistant building. No information on the cross sectional properties of the test panels was provided, but the researchers performed SDOF analyses of all their tests and provide the properties of the equivalent spring-mass systems for the test panels as shown in Table G-1. Applied blast load information was also provided. The panels spanned 5 ft and were well attached to steel beams support, so that these panels probably could have developed significant tension membrane if they had undergone more severe support rotations. However, since almost all the measured support rotations were less than 4 degrees, no significant tension membrane was assumed for these tests. The LOP was assigned mainly based on the measured panel deflections and also descriptions and photographs of the most severely damaged panels.

Data from the proprietary 1997 Coop study described in Appendix E is also shown in Table G-1. Full-scale panels spanned 4 ft between girts in tests conducted in BakerRisk's full scale shock tube. The girts were supported by the shock tube frame. These data are for a standing seam roof deck (SSRD) and an insulated metal panel, where flat cold-formed steel panels are glued at each face to rigid insulation material. Measured reflected blast loads on the panels are shown in the table. The stiffness and ultimate capacity of the insulated panel is based on the assumption of a composite cross section. Both of these panel types inherently do not support tension membrane because of very low in-plane tension capacity of their connections to the girt framing. The measured loads from shock tube tests are shown in the table. The LOP were assigned to the data based on photographs of the tests and maximum panel deflections.

Table G-2 also shows data from corrugated steel panels with significant tension membrane conducted during several test programs as noted in the table scaled using the $Pbar_{TM}$ and $Ibar_{TM}$ terms in Equation 10. These terms are referred to as Pbar and Ibar in Table G-2. The Pbar and Ibar values in Table G-2 are plotted against scaled P-i curves in Section 6.1.

All the data in Table G-2 are from the proprietary 1997 Coop study conducted by BakerRisk that is described in Appendix E. In all these tests the panels were connected to the supporting girts with screws spaced at 6 inches or less. The maximum tension membrane force was assumed equal to the lesser of the ultimate shear capacity of the screws or the bearing capacity of the surrounding panel material. The panels were attached to a strengthened top girt, or eave girt, that supplied much more in-plane support to the panels than would be provided in a typical pre-engineered building. Photographs of the tests showed that panels without oversized washers failed by tearing away around the screws, indicating that the panels went into significant tension membrane response and the tension capacity was controlled by the connections. All the connections were standard #12 self-tapping screws. Measured reflected blast loads on the panels are shown in the table. All the panels had support rotations in the range of 4 degrees or larger.

Table G-1. Data for Cold-Formed Corrugated Steel Panels Without Significant Tension Membrane

Component [1,2,3]	L (in)	B (in)	Fdy (psi)	E (psi)	Z (in^3)	I (in^4)	Self Weight (psf)	M (lb-in)	Ru (psi)	K (psi /in)	Mass ($psi\text{-}ms^2/in$)	Max Defl (in)	Mu	Theta	P (psi)	I (psi-ms)	Support Rotation		Ductility Ratio		LOP
																	Pbar	Ibar	Pbar	Ibar	
BCEPB Test No.1	49	12	8.4e4	2.9e7	0.06	0.06	1.3	4.8e3	2.0	3.8	22.5	0.6	1.2	1.4	0.5	10	0.25	0.11	0.25	1.03	HLOP
BCEPB Test No.3	49	12	8.4e4	2.9e7	0.06	0.06	1.3	4.8e3	2.0	3.8	22.5	1.0	2.0	2.4	1.4	25	0.72	0.27	0.72	2.59	MLOP
BCEPB Test No.4	49	12	8.4e4	2.9e7	0.06	0.06	1.3	4.8e3	2.0	3.8	22.5	1.8	3.5	4.3	2.1	32	1.05	0.34	1.05	3.31	MLOP
BCEPB Test No.5	49	12	8.4e4	2.9e7	0.06	0.06	1.3	4.8e3	2.0	3.8	22.5	1.9	3.7	4.5	2.5	44	1.25	0.47	1.25	4.55	LLOP
BCEPB Test No.6	49	12	8.4e4	2.9e7	0.06	0.06	1.3	4.8e3	2.0	3.8	22.5				2.4	42	1.20	0.45	1.20	4.34	LLOP
1997 Coop SSRD, 24 g	45	12	6.7e4	2.9e7	0.07	0.13	1.3	4.4e3	2.2	12	22.5	10.5	58	25.1	4.2	55	1.92	0.58	1.92	9.13	VLLOP
1997 Coop, 2 in Insulated Panels	45	12	4.4e4	2.9e7	0.70	0.52	2.7	3.1e4	15.1	49	48.9	12.5	41	29.1	4.2	61	0.28	0.13	0.28	1.31	VLLOP
BCCSP Structure A roof	60						Note 4		2.7	2.6	32.0	1.5	1.4	2.8	2.0	30	0.75	0.20	0.75	1.55	MLOP
BCCSP Structure B roof	60						Note 4		5.3	11	60.0	0.9	1.9	1.8	4.5	59	0.85	0.20	0.85	1.98	MLOP
BCCSP Structure C roof	60						Note 4		7.7	17	80.9	0.7	1.4	1.3	5.6	76	0.73	0.17	0.73	1.74	MLOP
BCCSP Structure D roof	60						Note 4		7.0	30	51.2	1.0	4.1	1.8	7.0	91	1.00	0.29	1.00	4.01	MLOP
BCCSP Structure A roof	60						Note 4		3.3	6	32.7	1.7	2.9	3.2	3.2	48	0.97	0.29	0.97	2.83	MLOP
BCCSP Structure B roof	60						Note 4		6.8	14	66.8	0.7	1.4	1.3	4.5	63	0.66	0.17	0.66	1.68	MLOP
BCCSP Structure D roof	60						Note 4		8.3	36	60.8	1.7	7.4	3.3	9.5	114	1.14	0.30	1.14	4.05	LLOP
BCCSP Structure A roof	60						Note 4		5.0	8	45.7	1.4	2.3	2.6	4.5	65	0.90	0.26	0.90	2.40	MLOP

																	Support Rotation		Ductility Ratio		
BCCSP Structure B roof	60						Note 4		5.2	9	47.6	2.3	3.9	4.4	5.6	76	1.08	0.29	1.08	2.66	MLOP
BCCSP Structure C roof	60						Note 4		10.3	22	108.2	1.6	3.6	3.1	11	138	1.07	0.24	1.07	2.19	MLOP
BCCSP Structure D roof	60						Note 4		15.8	72	104.7	0.7	3.1	1.3	15	158	0.95	0.22	0.95	2.63	MLOP
BCCSP Structure B wall	60						Note 4		8.3	19	111.6	0.8	1.8	1.5	11.5	46	1.39	0.09	1.39	0.87	MLOP
BCCSP Structure B wall	60						Note 4		5.5	12	77.7	2.9	6.1	5.5	11.5	46	2.09	0.14	2.09	1.37	LLOP
BCCSP Structure B wall	60						Note 4		8.0	13	81.1	2.1	3.4	4.0	13.5	54	1.69	0.13	1.69	1.05	MLOP

Note 1: BCEPB are tests from Blast Capacity Evaluation of Pre-Engineered Building report
Note 2: BCCSP are tests from Blast-Resistant Capacities of Cold-Formed Metal Panels report
Note 3: Tests by Wilfred Baker Engineering for 1997 Petrochemical Industrial Research Cooperative
Note 4: Ru, K, and Mass properties calculated by researchers are used directly in table

Table G-2. Data for Cold-Formed Corrugated Steel Panels With Significant Tension Membrane

Component	L (in)	B (in)	Fdy (psi)	E (psi)	Z (in^3)	I (in^4)	Self Weight (psf)	Support	M (lb-in)	Max. Tension Force (lbs/in)	Ru (psi)	K (psi /in)	Mass (psi-ms^2/in)	Ktm (psi /in)	Max Defl. (in)	Mu	Theta	P (psi)	I (psi-ms)	Pbar	Ibar	LOP
1997 Coop 24 g M, 6 in screw sp.	87	12	6.7e4	2.9e7	0.05	0.03	1.3	Fixed	3.6e3	210	0.6	0.4	22.5	0.2	13.0	7.7	16.6	3.2	28	0.13	0.37	LLOP
1997 Coop, SSRD, 24 g w/ 22 g flat panel	45	12	6.7e4	2.9e7	0.07	0.13	2.5	Fixed-Simple	4.4e3	262	2.2	12	44.5	1.0	11.0	60	26.1	5.5	95	0.07	0.51	LLOP
1997 Coop Stromgard 26 g	45	12	8.4e4	2.9e7	0.02	0.02	1.0	Fixed-Simple	1.7e3	175	0.8	1.9	18.0	0.7	7.0	16	17.3	3.1	43	0.07	0.69	LLOP
1997 Coop 26 g R, flat 22 g	45	12	6.7e4	2.9e7	0.04	0.04	2.2	Fixed-Simple	2.8e3	333	1.4	3.8	40.0	1.3	9.0	25	21.8	4.2	72	0.05	0.49	LLOP
1997 Coop 24 g M, 6 in screw sp.	45	12	6.7e4	2.9e7	0.05	0.03	1.3	Fixed-Simple	3.6e3	210	1.8	2.7	22.5	0.8	3.0	4.6	7.6	2.5	34	0.02	0.24	LLOP
1997 Coop Nested 22 g R	45	12	6.7e4	2.9e7	0.14	0.14	3.1	Fixed-Simple	9.3e3	333	4.6	13	55.4	1.3	4.8	14	12.1	8.2	137	0.06	0.41	LLOP
1997 Coop Nested 22 g R	45	12	6.7e4	2.9e7	0.14	0.14	3.1	Fixed-Simple	9.3e3	333	4.6	13	55.4	1.3	1.4	4.0	3.5	5.0	100	0.01	0.18	MLOP

APPENDIX H.
DATA FROM SHOCK LOADING TESTS ON WOOD STUD WALLS

Table H-1 shows data from wood buildings and wood wall panels subjected to high explosive and shock tube loads scaled using the Pbar1 and Ibar1 terms in Equation 10. These terms are referred to as Pbar and Ibar in Table H-1. The Pbar and Ibar values in Table H-1 are plotted against scaled P-i curves in Section 6.9.

Data shown in Table H-1 from the BAITS tests (Marchand, 2000) are from light wood SEA huts subject to blast loads from large high explosive charges at large standoff distances. Measured reflected blast loads are shown in the table. The SEA huts had 2 inch x 4 inch wood studs at 16 inch spacing with a 8 ft clear span supporting 5/8 inch plywood cladding. All the data in Table H-1 is for response of the reflected walls. The LOP are based on descriptions of the damage in each test and photographs. No information is available on the yield strength and modulus of elasticity of the wood used to construct the SEA huts. The yield strengths in Table H-1 are estimated from a typical allowable yield strength of 1,300 psi for construction quality visually graded lumber multiplied by 2.5 to account for the safety factor and then 2.0, which is the maximum allowable impact factor for wood design. The modulus of elasticity is estimated as 1.4e6 psi, which is in the range of typical values for construction quality lumber. There is considerable variation in wood stud strength and modulus of elasticity based on moisture content and density. The values in Table H-1 are considered reasonable estimates and they cause scaled Pbar and Ibar values for data with response ranging from light damage to failure that are consistent with scaled P-i diagrams based on SDOF analyses with ductility ratios in the range of 1 to 3. These ductility ratios are within the expected response range for a material like wood with limited ductility.

The WBE data in Table H-1 is from shock tube tests performed by Wilfred Baker Engineering, Inc. (now BakerRisk) for a commercial client where wood stud walls were tested in BakerRisk's large shock tube. The walls were intended to be blast resistant and were constructed with closely spaced studs that were nailed to 0.5 inch thick plywood cladding on one face or two faces with nails as close as 3 inches on center. The measured peak dynamic reactions were close to values calculated using the assumed yield strength values in Table H-1 and the assumption of no composite action for walls where the cladding was cut horizontally at midspan so that it could not contribute to the overall flexural capacity of the wall system and for tests where the cladding was not cut. Also, very similar peak dynamic reactions were calculated for otherwise identical test walls where cladding was very well nailed to one and two sides of the studs. Therefore, no composite action is assumed for any of the tests in Table H-1 or in the CEDAW program. The studs were Southern Pine No. 2 visually graded lumber. The blast load durations for these tests ranged from 40 ms to 80 ms, which were two to four times the natural periods of the test walls assuming no composite action between the studs and cladding.

Table H-1. Data for Cold-Formed Corrugated Steel Panels without Significant Tension Membrane

Test No.	L	Stud Width (inch)	Stud Depth (inch)	Spacing (inch)	Fdy (psi)	E (psi)	I (in^4))	S (in^3	Supported Weight (psf)	M (lb-in)	Ru (psi)	K (psi /in)	Mass[1] (psH-ms^2/in)	P (psi)	I (psi-ms)	Pbar	Ibar	LOP
Baits Test SH 1	96	1.5	3.5	16	6.5e3	1.4e6	5.4	3.1	1.6	2.0e4	1.1	0.4	45	4.5	14	4.2	0.66	LLOP
Baits Test SH 2	96	1.5	3.5	16	6.5e3	1.4e6	5.4	3.1	1.6	2.0e4	1.1	0.4	45	2.0	8	1.8	0.42	HLOP
Baits Test SH 1	96	1.5	3.5	16	6.5e3	1.4e6	5.4	3.1	1.6	2.0e4	1.1	0.4	45	10.8	64	10.0	2.95	Collapse
Baits Test SH 2	96	1.5	3.5	16	6.5e3	1.4e6	5.4	3.1	1.6	2.0e4	1.1	0.4	45	3.0	36	2.8	1.77	VLLOP
Baits Test SH 3	96	1.5	3.5	16	6.5e3	1.4e6	5.4	3.1	1.6	2.0e4	1.1	0.4	45	1.0	8	0.9	0.40	MLOP
Baits Test SH 3	96	1.5	3.5	16	6.5e3	1.4e6	5.4	3.1	1.6	2.0e4	1.1	0.4	45	1.7	12	1.6	0.60	MLOP
Baits Test SH 3	96	1.5	3.5	16	6.5e3	1.4e6	5.4	3.1	1.6	2.0e4	1.1	0.4	45	3.4	18	3.1	0.89	MLOP
Baits Test SH 4	96	1.5	3.5	16	6.5e3	1.4e6	5.4	3.1	1.6	2.0e4	1.1	0.4	45	4.3	46	3.9	2.24	VLLOP
Baits Test SH 8	96	1.5	3.5	16	6.5e3	1.4e6	5.4	3.1	1.6	2.0e4	1.1	0.4	45	11.7	69	10.8	3.17	Collapse
Baits Test SH 7 (end-on)	96	1.5	3.5	16	6.5e3	1.4e6	5.4	3.1	1.6	2.0e4	1.1	0.4	45	5.9	38	5.4	1.80	Collapse
Baits Test SH 10	96	1.5	3.5	16	6.5e3	1.4e6	5.4	3.1	1.6	2.0e4	1.1	0.4	45	35.9	127	33.2	5.60	Collapse
Baits Test Long SEA Hut	96	1.5	3.5	16	6.5e3	1.4e6	5.4	3.1	1.6	2.0e4	1.1	0.4	45	4.9	33	4.6	1.60	Collapse
Baits Test SH 7	96	1.5	3.5	16	6.5e3	1.4e6	5.4	3.1	1.6	2.0e4	1.1	0.4	45	19.9	101	18.4	4.57	Collapse
WBE Test 2	96	1.5	5.5	6	6.5e3	1.4e6	20.8	7.6	3.1	4.9e4	7.1	4.4	128	6.0	185	0.8	2.39	MLOP
WBE Test 3	96	1.5	5.5	6	6.5e3	1.4e6	20.8	7.6	3.1	4.9e4	7.1	4.4	128	7.5	181	1.1	2.38	LLOP
WBE Test 4	96	1.5	7.5	6	6.5e3	1.4e6	52.7	14.1	1.6	9.1e4	13.2	11.2	126	12.3	244	0.9	2.63	VLLOP
WBE Test 5	96	1.5	7.5	6	6.5e3	1.4e6	52.7	14.1	3.1	9.1e4	13.2	11.2	155	10.0	388	0.8	3.70	MLOP
Note 1: Stud self-weight estimated based on 35 lb/ft^3 density.																		

APPENDIX I.
DATA FROM SHOCK LOADING TESTS ON REINFORCED CONCRETE COLUMNS RESPONDING IN SHEAR

Table I-1 shows data from reinforced concrete columns subjected to high explosive loads scaled using the Pbar1 and Ibar1 terms in Equation 10. These terms are referred to as Pbar and Ibar in Table I-1. The ultimate resistances used in the Pbar and Ibar terms are based on the ultimate concrete shear capacity, as described in Section 6.10. The Pbar and Ibar values in Table I-1 are plotted against scaled P-i curves in Section 6.10.

The data in Table I-1 is from the Devine Buffalo (DB) test series (Plamondon and Sheffield, 1999), the Murrah Building near the 1995 Oklahoma City bombing (FEMA, 1996), and the Kansallis House near the Bishopgate IRA bombing in London. The DB tests were conducted outside a typical concrete frame building with infill CMU walls. The Kansallis House and Murrah Buildings were concrete frame buildings with lightweight cladding located near the Bishopgate and Oklahoma City terrorist bombs. The blast loads from these two bombings are calculated from estimated explosive charge weights by U.S. and U.K. government engineers based on a number of factors including vehicle size, crater dimensions, and radius of window breakage. Column damage was based on post–test and post-explosion photographs of the buildings.

Detailed information was available on the G Line columns of the Murrah Building nearest the Oklahoma City bombing, which were free standing columns located under the third floor above (FEMA, 1996). The net blast loads on these columns in Table I-1 were calculated at mid-height using methods from TM 5-1300 (1990) assuming a surface burst explosion. The reflected blast load was calculated on the side of the column facing the explosion, which is shown as the width in Table I-1, including angle of incidence and clearing effects. The side-on blast load was calculated on the back side of the columns and subtracted from the reflected blast load to obtain a net impulse. The load durations were short compared to the column natural period. The columns were supported with a compression strut back to the second floor in their strong bending axis, but no support at the second floor was assumed for loading in the weak-bending axis. Since Columns G16 and G24 were loaded primarily in their weak-bending axis, these column heights were based on the third floor support. The design concrete strength of 4000 psi is shown in Table I-1. The column ties in Columns G16 and G24 were spaced at more than one-half the depth to the reinforcing steel and were therefore not included in the shear strength.

Information on the Kansallis House columns is based on scaled dimensions off a plan drawing of the building showing the approximate bomb location. The column concrete strength is estimated based on typical construction values. The column ties were assumed to be spaced at more than a distance of one-half the reinforcing steel depth and were therefore not included in the shear strength calculations. The reflected blast loads were calculated using the methods in TM 5-1300 for a surface burst including the effects of the angle of incidence.

Information on the DB test series, including charge size, location, and column dimensions, was obtained from Plamondon and Sheffield (1999). The reported charge size and location was used to calculate reflected blast loads at midheight on the columns including the effects of angle of incidence using the methods in TM 5-1300 (1990) for a surface burst. The column ties spaced at more than a distance of one-half the reinforcing steel depth and were therefore not included in

the shear strength calculations.

Table I-1. Summary of Reinforced Concrete Column Blast Data

Column	Standoff (ft)	Concrete Compression Strength (psi)	Width (in)	Depth (in)	Height (in)	Peak Pressure (psi) [2]	Impulse (psi-ms) [2]	Pbar[1]	Ibar[1]	Damage
Murrah Bldg G20	16	4000	20	36	108	6960	1995	14.6 [3]	3.1 [3]	Fail
Murrah Bldg G16	47	4000	36	20	252	635	1099	17.7	2.2	Fail
Murrah Bldg G24	38	4000	36	20	252	1060	1421	29.5	2.8	Fail
Murrah Bldg G12	86	4000	36	20	252	116	400	4.6	1.1	No Fail
Kansallis House A8	22	4000	10	8	132	3681	1025	168.7	3.7	Fail
Kansallis House A9, A10	16	4000	8	10	132	7066	1880	236.5	6.8	Fail
Kansallis House A7	35	4000	10	8	132	1200	470	78.5	2.4	No Fail
DB23	25	5000	12	12	129	1500	1000	19.5	2.7	Fail
DB20	13	5000	14	14	129	6000	2500	61.1	6.5	Fail
DB30	20	5000	15	15	129	2100	1400	20.3	3.8	Fail
DB6 A4	25	5000	14	14	147	600	550	18.3	2.4	No Fail

Note 1: Pbar1 and Ibar1 terms in Equation 8, where Y=1
Note 2: Charge weights from terrorist bombings estimated by U.S. and U.K. government engineers based on a number of factors including vehicle size, crater dimensions, and radius of window breakage
Note 3: Includes 165 psi of shear capacity from ties spaced at less than Depth/2

APPENDIX J.
DATA FROM SHOCK LOADING TESTS ON STEEL COLUMNS LIMITED BY CONNECTION CAPACITY

Table J-1 shows data from steel columns with typical anchor bolts connecting the column baseplate to the slab subjected to high explosive loads scaled using the Pbar1 and Ibar1 terms in Equation 10. These terms are referred to as Pbar and Ibar in Table J-1. The ultimate resistances used in the Pbar and Ibar terms are based on the ultimate connection shear capacity, as described in Section 6.11. The Pbar and Ibar values in Table J-1 are plotted against scaled P-i curves in Section 6.11. The very limited available data in Table J-1 is taken from Stanley and Osowski (2002), which gives details on the column and connection sizes and properties and the charge weight and standoff. The reflected blast loads were calculated at mid-height over the column width using the methods of TM 5-1300 for a surface burst. This test data showed that connection failure was the weakest response mode when conventional types of column baseplate connections were used. Other tests were performed where strengthened connections were used to prevent connection failure.

Table J-1. Summary of Available Steel Column Blast Test Data

Case	Size	Loaded Axis	No. Bolts	Bolt Dia. (in)	Loaded Width (in)	Span (in)	Ultimate Resistance[1] (psi)	Peak Pressure (psi)	Impulse (psi-ms)	Pbar	Ibar
Matrix 2, Test 1	W14x53	Strong	8	1	8	165	550	4000	2000	7.4	2.2
Matrix 2, Test 2	W14x53	Weak	8	1	14	165	308	4000	2000	13.0	1.5
Arena, Column C	W14x53	Strong	8	0.75	8	240	210	4000	2000	19.2	2.7
Note 1: Based on F_{dv}=56,000 psi for A325 anchor bolts											

APPENDIX K.
COMPARISON OF P-I DIAGRAMS CALCULATED WITH CEDAW AND SDOF ANALYSES

Table K-1 and K-2 show comparisons of pressure and impulse values from P-i diagrams calculated with SDOF analyses and with CEDAW as described in Section 7.1 of the report. The SDOF analyses were made with the SBEDS computer program (Nebuda and Oswald, 2004). Comparisons were made for each component type using component properties that are typical for conventional construction. Numerous comparisons were made for unreinforced masonry walls because the CEDAW curve-fits for this component type is also dependent on the ratio of resistance from axial load arching to resistance from flexural resistance, as discussed in Section 3.0 and Section 4.3. The cases in Table K-1 with low, medium, and high axial load correspond to ratios of resistance from axial load arching to resistance from flexural resistance of 17%, 60%, and 100%, respectively. Table K-1 also shows comparisons for components spanning in one and two directions for reinforced concrete slabs and unreinforced masonry walls, which are the two component types in CEDAW that can have two-way spans.

The tables show that pressure and impulse values calculated with CEDAW are almost always within 15% of comparable values calculated with SBEDS. This is least true for the pressure point on the inflection point of the P-i diagrams, but this point is the most difficult to define since the P-i curves are relatively flat in this region. The overall trend is for CEDAW to slightly overestimate the pressure point at the point of minimum impulse, indicated by a P-ratio greater than 1.0 in Tables K-1 and K-2. See Section 7.1 for average values and standard deviations of the ratios of CEDAW to SDOF P-i curve values shown in Tables K-1 and K-2.

Table K-1. Comparison of P-i Diagrams Calculated with CEDAW and SDOF Analyses in English Units

Component	Pressure Asymptote Comparison			Point of Minimum Impulse Comparison						Comparison at High Pressure Value					
	SBEDS	CEDAW	CEDAW/ SBEDS	SBEDS		CEDAW		CEDAW/ SBEDS		SBEDS		CEDAW		CEDAW/ SBEDS	
	Pressure (psi)	Pressure (psi)	P-ratio	Impulse (psi-sec)	Pressure (psi)	Impulse (psi-sec)	Pressure (psi)	P-ratio	I-ratio	Impulse (psi-sec)	Pressure (psi)	Impulse (psi-sec)	Pressure (psi)	P-ratio	I-ratio
Steel Beams (No Tension Membrane)	0.5	0.55	1.10	0.015	2	0.015	2	1.00	1.00	0.032	100	0.035	100	1	1.09
	0.85	0.9	1.06	0.035	3.5	0.038	4.3	1.23	1.09	0.065	100	0.067	100	1	1.03
	0.9	0.95	1.06	0.055	3.6	0.064	5	1.39	1.16	0.09	100	0.095	100	1	1.06
	1	1	1.00	0.08	4.8	0.08	5.5	1.15	1.00	0.14	100	0.14	100	1	1.00
Steel Beams (Tension Membrane)	0.5	0.55	1.10	0.015	2	0.016	2	1.00	1.07	0.022	100	0.025	100	1	1.14
	1.2	1.2	1.00	0.055	5	0.059	3	0.60	1.07	0.1	100	0.088	100	1	0.88
	1.5	1.6	1.07	0.095	7	0.093	7	1.00	0.98	0.15	100	0.14	100	1	0.93
	1.9	1.9	1.00	0.14	10	0.13	8	0.80	0.93	0.2	100	0.22	100	1	1.10
Metal Panels	1	1.05	1.05	0.012	3.3	0.013	4.1	1.24	1.08	0.02	100	0.022	100	1	1.10
	1.65	1.75	1.06	0.025	7.15	0.028	9	1.26	1.12	0.037	100	0.038	100	1	1.03
	1.87	2	1.07	0.039	9.9	0.041	10	1.01	1.05	0.053	100	0.054	100	1	1.02
	2	2.2	1.10	0.05	11	0.058	10.4	0.95	1.16	0.07	100	0.073	100	1	1.04
Open Web Steel Joists (No Tension Membrane)	0.4	0.4	1.00	0.054	1.8	0.055	1.5	0.83	1.02	0.13	100	0.14	100	1	1.08
	0.6	0.6	1.00	0.09	2.5	0.083	3.2	1.28	0.92	0.2	100	0.18	100	1	0.90
	0.7	0.7	1.00	0.15	3	0.15	4	1.33	1.00	0.3	100	0.27	100	1	0.90
	0.8	0.8	1.00	0.2	4	0.18	4	1.00	0.90	0.38	100	0.38	100	1	1.00
One-Way Reinforced Concrete (RC) Slab	1.7	1.6	0.94	0.028	7	0.029	8	1.14	1.04	0.041	100	0.04	100	1	0.98
	3	2.7	0.90	0.13	20	0.14	25	1.25	1.08	0.16	100	0.16	100	1	1.00
	3.1	2.9	0.94	0.21	28	0.21	30	1.07	1.00	0.32	100	0.24	100	1	0.75
	3.3	3.2	0.97	0.3	28	0.31	30	1.07	1.03	0.35	100	0.35	100	1	1.00
Two-Way RC Slab (Two-side supported)	2.9	3	1.03	0.18	18	0.19	17	0.94	1.06	0.23	100	0.23	100	1	1.00
	3.8	4.9	1.29	0.25	30	0.3	50	1.67	1.20	0.29	100	0.31	100	1	1.07
	5	5	1.00	0.46	45	0.48	60	1.33	1.04	0.5	100	0.59	100	1	1.18
	5.5	5.9	1.07	0.7	50	0.7	70	1.40	1.00	0.75	100	0.7	100	1	0.93
Two-Way RC Slab (Three-side	21	18	0.86	0.17	250	0.18	223	0.89	1.06	0.18	100	0.18	100	1	1
	35	30	0.86	0.53	600	0.48	600	1.00	0.91	0.65	100	0.65	100	1	1
	37	35	0.95	0.9	700	0.7	800	1.14	0.78	1.2	100	1	100	1	0.83

Component	Pressure Asymptote Comparison			Point of Minimum Impulse Comparison						Comparison at High Pressure Value					
	SBEDS	CEDAW	CEDAW/ SBEDS	SBEDS		CEDAW		CEDAW/ SBEDS		SBEDS		CEDAW		CEDAW/ SBEDS	
	Pressure (psi)	Pressure (psi)	P-ratio	Impulse (psi-sec)	Pressure (psi)	Impulse (psi-sec)	Pressure (psi)	P-ratio	I-ratio	Impulse (psi-sec)	Pressure (psi)	Impulse (psi-sec)	Pressure (psi)	P-ratio	I-ratio
supported)	39	38	0.97	1.3	700	1.1	800	1.14	0.85	1.8	100	1.6	100	1	0.89
RC Beam	0.6	0.6	1.00	0.016	2.7	0.014	3	1.11	0.88	0.03	100	0.03	100	1	1.00
	1.1	1.2	1.09	0.055	6.5	0.057	7	1.08	1.04	0.085	100	0.09	100	1	1.06
	1.2	1.3	1.08	0.087	6.8	0.09	8	1.18	1.03	0.13	100	0.14	100	1	1.08
	1.3	1.4	1.08	0.12	6.8	0.14	8	1.18	1.17	0.19	100	0.2	100	1	1.05
Reinforced Masonry Wall	7	6	0.86	0.04	45	0.046	50	1.11	1.15	0.05	100	0.048	100	1	0.96
	11.5	11	0.96	0.28	150	0.28	200	1.33	1.00	0.28	100	0.28	100	1	1.00
	13	13	1.00	0.55	200	0.52	250	1.25	0.95	0.55	100	0.58	100	1	1.05
	14	16	1.14	0.75	300	0.75	300	1.00	1.00	0.8	100	0.8	100	1	1.00
One-Way Unreinforced Masonry Wall (URM) with No Axial Load)	0.4	0.4	1	0.0048	1.6	0.0042	1.7	1.06	0.88	0.012	100	0.012	100	1	1
	0.55	0.55	1	0.022	0.8	0.022	0.9	1.13	1.00	0.07	100	0.071	100	1	1.01
	0.55	0.55	1.00	0.037	0.85	0.036	1	1.18	0.97	0.13	100	0.12	100	1	0.92
Two-Way URM Wall with Small Axial Load	2	2.1	1.05	0.009	9	0.009	11	1.22	1.00	0.009	10	0.009	10	1	1.00
	2.5	2.4	0.96	0.075	6	0.085	8	1.33	1.13	0.08	10	0.087	10	1	1.09
	2.5	2.5	1.00	0.15	7	0.15	8.5	1.21	1.00	0.15	10	0.15	10	1	1.00
One-Way URM Wall with Medium Axial Load	Scaled standoff too large in SDOF analyses			0.0067	1.5	0.0063	1.5	1.00	0.94	0.01	10	0.009	10	1	0.90
				0.048	2.3	0.045	2.4	1.04	0.94	0.06	10	0.058	10	1	0.97
				0.075	2.2	0.075	2.4	1.09	1.00	0.1	10	0.09	10	1	0.90
One-Way URM Wall with Large Axial Load	Scaled standoff too large in SDOF analyses			0.0058	0.8	0.0052	0.8	1.00	0.90	0.012	10	0.0097	10	1	0.81
				0.032	1.5	0.033	1.4	0.93	1.03	0.05	10	0.049	10	1	0.98
				0.048	1.5	0.053	1.5	1.00	1.10	0.075	10	0.078	10	1	1.04
Steel Column	50	50	1.00	No inflection point because of different shape of scaled P-i diagram						0.35		0.34			0.97
RC Column	700	700	1.00							1.5		1.5			1.00

Table K-2. Comparison of P-i Diagrams Calculated with CEDAW and SDOF Analyses in Metric Units

Component	Pressure Asymptote Comparison			Point of Minimum Impulse Comparison						Comparison at High Pressure Value					
	SBEDS	CEDAW	CEDAW/ SBEDS	SBEDS		CEDAW		CEDAW/ SBEDS		SBEDS		CEDAW		CEDAW/ SBEDS	
	Pressure (kPa)	Pressure (kPa)	P-ratio	Impulse (kPa-sec)	Pressure (kPa)	Impulse (kPa-sec)	Pressure (kPa)	P-ratio	I-ratio	Impulse (kPa-sec)	Pressure (kPa)	Impulse (kPa-sec)	Pressure (kPa)	P-ratio	I-ratio
Steel Beams (No Tension Membrane)	3.5	3.5	1.00	0.28	13	0.28	13	1.00	1.00	0.4	100	0.4	100	1	1.00
	6.1	5.1	0.84	0.7	25	0.65	25	1.00	0.93	0.8	100	0.78	100	1	0.98
	7	6.1	0.87	1.6	40	1.5	35	0.88	0.94	1.7	100	1.6	100	1	0.94
	7.5	7	0.93	2.1	40	2	45	1.13	0.95	2.2	100	2.2	100	1	1.00
Steel Beams (Tension Membrane)	3.5	3.5	1.00	0.28	13	0.28	13	1.00	1.00	0.4	100	0.4	100	1	1.00
	6.1	4.1	0.67	0.7	25	0.65	25	1.00	0.93	0.9	100	0.8	100	1	0.89
	10	10	1.00	1.6	45	1.7	60	1.33	1.06	1.8	100	1.7	100	1	0.94
	15	13	0.87	2.6	75	2.4	80	1.07	0.92	2.8	100	2.5	100	1	0.89
Metal Panels	7.15	7	0.98	0.08	30	0.09	30	1.00	1.13	0.1	100	0.1	100	1	1.00
	12.1	12	0.99	0.17	52	0.19	65	1.25	1.12	0.28	1000	0.28	1000	1	1.00
	13.2	15	1.14	0.26	65	0.28	70	1.08	1.08	0.4	1000	0.4	1000	1	1.00
	14.3	16	1.12	0.35	75	0.4	75	1.00	1.14	0.5	1000	0.52	1000	1	1.04
Open Web Steel Joists (No Tension Membrane)	2.8	2.9	1.04	0.38	10	0.38	10	1.00	1.00	0.62	100	0.6	100	1	0.97
	4	4.2	1.05	0.58	27	0.58	28	1.04	1.00	0.9	100	0.71	100	1	0.79
	5	4.7	0.94	1	25	0.93	30	1.20	0.93	1.3	100	1.3	100	1	1.00
	5.8	5.6	0.97	1.4	25	1.4	30	1.20	1.00	1.7	100	1.6	100	1	0.94
One-Way Reinforced Concrete (RC) Slab	11	11	1.00	0.19	50	0.19	60	1.20	1.00	0.31	1500	0.33	1500	1	1.06
	20	19	0.95	0.9	150	0.95	180	1.20	1.06	1.3	1500	1.2	1500	1	0.92
	21	20	0.95	1.5	160	1.6	180	1.13	1.07	1.8	1500	1.8	1500	1	1.00
	23	22	0.96	2	170	2.2	200	1.18	1.10	2.6	1500	2.7	1500	1	1.04
RC Beam	3	3	1.00	0.06	15	0.069	10	0.67	1.15	0.12	100	0.11	100	1	0.92
	6	5	0.83	0.3	25	0.34	30	1.20	1.13	0.4	100	0.39	100	1	0.98
	6.1	5.5	0.90	0.5	30	0.53	35	1.17	1.06	0.6	100	0.6	100	1	1.00
	6.5	6	0.92	0.7	30	0.8	38	1.27	1.14	0.8	100	0.85	100	1	1.06
Reinforced Masonry	50	40	0.80	0.35	300	0.34	300	1.00	0.97	0.36	1000	0.37	1000	1	1.03
	80	75	0.94	2	1200	1.8	1400	1.17	0.90	2	1000	1.9	1000	1	0.95

Component	Pressure Asymptote Comparison			Point of Minimum Impulse Comparison						Comparison at High Pressure Value					
	SBEDS	CEDAW	CEDAW/ SBEDS	SBEDS		CEDAW		CEDAW/ SBEDS		SBEDS		CEDAW		CEDAW/ SBEDS	
	Pressure (kPa)	Pressure (kPa)	P-ratio	Impulse (kPa-sec)	Pressure (kPa)	Impulse (kPa-sec)	Pressure (kPa)	P-ratio	I-ratio	Impulse (kPa-sec)	Pressure (kPa)	Impulse (kPa-sec)	Pressure (kPa)	P-ratio	I-ratio
Wall	85	85	1.00	4	1800	3.8	2000	1.11	0.95	3.9	1000	3.8	1000	1	0.97
	95	100	1.05	5.1	1900	5	1900	1.00	0.98	5.2	1000	5.2	1000	1	1.00
One-Way URM Wall with No Axial Load	Scaled standoff too large in SDOF analyses			0.032	12	0.031	10	0.83	0.97	0.05	100	0.048	100	1	0.96
				0.16	6.2	0.16	6	0.97	1.00	0.3	100	0.3	100	1	1
				0.3	6	0.26	6.5	1.08	0.87	0.6	100	0.5	100	1	0.83
Steel Column	95	95	1.00	No inflection point because of different shape of scaled P-i diagram						0.9		0.85			0.94
RC Column	5000	5000	1.00							12		12			1

APPENDIX L.
COMPARISON OF SCALED P-I DIAGRAMS

Figure L-1 through L-14 show comparisons of scaled P-i curves developed from SDOF analyses for different components of the same component type, response level, and non-dimensional response level should be identical, as described in Section 7.2. The scaling is performed with the applicable Pbar and Ibar terms for each component type and non-dimensional response type (i.e., ductility ratio or support rotation) from Table 2. The comparisons were made for components with a variety of spans, thicknesses, mass, strength and stiffness terms. The SDOF properties for each case are shown in the figures. Ideally, the scaled P-i curves for all cases would be identical, indicating perfect accuracy of the Pbar and Ibar scaling approach, except for Figure L-13 and L-14 discussed below. See Section 7.2 for a discussion of accuracy of the scaling approach based on the relatively minor differences between the analyzed cases, especially in the realms of primary interest.

Figure L-13 and L-14 show scaled P-i curves for unreinforced masonry components responding in brittle flexural with arching from axial load. As described in Equation 2, the scaled P-i curve-fits for this case are a function of the peak resistance from axial load arching divided by the ultimate flexural resistance. As shown in the information boxes at the top of these figures, this ratio is different for each case and therefore there are different CEDAW scaled P-i curves representing the same response levels for each case in the figures. Ideally, the points in the figures representing from the SDOF analyses for all cases would lie along the CEDAW curves.

Case	Ductility Ratio	Ru (psi)	K (psi/in)	Mass (psi-ms^2/in)
Case 1	1	1.1438281	0.9651	128.4542314
Case 2	1	4.5753125	15.442	128.4542314
Case 3	1	7.9305417	20.885	102.5474957
Case 4	1	13.05439	31.832	102.5474957

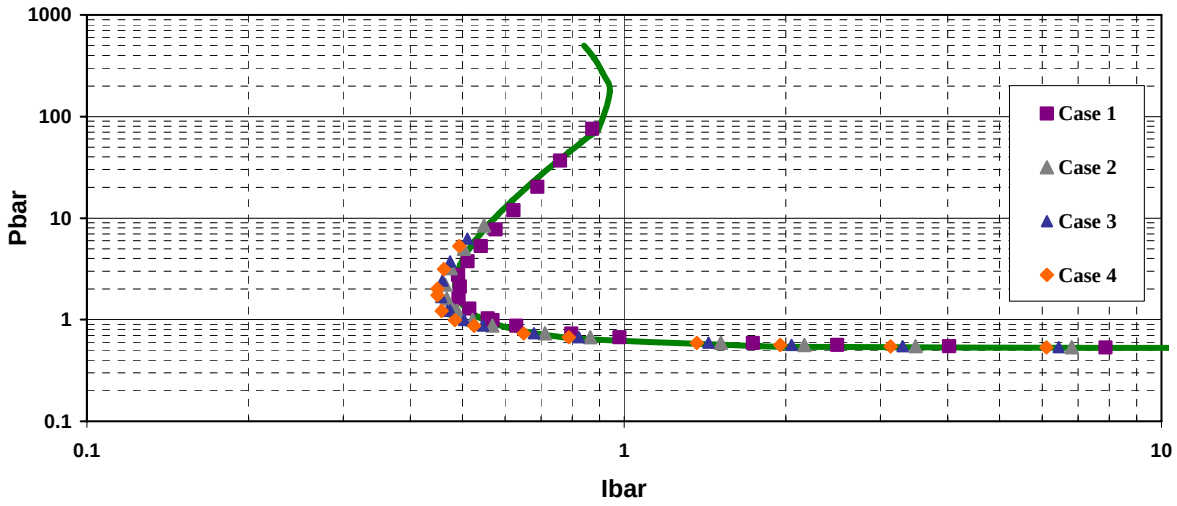

Figure L- 1. Comparison of Scaled P-i Curves Controlled by Ductility Ratio for Corrugated Steel Panels for HLOP Response

Case	Ductility Ratio	Ru (psi)	K (psi/in)	Mass (psi-ms^2/in)
Case 1	3	11.804	4.3467	1500
Case 2	3	4.8567	2.4839	1500
Case 3	3	2.1585	0.4906	1500
Case 4	3	1.1101	0.1854	1500

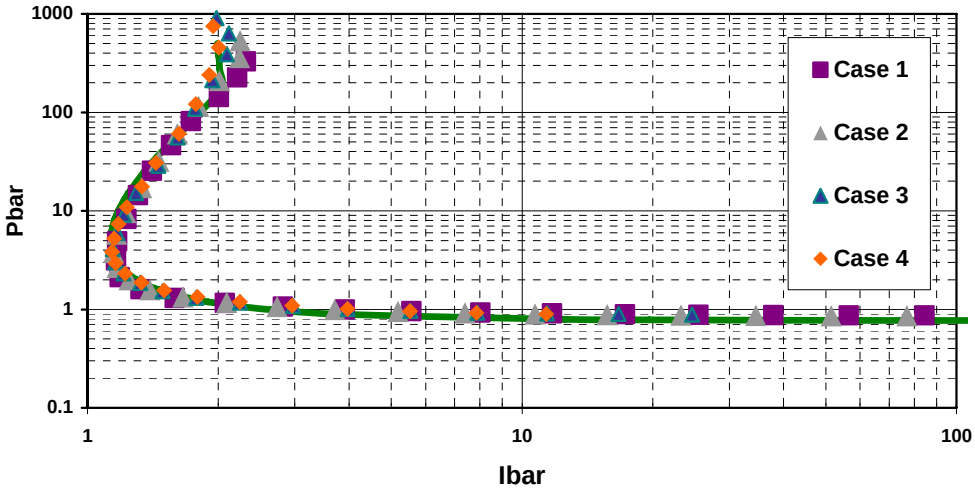

Figure L- 2. Comparison of Scaled P-i Curves Based on Ductility Ratio for Steel Beams with LOP Response

Case	Support Rotation	Ru (psi)	K (psi/in)	Mass (psi-ms^2/in)
Case 1	3	0.3681	0.117188	143.9263097
Case 2	3	0.8833	0.369688	143.9263097
Case 3	3	1.4722	0.598958	179.9078872
Case 4	3	2.0243	1.197917	197.8986759

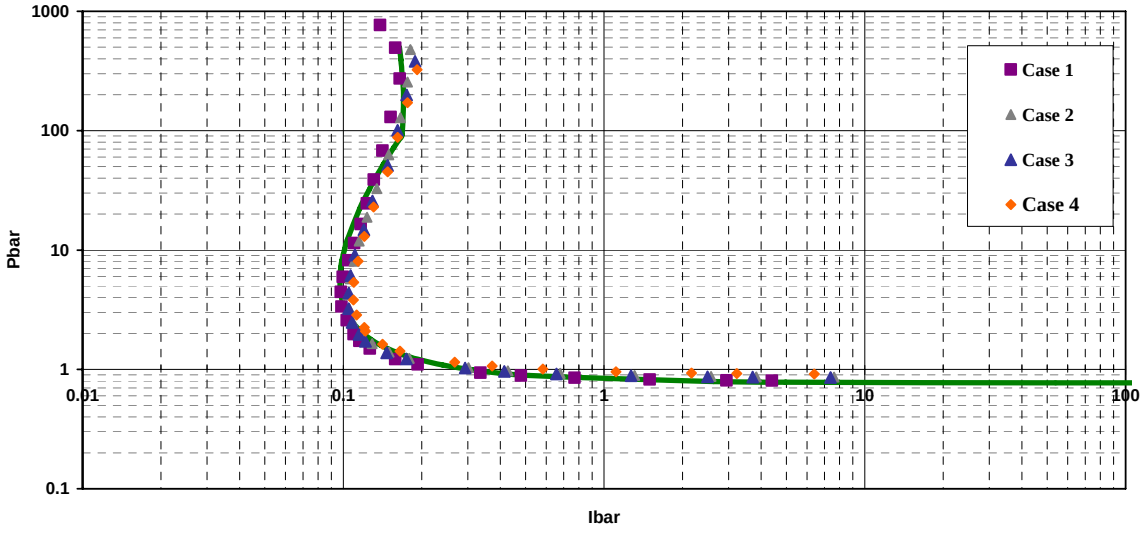

Figure L- 3. Comparison of Scaled P-i Curves Based on Support Rotation for Open Web Steel Joists without Tension Membrane for MLOP Response

Case	Support Rotation	Ru (psi)	K (psi/in)	Mass (psi-ms^2/in)
Case 1	5	0.325	0.34483241	1336.787565
Case 2	5	0.7752	0.84187599	1336.787565
Case 3	5	1.3781	2.66074388	1336.787565
Case 4	5	7.3785	107.760127	2673.57513

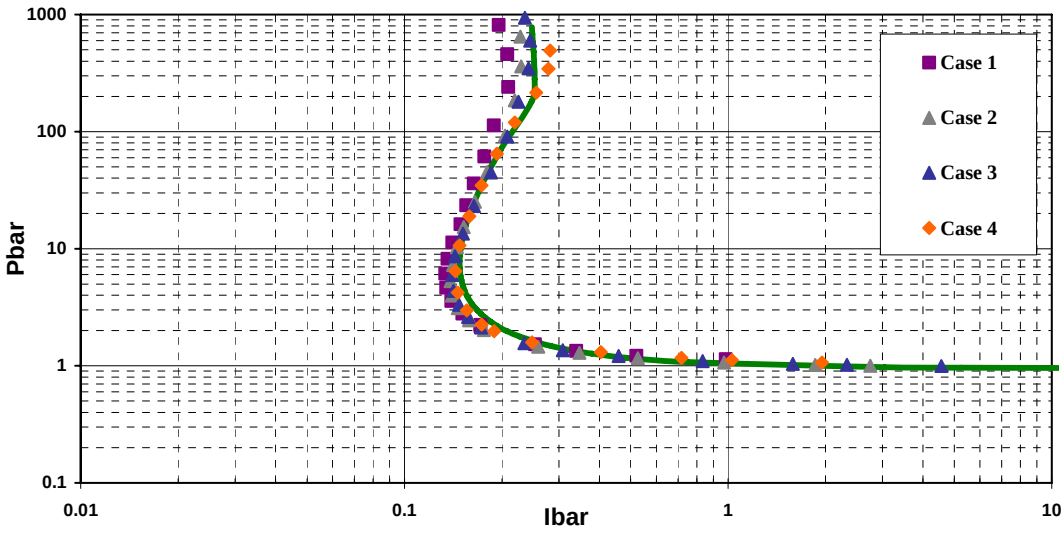

Figure L- 4. Comparison of Scaled P-i Curves Based on Support Rotation for Reinforced Concrete Slabs for MLOP Response (Uniform Load and Simple Supports)

Case	Support Rotation	Ru (psi)	K (psi/in)	Mass (psi-ms^2/in)
Case 1	5	0.366	1.37485128	1336.787565
Case 2	5	0.866	3.35657052	1336.787565
Case 3	5	1.5396	10.6084204	1336.787565
Case 4	5	8.1696	429.641027	2673.57513

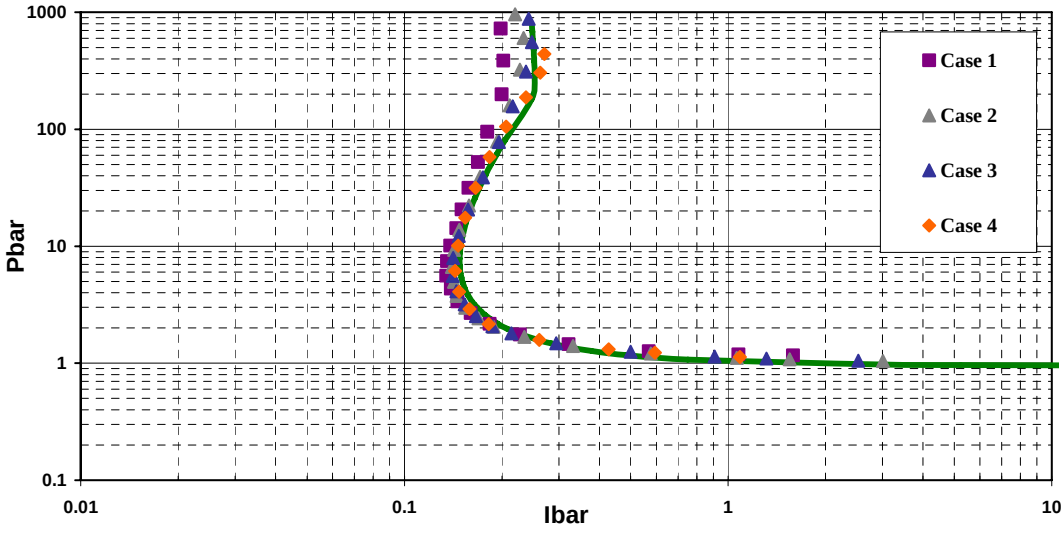

Figure L- 5. Comparison of Scaled P-i Curves Based on Support Rotation for Reinforced Concrete Slabs for MLOP Response (Uniform Load and Fixed Supports)

Case	Support Rotation	Ru (psi)	K (psi/in)	Mass (psi-ms^2/in)
Case 1	5	0.1625	0.21496046	1336.787565
Case 2	5	0.3876	0.52480581	1336.787565
Case 3	5	0.689	1.65864554	1336.787565
Case 4	5	3.6892	67.1751442	2673.57513

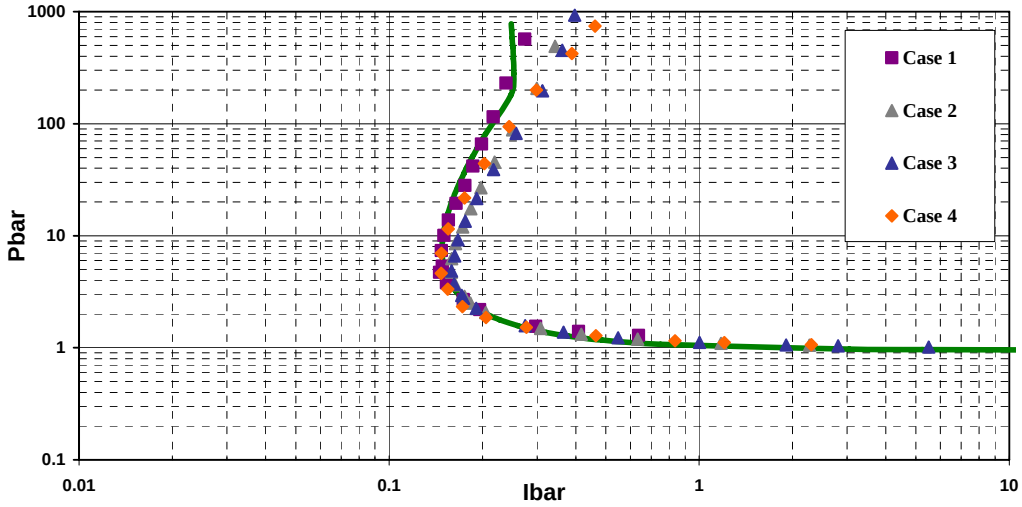

Figure L- 6. Comparison of Scaled P-i Curves Based on Support Rotation for Reinforced Concrete Slabs for MLOP Response (Central Load and Simple Supports)

Note: The case in Figure L-6 for Non-Uniform Load is not in CEDAW and is shown for illustrative purposes only.

Case	Support Rotation	Ru (psi)	K (psi/in)	Mass (psi-ms^2/in)
Case 1	6	1.14	0.97	128
Case 2	6	4.58	15.44	128
Case 3	6	7.93	20.88	103
Case 4	6	13.05	31.83	103

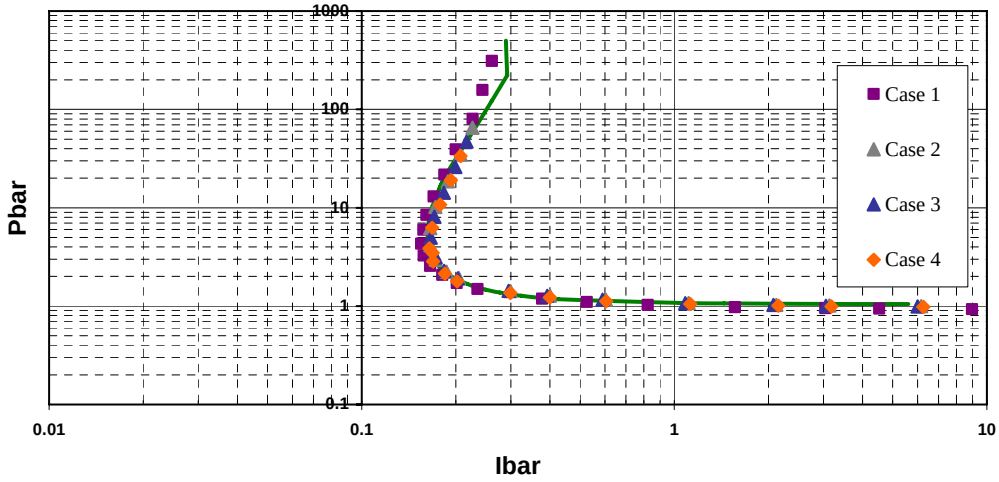

Figure L- 7. Comparison of Scaled P-i Curves Controlled by Support Rotation for Corrugated Steel Panels for LLOP Response

Case	Support Rotation	Ru (psi)	K (psi/in)	Mass (psi-ms^2/in)
Case 1	10	11.80	4.35	1079
Case 2	10	4.86	2.48	1002
Case 3	10	2.16	0.49	1002
Case 4	10	1.11	0.19	972

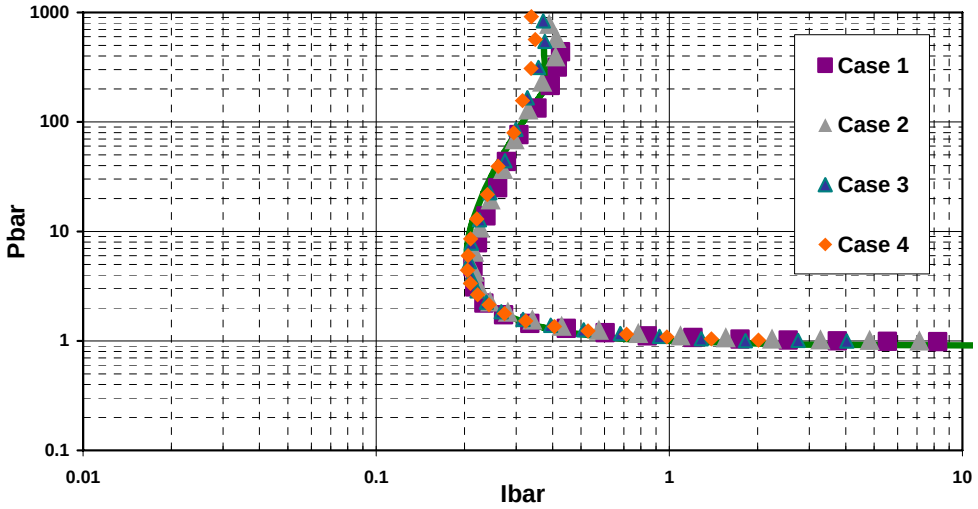

Figure L- 8. Comparison of Scaled P-i Curves Based on Support Rotation for Steel Beams for LLOP Response

Case	Support Rotation	Ru (psi)	K (psi/in)	Mass (psi-ms^2/in)	Ktm psi/in
Case 1	10	0.36805556	0.078125	143.9263097	0.03
Case 2	10	0.88333333	0.3696875	143.9263097	0.10
Case 3	10	1.47222222	0.59895833	179.9078872	0.13
Case 4	10	2.02430556	1.19791667	197.8986759	0.13

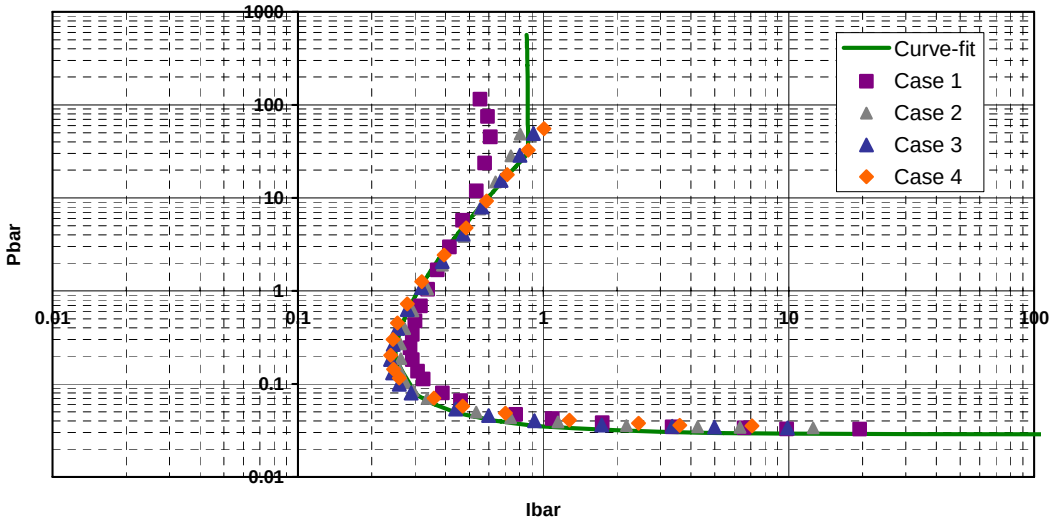

Figure L- 9. Comparison of Scaled P-i Curves for Open Web Steel Joists with Tension Membrane for LLOP Response

Case	Support Rotation	Ru (psi)	K (psi/in)	Mass (psi-ms^2/in)	Ktm (psi/in)
Case 1	12	0.2666481	0.0693236	913.4283247	0.0463
Case 2	12	0.5605671	0.2019133	913.4283247	0.0463
Case 3	12	0.9965638	0.6381459	913.4283247	0.0823
Case 4	12	3.7707819	2.8362038	927.3172136	0.3292

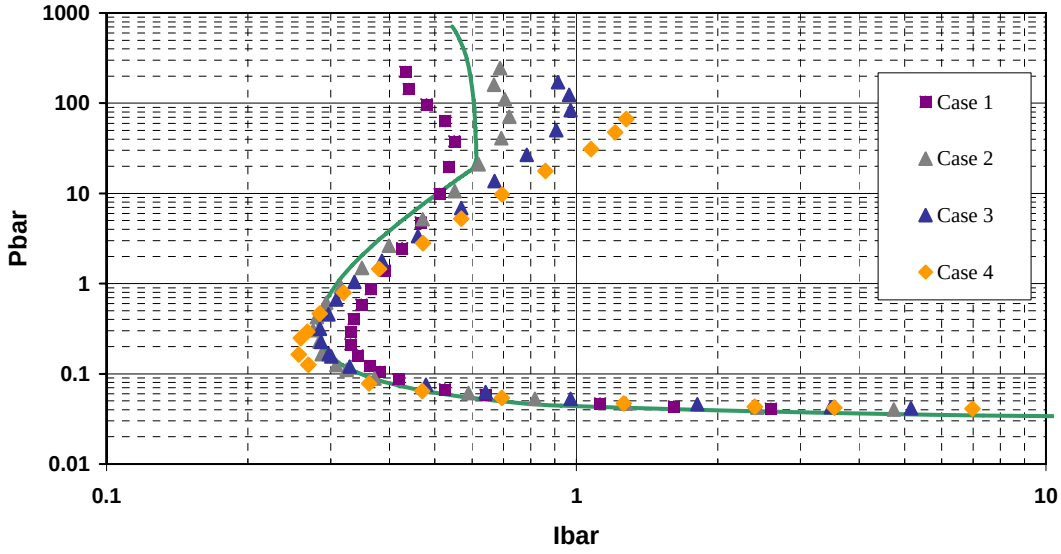

Figure L- 10. Comparison of Scaled P-i Curves For Cold-formed Beams with Significant Tension Membrane for LLOP Response

Case	Support Rotation	Ru (psi)	K (psi/in)	Mass (psi-ms^2/in)	Ra/Ru
Case 1	1.50	0.82	18.89	665.66	0.08
Case 2	1.50	0.82	18.89	665.66	0.34
Case 3	1.50	0.82	18.89	665.66	0.60
Case 4	1.50	0.82	18.89	665.66	1.11

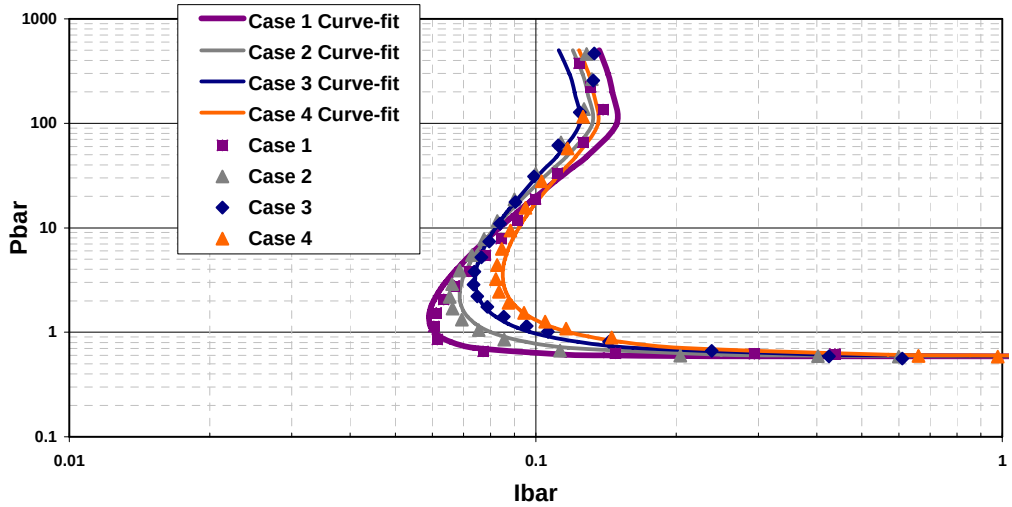

Figure L- 11. Comparison of Scaled P-i Curves Controlled for Unreinforced Masonry Wall with Constant Ultimate Resistance and Variable Axial Load for MLOP Response

Case	Support Rotation	Ru (psi)	K (psi/in)	Mass (psi-ms^2/in)	Ra/Ru
Case 1		0.36	9.33	665.66	0.12
Case 2		0.82	18.89	665.66	0.34
Case 3	1.5	1.83	86.76	665.66	0.53
Case 4		3.00	167.56	544.04	0.94

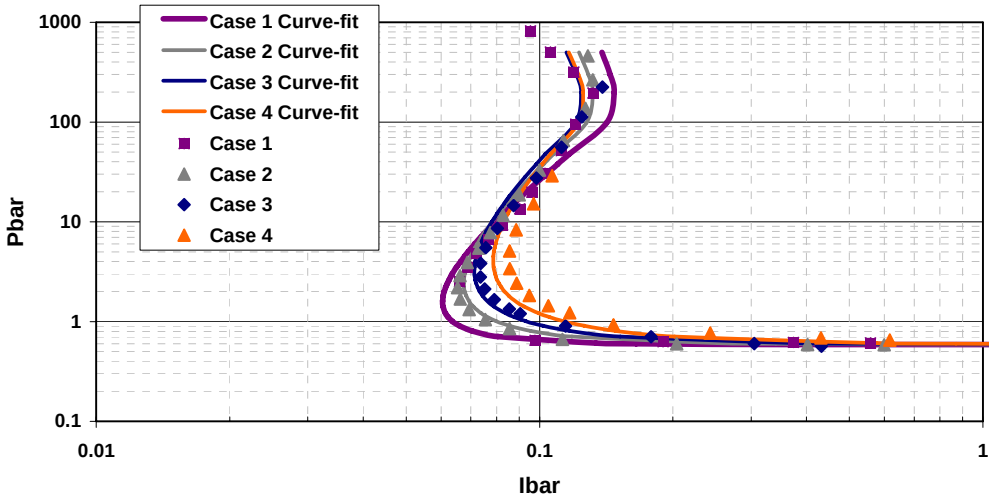

Figure L- 12. Comparison of Scaled P-i Curves Controlled for Unreinforced Masonry Wall with Variable Ultimate Resistance and Axial Load for MLOP Response

Case	Support Rotation	Ru (psi)	K (psi/in)	Mass psi-ms^2/in)	Ra/Ru
Case 1	4.00	0.82	18.89	665.66	0.08
Case 2	4.00	0.82	18.89	665.66	0.34
Case 3	4.00	0.82	18.89	665.66	0.60
Case 4	4.00	0.82	18.89	665.66	1.11

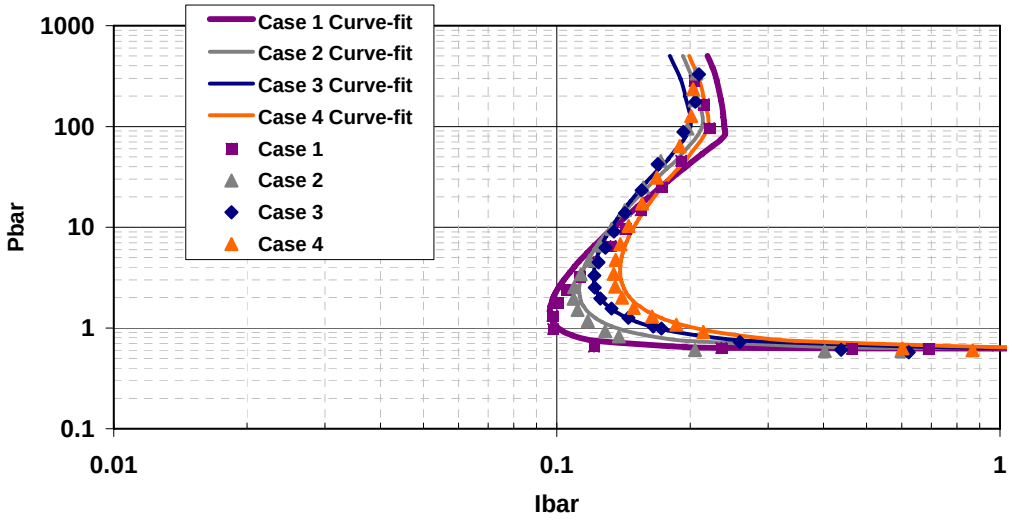

Figure L- 13. Comparison of Scaled P-i Curves Controlled for Unreinforced Masonry Wall with Constant Ultimate Resistance and Variable Axial Load for LLOP Response

Case	Support Rotation	Ru (psi)	K (psi/in)	Mass psi-ms^2/in)	Ra/Ru
Case 1	4.00	0.38	8.74	665.66	0.14
Case 2	4.00	0.82	18.89	665.66	0.34
Case 3	4.00	1.83	86.76	665.66	0.53
Case 4	4.00	3.00	223.41	665.66	0.95

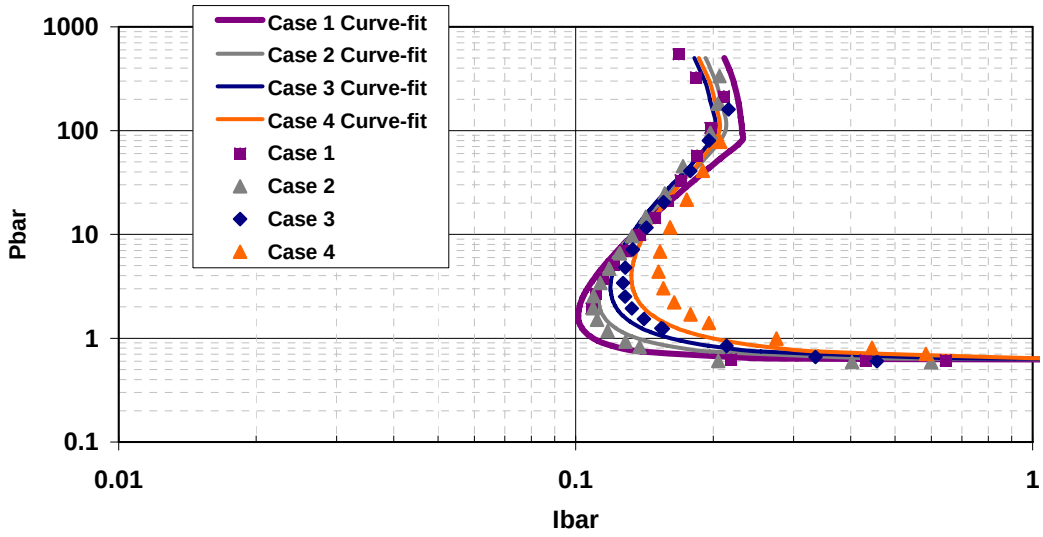

Figure L- 14. Comparison of Scaled P-i Curves Controlled for Unreinforced Masonry Wall with Variable Ultimate Resistance and Axial Load for LLOP Response

APPENDIX M.
CURVE-FITTING PARAMETERS FOR CEDAW P-I CURVES FOR EACH COMPONENT TYPE

As described in Section 3.0, the blast loads causing given levels of non-dimensional response in SDOF analyses were scaled to create Pbar and Ibar values defining scaled blast load points. Equation 1 and Equation 3 in Section 3.0 were used to create curve-fit equations through the scaled points. Equation 1, which is used to curve-fit the scaled blast load points for the large majority of the component types, requires seven curve-fitting parameters designated as A through G. Equation 3, which is used to curve-fit the scaled blast load points for the reinforced concrete columns and steel columns subject to connection failure, requires three curve-fitting parameters designated as A through C.

The curve-fitting parameters A through G in Equation 1 and A through C in Equation 3 were fit to scaled blast loads from SDOF analyses for each component type, LOP, and applicable non-dimensional response parameter as discussed in Section 6.0 and the resulting parameters are shown in Table L-1 and Table L-2. Table L-1 shows the curve-fit equation parameters for cases where the scaled blast loads were from SDOF analyses where the response was defined in terms of ductility ratio. Table L-2 shows the curve-fit equation parameters for cases where the scaled blast loads were from SDOF analyses where the response was defined in terms of support rotation. As noted in Table L-2, Equation 2 in Section 3.0 shows a special case where A and D in Equation 1 for the unreinforced masonry wall component type are functions of input properties of the wall, including the applied axial load. In all other case the curve-fitting parameters are only functions of the LOP, component type, and applicable non-dimensional response parameter (i.e., ductility ratio or support rotation).

Table L-1. Curve-fitting Parameters for Component Types and LOP with Scaled P-i Curves Based on Ductility Ratio Criteria

Component Type	HLOP							MLOP							LLOP							VLLOP						
	A	B	C	D	E	F	G	A	B	C	D	E	F	G	A	B	C	D	E	F	G	A	B	C	D	E	F	G
One-Way Corrugated Metal Panel	0.44	1.90	0.36	0.50	80	0.95	-.1	0.95	1.30	0.40	0.75	150	2.03	-.1	1.30	1	0.40	0.75	150	2.88	-.1	1.90	1	0.40	0.75	150	4.21	-.1
Steel Beam	0.44	1.90	0.36	0.50	80	0.95	-.1	0.95	1.30	0.40	0.75	150	2.03	-.1	1.90	1	0.40	0.75	150	4.21	-.1	2.76	0.90	0.39	0.75	200	6.34	-.1
Metal Studs with Sliding Connection	0.28	3.80	0.40	0.55	50	0.54	-.1	0.36	2.50	0.37	0.50	60	0.73	-.1	0.41	2.10	0.36	0.50	70	0.85	-.1	0.44	1.90	0.36	0.50	80	0.95	-.1
Metal Studs Connected Top and Bottom	0.28	3.80	0.40	0.55	50	0.54	-.1	0.44	1.90	0.36	0.50	100	1.01	-.2	0.76	1.40	0.34	0.60	150	1.53	-.2	0.95	1.30	0.40	0.75	150	2.03	-.2
Open-Web Steel Joist	0.44	1.90	0.36	0.50	80	0.95	-.1	Scaled P-i Curves only based on support rotation for this LOP and these component types							Scaled P-i Curves only based on support rotation for this LOP and these component types							Scaled P-i Curves only based on support rotation for this LOP and these component types						
Reinforced Concrete Slab	0.44	1.90	0.36	0.50	80	0.95	-.1																					
Reinforced Concrete Beam	0.44	1.90	0.36	0.50	80	0.95	-.1																					
Reinforced Masonry	0.44	1.90	0.36	0.50	80	0.95	-.1																					
Unreinforced Masonry	0.44	1.90	0.36	0.50	80	0.95	-.1																					
Wood Beam	0.44	1.90	0.36	0.50	80	0.95	-.1	0.76	1.40	0.34	0.60	150	1.53	-.1	0.95	1.30	0.40	0.75	150	2.03	-.1	1.10	1.20	0.40	0.77	150	2.30	-.1
Reinforced Concrete Column	No scaled P-i curves for this LOP for these component types							No scaled P-i curves for this LOP for these component types							3.70	0.95	1.50	Curve-fit using Equation 3 in Section 3.0 only requires A, B, and C parameters				No scaled P-i curves for this LOP for these component types						
Steel Column (Connection Failure)															1.00	0.50	0.70											
Steel Column (Flexural Response)															1.30	1.10	0.40	0.75	150	2.84	-.30							
See Equation 3 in Section 3.0 for curve-fit equation for column components as noted above and Equation 1in Section 3.0 for curve-fit equation for all other component types.																												

Table L-2. Curve-fitting Parameters for Component Types and LOP with Scaled P-i Curves Based on Support Rotation Criteria

Component Type	MLOP							LLOP							VLLOP						
	A	B	C	D	E	F	G	A	B	C	D	E	F	G	A	B	C	D	E	F	G
One-Way Corrugated Metal Panel	0.09	1.15	0.35	0.60	200	0.20	-.01	0.12	0.95	0.34	0.55	200	0.29	-.01	0.16	0.90	0.31	0.50	200	0.36	-.01
Steel Beam without Tension Membrane	0.08	1.30	0.40	0.70	200	0.20	-.01	0.16	1.10	0.40	0.75	200	0.38	-.01	0.22	1	0.43	0.85	200	0.52	-.01
Steel Beam without Tension Membrane	2.40	250	0.51	1.60	15	0.33	-.10	1.03	30	0.45	1	25	0.66	-.10	1.20	17	0.48	1	30	0.98	-.10
Open-Web Steel Joist without Tension Membrane	0.08	1.30	0.51	1	100	0.17	-.02	0.13	1.20	0.48	1	100	0.25	-.02	0.15	1	0.46	0.83	100	0.35	-.02
Open-Web Steel Joist with Tension Membrane	1	75	0.47	1	25	0.60	-.02	1.10	35	0.50	1	30	0.87	-.02	1	75	0.47	1	25	0.60	-.02
Reinforced Concrete Slab	0.08	1.20	0.42	0.90	200	0.16	-.01	0.12	1.05	0.41	0.85	200	0.25	-.01	0.18	1.00	0.41	0.85	200	0.38	-.01
Reinforced Concrete Beam	0.08	1.20	0.42	0.90	200	0.16	-.01	0.12	1.05	0.41	0.85	200	0.25	-.01	0.18	1.00	0.41	0.85	200	0.38	-.01
Reinforced Masonry	0.08	1.10	0.42	0.90	200	0.16	-.01	0.17	1	0.41	0.96	300	0.33	-.01	0.21	0.82	0.43	0.97	300	0.47	-.01
Unreinforced Masonry	Note[1]	1.70	0.36	Note[1]	80	0.16	-.03	Note[1]	1.60	0.36	Note[1]	80	0.25	-.05	Note[1]	1	0.36	Note[1]	80	0.48	-.10
Steel Column (Flexural Response)	No scaled P-i curves for this LOP for this component type							0.10	1.20	0.40	0.70	150	0.22	-.01	No scaled P-i curves for this LOP for this component type						

Note 1: See Equation 2 in Section 3.0 for equation defining A and D in terms of ratio of resistance from arching to resistance from flexure.
General Note: See Equation 1 in Section 3.0 for curve-fit equation for all component types.